The relationships between rapid urban development and vegetation in the pan Pacific region: spatio-temporal quantification using satellite images

by

Yuhao Lu

B.Sc., The University of British Columbia, 2014

A THESIS SUBMITTED IN PARTIAL FULFILLMENT OF

THE REQUIREMENTS FOR THE DEGREE OF

DOCTOR OF PHILOSOPHY

in

The Faculty of Graduate and Postdoctoral Studies

(Forestry)

The University of British Columbia

(Vancouver)

April 2018

The following individuals certify that they have read, and recommend to the Faculty of Graduate and Postdoctoral Studies for acceptance, the dissertation entitled:

Relationship between rapid urban development and vegetation in pan Pacific regions: spatio-temporal quantification using satellite images

submitted by Yuhao Lu in partial fulfilment of the requirements for

the degree of Doctor of Philosophy

in The Faculty of Graduate and Postdoctoral Studies (Forestry)

Examining Committee:

Dr. Nicholas Coops

Supervisor

Dr. Tongli Wang

Supervisory Committee Member

Dr. Jeanine Rhemtulla

Supervisory Committee Member

Dr. Mark Johnson

University Examiner

Dr. Cecil Konijnendijk

University Examiner

Additional Supervisory Committee Members:

NA

Supervisory Committee Member

NA

Supervisory Committee Member

Abstract

Cities strive for economic strength while recognize the necessity of being environmentally sustainable. The balance between economic development and the environment has been challenging particularly for cities in the pan Pacific region, which is seeing some of the most rapid urban growth rates. Remotely sensed satellite images offer much larger and more consistent spatial and temporal coverages than conventional census data therefore are increasingly being utilized for regional and global urban studies. Two key remote sensing datasets, namely urban vegetation cover derived from Landsat time series, and brightness generated from NOAA's nighttime lights datasets to represent urban development were the focus of this dissertation. I first extracted annual urban vegetation characteristics using spectral indices (e.g. EVI) as well as a spectral mixture analysis from 1984 to 2012. Nighttime lights brightness was used to assess urban expansion and its relationship with census-derived variables. Lastly, I examined the relationships between urban development and the environment using Environment Kuznets Curve (EKC) theory as a lens, addressing how urban vegetation responds to urban nighttime brightness in 25 cities across the pan Pacific region.

I identified inter- and intra-city patterns of vegetation and brightness changes that were strongly related to social and economic contexts. Spectral indices demonstrated opposing trends between urban vegetation and built-up area both spatially and temporally. Spectral mixture analysis successfully extracted the urban vegetation fraction at a sub-pixel level, setting a robust base for cross-city comparisons. I found that urban vegetation changed linearly both positively and negatively with urban brightness, particularly in higher income cities in North America. Pixels with statistically strong quadratic relationships between vegetation and brightness were less prevalent but more spatially clustered in comparison to those that expressed a linear relationship. Overall, there are three key contribution of this dissertation. Firstly, the integration of gap-free satellite images and innovative processing techniques unlocked new ways of informing urban environmental and socio-economic dynamics. Secondly, a classic econometric model (i.e. Granger causality test) was used to examine the casual relationship between census and remote sensing nighttime lights data. Lastly, a pixel-based model fitting was use to confirm EKC at a sub-city scale.

Lay Summary

This dissertation investigated the spatial and temporal dynamics between the urban environment and economic development using satellite images for 25 cities in the pan Pacific region from 1984 to 2012. This dissertation made key contributions to practical urban management. Gap-free satellite time series revealed both with- and across- vegetation and nighttime brightness dynamics at a pixel level. Comparing to conventional census data, satellite-derived information is more spatially comparable, unlocking new ways of regional and global urbanization studies. The relationship between vegetation and nighttime lights brightness was primarily linear yet varying degrees of quadratic relationship was also present at a pixel scale, confirming the existence of the Environmental Kuznets Curve.

Preface

The research questions and objectives of this dissertation were originally conceived from discussions between me and my supervisory committee. Portions of this dissertation appear as co-authored, peer-reviewed journal articles. For these publications, I performed the primary research, data analysis and interpretation, and prepared the final manuscript:

- Chapter 3: **Lu, Y.**, Coops, N. C., & Hermosilla, T. (2016). Regional assessment of pan Pacific urban environments over 25 years using annual gap free Landsat data. *International Journal of Applied Earth Observation and Geoinformation*, 50, 198-210.

- Chapter 4: **Lu, Y.**, Coops, N. C., & Hermosilla, T. (2017). Estimating urban vegetation fraction across 25 cities in pan Pacific using Landsat time series data. *ISPRS Journal of Photogrammetry and Remote Sensing*, 126, 11-23.

- Chapter 4: **Lu, Y.**, Coops, N. C., & Hermosilla, T. (2017). Chronicling urbanization and vegetation changes using annual gap free Landsat composites from 1984 to 2012. In *Urban Remote Sensing Event (JURSE), 2017 Joint* (pp. 1-4). IEEE.

- Chapter 5: **Lu, Y.**, Coops, N.C. Bright lights, Big City: Causal effects of population and GDP on urban brightness (in press Plos One).

- Chapter 6: **Lu, Y.**, Coops, N.C., Wang, T. (under review). Confirming the EKC theory at a pixel scale.

Table of Contents

List of Tables

List of Figures

List of Abbreviations

AIC – Akaike information criterion

BAP – Best available pixel

BSS/TSS – Ratio of the between to the total sum of square

CBD – Central business district

DN – Digital number

DTW – Dynamic time warping

EKC—Environmental Kuznets Curve

EVI – Enhanced Vegetation Index

GADM – Global administrative Data

GDP – Gross domestic product

NDBI – Normalized Differenced Built-up Index

NDI – Normalized Distance Index

NDVI – Normalized Differenced Vegetation Index

NTL – Nighttime lights

PBC – Pixel based compositing

POP – population

SMA – Spectral mixture analysis

TDN – Total digital number

TGDP – Total gross domestic product

TPOP – Total population

TS – Theil Sen slope

VF – Vegetation fraction

bak – Bangkok

cal – Calgary

csx – Changsha

dal – Dalian

den – Denver

edm – Edmonton

fuz – Fuzhou

hak – Haikou

har – Harbin

hksz – Hong Kong-Shenzhen

kul – Kuala Lumpur

lav – Las Vegas

man – Manila

mel – Melbourne

mex – Mexico City

ncx – Nanchang

phx – Phoenix

sea – Seattle

sel – Seoul

shh – Shanghai

sin – Singapore City

tjn – Tianjin

tko – Tokyo

van – Vancouver

Acknowledgements

This dissertation was supported by funding provided to Dr. Nicholas Coops from Natural Sciences and Engineering Research Council of Canada (NSERC, RGPIN 31 1926-13) as well as the Asia-Pacific Network for Sustainable Forest Management and Rehabilitation through Dr. Guangyu Wang. The images used in this dissertation are archived and distributed by United States Geological Survey and National Oceanic and Atmospheric Administration.

My committee members, Dr. Jeanine Rhemtulla and Dr. Tongli Wang, have offered tremendous support since entering graduate school. Dr. Jeanine Rhemtulla has always brought unique and fresh perspectives to my research and constantly reminded me to think broader. The knowledge and expertise on modelling and spatial data analysis from Dr. Tongli Wang is more than I could ever asked.

Dr. Nicholas Coops is more than just a supervisor. He created and maintained a friendly, productive, and enjoyable environment for all IRSS members and alumni. His passion and work ethic towards remote sensing is mind-blowing. He is a great mentor and a best friend.

The time at the IRSS lab is a life changing experience. I wrote my very first piece of code with Dr. Txomin Hermosilla. I could not recall how many times Dr. Paul Pickell proofread and edited my broken manuscripts. It was always fun to discuss mapping ideas and colour options with Andrew Plowright. Dr. Ryan Frazier was always happy and uplifting no matter how early the hours were in. IRSS is also full of some of the greatest athletes: Dr. Ricardo Tortini, Chris Mulverhill, Ethan Berman, Lukas Jarron etc. They are humble, strong, and taught me a lot of lessons that will be carried on beyond my career.

I did not spend too much time with my parents during my time in Canada. They are the most incredible human beings I know. They are my closest friends. I am thankful for everything they have done and sacrificed for me. Yang is the silliest golden retriever. I left home when he was just 5 years old. I hope he will stay strong and healthy.

I have also met many new friends from all of the world. Some of them I have never had a chance to meet in person (yet). A special thank-you to all the places I visited in Iceland and Canada, and all the members in eARTh. There are simply too many of you.

Y.L.
April 18, 2018

Chapter 1

1. Introduction

1.1. Urbanization worldwide

The rate of human modification of the terrestrial biosphere has intensified over the past several decades (Hugo, 2017). The term urbanization describes not only the physical expansion and densification of cities but also implies the complex transformation of human society, demography, and, more importantly, the relationship among them (Boone & Fragkias, 2012). Cities and their surroundings (synonymous with urban environments in this dissertation) cause some of the most profound anthropogenic impacts on Earth in spite of their disproportionately small spatial footprint. Covering approximately 3% of the landscape, cities are responsible for three quarters of global energy consumption and approximately 80% of greenhouse gas emissions (Ash, Jasny, Roberts, Stone, & Sugden, 2008) in accommodating over 54% of the global population, a number that is expected to exceed 70% by 2050 (UNDESA, 2014, 2017).

Concepts of urbanization have now evolved to not only refer to a collection of isolated, locally dense, commercial districts of concrete and artificial lights, but extend to *networks* of social, ecological, and economic mosaics functioning interdependently as a whole (Pickett & Zhou, 2015). The classic view of urbanization patterns is now being challenged by a more connected and heterogeneous decentralizing trend. The localizing mindset of "the closer the cheaper" that drove early urban development is no longer a primary objective espoused by city planners. Efficient transportation and global trading networks have nodalized cities worldwide regardless of their physical distances and, as a result, urbanization has become a global phenomenon with unprecedented rates of growth (Lee, 2013; Martinus & Tonts, 2015).

Despite decentralization, there remains recognition that cities are driven by local geopolitical, social, and ecological environments (K. C. Y. Seto, 2014), making models of urban development both conceptually and practically challenging. The scale and pace of modern urbanization also affect spatial urbanization processes. In the early 20th century, cities were conceptualized by a series of concentric circles (Burgess, 1925) that expand radially from the city centre. Around the central core is a buffer area, also known as a loop, which isolates the core from the third, or workmen's, zone inhabited by industrial

workers. Beyond that is the fourth, residential zone with high class apartments and single family houses. Outside the city limits lies the commuters' zone, which includes all suburban areas and other satellite cities within a 30 to 60 minutes drive from the city centre (Burgess, 1925).

Spatially, contemporary urbanization posits two general models: *fragmentation* and *polycentrism* (Jenks et al., 2008). Particularly in developing regions, cities render spatial patterns that are recognized as urban fragmentation (Balbo & Navez-Bouchanine, 1995). The concept of fragmentation is described and interpreted as the "dividing" and "partitioning" of modern metropolises (Jenks et al., 2008) or is the result of a combination of urban dislocation and discontinuity (Mieg & Töpfer, 2013). Burgess (1925) defined urban fragmentation as "a spatial phenomenon that results from the act of breaking up, breaking off from, or disjointing the pre-existing form and structure of the city and systems of cities." Although the phenomenon of urban fragmentation is often understood to have a negative impact on urban demography, many cities have experienced decentralization throughout their developing stages.

In contrast, the polycentrism model allows for regions that contain separate and distinct cities or small human settlements with substantial interactions (Gordon et al., 1986) while fragmented urban structures display disconnection and highly heterogeneous patterns. Although it would appear to integrate small cites, the polycentric urban form often intensifies fragmentation instead of reversing it (Jenks et al., 2008). Infrastructure used to reduce urban fragmentation, such as mass public transit or freeways, may in fact exacerbate it. Despite these two theoretical models, the scarcity of knowledge about how cities grow and interact spatially and temporally limits the advancement of healthy and efficient urban structure and organization.

1.2. Big city versus green city

Urbanization today strives to grow not only economically strong but also environmentally sustainable during the process of urbanization. The perception that "big cities" yield overwhelmingly positive outcomes for the population has started to lose momentum over time. Urbanization has not only caused economic saturation (Wheaton & Shishido, 1981) but also numerous social, health, and environmental challenges such as increased crime (Shelley, 1981), disease (Nicolaou, Siddique, & Custovic, 2005), urban heat island effect (Oke, 1982), and water and air pollution (Beckerman, 1992).

As a result, there has been a recent increase in the value placed on urban greenspace, or urban vegetation, by both the scientific and political communities (Zhao, Liu, & Zhou, 2016). Definitions of urban greenspace and urban vegetation are just as complicated as urbanization itself; however, they are often used interchangeably to include any functional vegetated land-cover and land use type within an urban setting, exclusive of agriculture and cropland.

The presence of urban vegetation is known to be beneficial to the local climate, and thus also to the social, and physical environments through temperature control (Oke, 1982), air pollution reduction (Nowak, Crane, & Stevens, 2006), noise and storm water control (Glass & Singer, 1972), and habitat preservation (Nowak & Dwyer, 2007). Studies have also indicated significant social (Grahn & Stigsdotter, 2003), economic (Tyrväinen, Pauleit, Seeland, & De Vries, 2005), and aesthetic values associated with urban vegetation (Jim & Chen, 2006; Tyrväinen et al., 2005). Such greenspace has been utilized as an effective tool to achieve sustainable and functional urban environments. Efforts towards preserving healthy urban vegetation can be found worldwide, particularly in developed regions, such as in North America and Europe (Nowak et al., 2006).

The question many researchers and planners have raised however is at which urbanization stage a city can afford to be moving towards environmentally sustainability or "being green" (Stern, 1998). In less developed areas, urbanization often receive higher prioritization than preserving and maintaining urban vegetation, despite the resulting benefits and services (Grimm et al., 2008). Vegetation in these urban environments often grows in more isolated and fragmented patches compared to that in novel and well managed urban environments, making it more challenging to manage for local urban planners in these areas. Another concern associated with poorly managed and fragmented urban vegetation is ecological inequity (N. Heynen, Perkins, & Roy, 2006), which causes uneven access to quality urban green space among local residents.

It is evident worldwide that growing or maintaining economic development in an environmentally sustainable manner is difficult, particularly for less developed regions (Egli & Steger, 2007; Glaeser, 2011; Stern, 2004). The interplay between economic growth and urban greenspace has spurred debate, forming various theories to better understand the tensions that divide economic development and environmental sustainability. The *Environmental Kuznets Curve* (EKC) theory (Kuznets, 1955) hypothesises a non-linear, U-shaped relationship between environmental quality and economic development where environmental performance decreases at early stages of economic development and recovers as the economy reaches a certain turning point. However, the scarcity of reliable and

consistent assessment of the relationship between economic growth and environmental degradation limits our ability to understanding and testing theories such as the EKC.

1.3. The opportunity of studying urbanization using remote sensing

Remote sensing derived metrics have been widely used to assess urban vegetation and economic development in a more spatially and temporally consistent manner than conventional census and ground measurements. New imaging and mapping technologies such as Geographic Information Systems (GIS) and remotely sensed imagery have simplified the geographic identification of cities. The age of open access satellite images has arrived (Woodcock et al., 2008; Wulder et al., 2008; Wulder & Coops, 2013). These freely accessible remotely sensed time series data pose many strengths in urban contexts, including: (i) the capability to capture the full temporal profile of urbanization rather than snapshots of individual time periods; (ii) pixel-based compositing (PBC) which unlocks the limit of the traditional scene-based analysis approach; (iii) continuous measurement of the spectral response in urbanization and urban greenspace that allows for the application of various modelling options; and (iv) enables large-scale systematic and compatible comparisons across countries.

As a result, remotely sensed data allow monitoring, extracting, and estimating changes in three key components of urban environments: namely, urban built-up/impervious area, urban vegetation, and socio-economic indicators. The literature on urban remote sensing indicates a substantial amount of diversity in terms of study locations, temporal, and spatial scales (Table 1.1). Zha, Gao, & Ni (2003) proposed a new spectral index – Normalized Difference Built-up Index (NDBI) for a fast urban impervious mapping and classification. Bagan & Yamagata (2014) studied 50 cities globally using Landsat TM/ETM+ imagery at 30m spatial resolution, and used a maximum likelihood classifier to classify urban land use patterns between 1985 and 2010.

For vegetation, various spectral indices such as Normalized Difference Vegetation Index (NDVI, e.g. Boone & Fragkias, 2012; Lin, Liu, Li, & Li, 2014), and Enhanced Vegetation Index (EVI, e.g. Zhang et al., 2003) have been used to extract and monitor urban vegetation dynamics. Sub-pixel or spectral unmixing analysis (SMA) is also a popular method for investigating urban vegetation trends (Phinn, Stanford, Scarth, Murray, & Shyy, 2002; Ridd, 1995; Tooke, Coops, Goodwin, & Voogt, 2009). SMA spectrally decomposes a given pixel, allowing users to pre-define pure spectra and compute a fractional score that represents the abundance of a given land use or land-cover type (i.e. vegetation). Compared to

conventional spectral indices such as NDVI, SMA derived vegetation estimation is less likely to be saturated (Ridd, 1995).

Historically, accurate spatial representation of socio-economic activities was dominated by local census data with little use of remote sensing. Welch (1980) discovered the potential of utilizing nighttime light images (NTL) to map urban population and energy consumption. Ever since, NTL data have been used at local (Ma, Zhou, Pei, Haynie, & Fan, 2012), regional (Klotz, Kemper, Geiß, Esch, & Taubenböck, 2016), and global scales (Small, Pozzi, & Elvidge, 2005), representing a variety of urbanization indicators such as population density (P. Sutton, Roberts, Elvidge, & Baugh, 2001), income level (Ebener, Murray, Tandon, & Elvidge, 2005), GDP (P. C. Sutton, Elvidge, Ghosh, & others, 2007), light pollution (Bennie, Davies, Duffy, Inger, & Gaston, 2015), and even carbon emissions (Ghosh et al., 2010).

A literature review (Table 1.1) reveals three key findings on the use of the remote sensing of urban environments. First, despite the increasing use of remote sensing in urban studies, it is apparent that the value of remote sensing at a global scale is limited by the availability and quality of continuously collected image data. Studies involve either monitoring a small number of cities over a long continuous period, or monitoring a large number of cities at fewer time steps. For example, Wang et al. (2014) covered 1985 to 2013 using data acquired from alternative years for a single city (Toronto) while Bagan & Yamagata (2014) analysed 50 cities but only using imagery acquired in 1986 and 2010. In addition, recent urban expansion studies (e.g. Castrence et al., 2014; Chen et al., 2014; T. Liu & Yang, 2015; Ma et al., 2012), despite analysing a moderate number of cities and data, tended to focus on local urban dynamics with limited regional- and global-scale synthesis. Lastly, literature reviews confirm the Landsat data archive is the dominant spatial data source in urban studies with over 80% of papers reviewed using data from the Landsat series of satellites. The overall theme of previous literature focuses primarily on image classification using images from a limited number of cities. Although Landsat is the longest and most consistent Earth observation program, urban time series studies are still scarce in the current literatures.

Table 1.1 Literature review on previous urban remote sensing studies

Article	Data	Scale	Attribute(s) measured
Tooke et al. 2009	LiDAR	Metropolitan	Urban greenspace
Rottensteiner & Briese, 2002	LiDAR	Metropolitan	Building extraction
Secord & Zakhor, 2006	LiDAR	City blocks	Urban tree detection
Singh, Vogler, Shoemaker, & Meentemeyer, 2012	LiDAR and Landsat TM	Metropolitan	Land-cover classification
Fauvel & Benediktsson, 2008	Hyperspectral images	City blocks	Land-cover classification
Kong, Yin, and Nakagoshi 2007	SPOT-4	Province/State	Green space
Marconcini et al. 2014	TSX/TDX	Global	Urban extent
Small 2003	IKONOS	Global	Reflectance properties
Cheng et al. 2007	Landsat TM	Metropolitan	Urban park cooling effect
Wang et al. 2014	Landsat TM	Metropolitan	Urban extent
Zheng et al. 2014	Landsat-8 OLI	Rural	Impervious surface
Yang et al. 2014	Landsat ETM+	Metropolitan	Green space
Waqar et al. 2012	Landsat TM	Metropolitan	Built-up and bare soil
Chen et al. 2014	Landsat TM	Province/State	Urban extent
Schneider & Woodcock 2008	Landsat TM	Global	Urban fragmentation
Ward, Phinn, & Murray 2000	Landsat TM	Province/State	Land-cover classification
Liu & Yang 2015	Landsat TM and WV-2	Metropolitan	Land-cover classification
Handayani & Rudiarto 2014	Landsat TM/ETM+	Metropolitan	Built-up and population
Fan & Fan 2014	Landsat TM/ETM+	Metropolitan	Urban extent
Yang et al. 2014	Landsat TM/ETM+	National	Urban greenspace
Ji et al. 2006	Landsat TM/ETM+	Metropolitan	Urban density
Griffiths et al. 2010	Landsat TM/ETM+	Metropolitan	Urban extent
Michishita, Jiang, & Xu 2012	Landsat TM/ETM+	Metropolitan	Reflectance properties
Xu and Min 2013	Landsat TM/ETM+, CBERS, HJ-1	National	Urban extent
Shen et al. 2015	Landsat TM/ETM+, MODIS	Metropolitan	Urban temperature

Tian et al. 2014	Landsat-MSS and TM	Metropolitan	Land-cover and land use
Bagan & Yamagata 2014	Lansat TM/ETM+	Global	Land-cover change
Gonçalves et al. 2014	MODIS, SPOT, AVHRR/NOAA	Metropolitan	Land use temporal trend
Li et al. 2013	DMSP/OLS Nighttime lights	Metropolitan	GDP
Ghosh et al., 2010	DMSP/OLS Nighttime lights	Global	CO_2 emission
Huang et al., 2015	DMSP/OLS Nighttime lights	National	Spatial distribution
Bennie et al., 2015	DMSP/OLS Nighttime lights	Regional	Light pollution
Welch, 1980	DMSP/OLS and Landsat	National	Energy consumption
Bennett & Smith, 2017	DMSP/OLS and Suomi NPP VIIRS	Global	Review
Small et al., 2005	DMSP/OLS Nighttime lights	Global	Urban extent

1.4. Research approach and objectives

Given the need for and scarcity of accurate spatio-temporally consistent records of urban vegetation and economic development, the overall research objective of this dissertation is to test what trends and interrelationships exist between remotely sensed derived vegetation and economic indicators within and across pan Pacific urban centres.

Three specific research questions are proposed:

1. How can metrics derived from remotely sensed data inform environmental and socio-economic dynamics within and across cities in the pan Pacific region?

2. What models exist to examine the relationship between urban environmental and socio-economic developments over time and space?

3. What similarities and differences exist across cities in the pan Pacific region both spatially and temporally?

These three questions are structured in such a way to allow examination of the EKC hypothesis (Figure 1.1). Research question 1 investigates how time series of satellite images can be used to spatially and temporally assess the dynamics of urban environment and development. Research question 2 examines the EKC theory at a pixel-level using measurements from research question 1. The final research question examines how individual cities conform to the hypothesis of EKC theory.

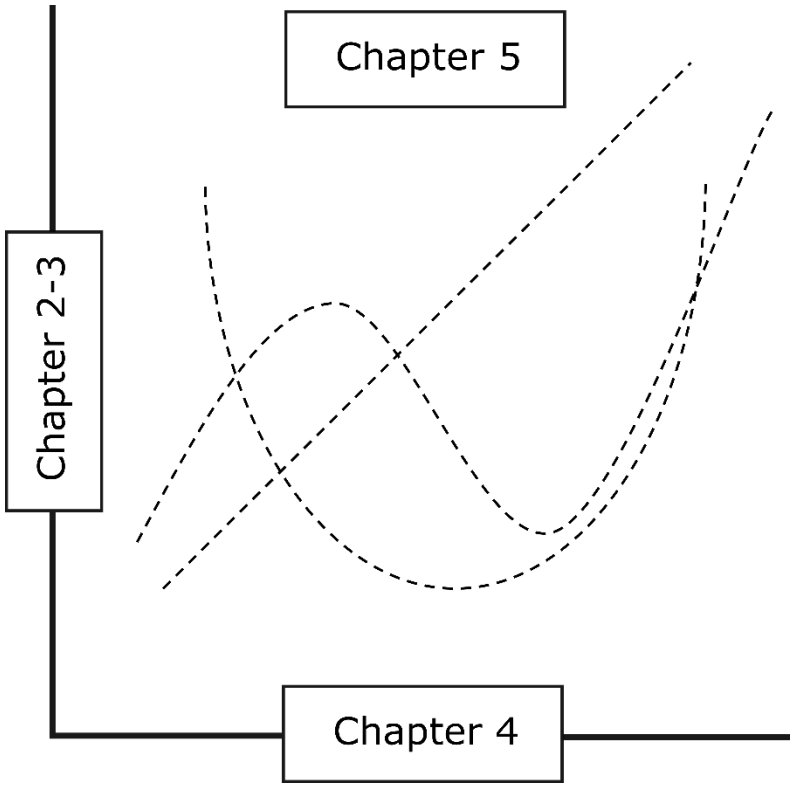

Figure 1.1 A conceptualized overview of the dissertation – An integration between Environmental Kuznets Curve (EKC) and 4 chapters of this dissertation. Chapter 2 and Chapter 3, addresses the challenges of measuring urban vegetation consistently over time. Chapter 4 utilizes the NTL image archive and local census economic data to examine the driving socio-economic variables behind Nighttime Lights (NTL) changes. Final research Chapter 5 utilizes results from previous chapters and further investigates and confirms the EKC hypothesis within 25 selected cities.

1.5. Dissertation overview

The structure of this dissertation is as follows.

Chapter 2 introduces the main study sites: 25 cities across the pan Pacific region, in terms of their geographic location, climate, and economic status. Chapter 2 also provides an overview of the two main remote sensing products used in this dissertation.

Chapter 3 addresses the first research question using a pixel-based image composite technique to generate annual gap-free surface reflectance Landsat composites from 1984 to 2012. Using time series composites, spectral indices were calculated and compared using a hexagonal grid ring model to assess

changes in vegetative and urban built-up patterns. Trajectories are then clustered to further investigate the spatio-temporal dynamics and relationships among the 25 cities. Outcomes from this chapter demonstrate the value of utilising annual Landsat time series composites for assessing urban vegetation and urban dynamics at regional scales and potential use in achieving and evaluating sustainable urban planning.

Chapter 4 focuses on extracting and characterizing urban vegetation by innovatively applying sub-pixel, spectral unmixing on Landsat time series composites from Chapter 2. Vegetation change trends were then analyzed using Mann-Kendall statistics and Theil-Sen slope estimators. The outcomes of this chapter indicate that unmixing approaches successfully map urban vegetation for pixels located in urban parks, forested mountainous regions, as well as agricultural land (correlation coefficient ranging from 0.66 to 0.77). Using temporal trend analysis, our results suggest that it is possible to reduce noise and outliers caused by phenological changes particularly in cropland using dense new Landsat time series approaches.

Chapter 5 focuses on the socio-economic aspects of urbanization in the pan Pacific region. It uses remotely sensed nighttime light images (NTL) as a proxy to map urbanization and subsequently examines the driving socio-economic variables in cities. Using a classic econometric approach, panel causality tests are undertaken to analyze causal relationships between NTL and socio-economic development across the pan Pacific region. Panel causality tests show a contrasting effect of population and gross domestic product (GDP) on NTL in fast and slowly changing cities. Information derived from this chapter quantitatively chronicles urban activities in the pan Pacific region and offers data for further studies on spatially tracking local policy progress on sustainable urban development.

Chapter 6 brings the results from Chapter 3 and 4 to spatially test the EKC hypothesis within the selected 25 cities. Three fitted models were developed (i.e. linear, polynomial, and cubic) and the best fit was selected using AIC (Akaike Information Criteria) scores. The results of this chapter suggested that in most cases, urban vegetation varies linearly with NTL however the relationship and the rate of change varies over time. Within individual cities polynomial models tend to spatially cluster together more than linear and cubic models. Further, this chapter bridges the gap between the conventional econometric theory (i.e. EKC) and advanced earth observation satellite data, thus overcoming some of the difficulties of using census data which are less suitable, updated infrequently, and spatially incompatible among cities.

Chapter 7 concludes with some key research findings, limitations, and possible opportunities for future research.

Chapter 2

2. Study area and Data

2.1. Study area

Defined by UNESCO, the pan Pacific, or Pacific Rim, region of the globe contains 50 countries (UNESCO, 2014) from the borders of China-Mongolia to the north, and the southern tips of Australia and New Zealand to the south. This region covers approximately 2.8 billion hectares of land, approximately 22% of the Earth's land surface, 30% of the world's natural forest, and 54% of the world's plantations (UNESCAP, 2012). In addition to Asia and Oceania, the pan Pacific region as recognised in this dissertation also contains North and Central America, producing a diversity of geopolitical, social, and ecological environments, making it an ideal regional focus area for the questions posed herein.

Throughout this dissertation I focused on 25 cities across the pan Pacific region covering a range of population sizes and economic development statuses (Table 2.1, Figure 2.1). Nine cities were selected in China, and six in Southern Asia and South America, all of which are highly dynamic urban areas. The rest of the cities are located in more developed areas with four in the United States, three in Canada, two in Australia, one in Japan, and one in South Korea. Among the 25 urban environments, eight are mega-cities (defined as having a population over 10 million), namely, Tokyo, Shanghai, Seoul, Mexico City, Tianjin, Bangkok, Shenzhen, and Harbin. Smaller cities, particularly those in developing regions, are often less studied (Bell & Jayne, 2009) and were thus included in this dissertation. As a result, the thesis includes cities such as Changsha that are not as economically developed as other selected mega-cities.

Urban environments were also located across a variety of landscapes from costal mountainous regions (e.g. Vancouver, Dalian) to plains and dry inland areas (e.g. Las Vegas, Denver). Climatically, using Köppen climate scheme (Kottek, Grieser, Beck, Rudolf, & Rubel, 2006), 10 cities are located within a temperate climate scheme (Class C) with the temperature of the coolest month at 18 °C or higher. The cold continental (Class D) climate scheme contained six cities dominantly from North America and East Asia. Cities located in South East Asia were primarily within the Tropic (Class A) climate scheme, and three cities from North America (i.e. Denver, Las Vegas, and Phoenix) were from the Arid (Class B) climate scheme.

Table 2.1 Summary table of studied cities.

City (code)	Country	Latitude/ Longitude [1]	Location	Köppen climate scheme*	Word Bank Economy Class*
Bangkok (bak)	Thailand	13.75°N/100.49°E	South East Asia	Tropical (Aw)	Upper middle
Calgary (cal)	Canada	51.05°N/114.08°W	North America	Continental (Dfb)	High
Changsha (csx)	China	28.20°N/112.92°E	East Asia	Temperate (Cfa)	Upper middle
Dalian (dal)	China	38.92°N/121.64°E	East Asia	Continental (Dwa)	Upper middle
Denver (den)	USA	39.75°N/111.00°W	North America	Arid (Bsk)	High
Edmonton(edm)	Canada	53.55°N/113.49°W	North America	Continental (Dfb)	High
Fuzhou (fuz)	China	26.08°N/113.31°E	East Asia	Temperate (Cfa)	Upper middle
Haikou (hak)	China	20.03°N/110.33°E	East Asia	Tropical (Am)	Upper middle
Harbin (har)	China	45.77°N/126.63°E	East Asia	Continental (Dwa)	Upper middle
Shenzhen (hksz)	China	22.53°N/114.05°E	East Asia	Temperate (Cwa)	High
Kuala Lumpur (kul)	Malaysia	3.16°N/101.70°E	South East Asia	Tropical (Af)	Upper middle
Las Vegas (lav)	USA	36.17°N/115.14°W	North America	Arid (Bwk)	High
Manila (man)	Philippines	14.58°N/120.99°E	South East Asia	Tropical (Af)	Lower middle
Melbourne (mel)	Australia	37.82°S/144.96°E	Oceania	Temperate (Cfb)	High
Mexico City (mex)	Mexico	19.42°N/99.13°W	Central America	Temperate (Cwb)	Upper middle
Nanchang (ncx)	China	28.67°N/115.90°E	East Asia	Temperate (Cfa)	Upper middle
Phoenix (phx)	USA	33.44°N/112.07°W	North America	Arid (Bwh)	High
Seattle (sea)	USA	47.61°N/122.34°W	North America	Temperate (Csb)	High
Seoul (sel)	South Korea	37.57°N/126.98°E	East Asia	Continental (Dwa)	High
Shanghai (shh)	China	31.24°N/121.50°E	East Asia	Temperate (Cfa)	Upper middle
Singapore City (sin)	Singapore	1.30°N/103.84°E	South East Asia	Tropical (Af)	High
Tianjin (tjn)	China	33.86°S/151.21°E	East Asia	Continental (Dwa)	Upper middle
Tokyo (tko)	Japan	39.13°N/117.20°E	East Asia	Temperate (Cfa)	High
Vancouver (van)	Canada	35.70°N/139.70°E	North America	Temperate (Cfb)	High

[1] Latitude/Longitude of each city is the location of the city center used in this dissertation

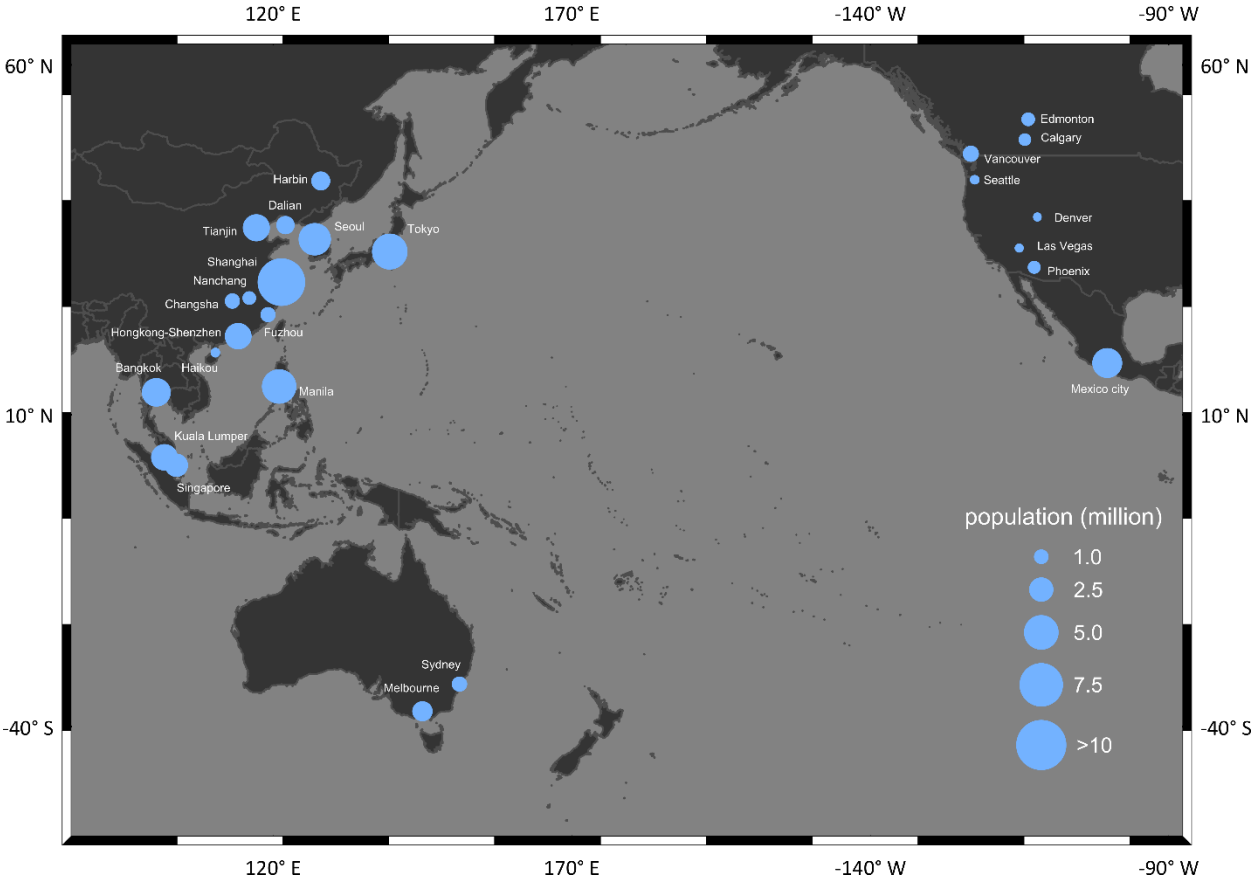

Figure 2.1 Geographic locations of studied cities.

2.2. Landsat time series

Landsat data have been recorded, organized, and distributed by the U.S. Geological Survey (USGS) since 1972. One of the most critical components of Earth Observation (EO) and land use monitoring is a continuous archive of images (Wulder et al., 2008). Landsat has continually imaged the Earth surface every 16 days for almost 40 years and become freely available since 2008. Data acquired by the Landsat program represent a unique combination of spatial, spectral, and temporal resolutions that are desirable to chronicle both anthropogenic and natural impacts of the land status and dynamics for the past three decades (Woodcock et al., 2008).

Launched in 1972, Landsat-1-3, the Multi-Spectral Scanner (MSS), pioneered some of the earliest planetary observation programmes. The onboard MSS sensor, capable of capturing multi-spectral

information at a 80-meter pixel size, covered four electromagnetic bands, namely, green (500-600nm), red (600-700nm), and near infrared (700-800nm, 800-1100nm).

The era of Thematic Mapper (TM) started with the launch of Landsat-4 in 1982. Comparing to MSS, the TM sensor was spatially and spectrally more capable, adding two critical spectra (i.e. shortwave infrared, and thermal infrared) at a 30-meter resolution. Landsat-5, launched in 1984, carried both MSS and TM, revolutionized Earth observation. Landsat-5 remained operational until 2011, ensuring a continuous time series despite the failure of Landsat-6 in 1993.

Landsat-7, carrying an Enhanced Thematic Mapper (ETM+), was launched in 1999 and continued imaging the Earth with the addition of a panchromatic band at a 15-meter spatial resolution that is finer than any other previous Landsat. Unfortunately from May 31 2003 onward, Landsat-7 suffered from a technical failure, causing approximately 22% per image area with no data collected. This issue was also known as the scanline off effect (SLC-off).

The Operational Land Imager (OLI) was introduced in 2013 with the launch of Landsat-8. The OLS added two more spectral bands, ultra blue for coastal application and another infrared band for cloud detection. At the same spatial and spectral resolution as the EMT+ sensor on Landsat-7, the addition of Landsat-8 continued the Landsat tradition, seamlessly collecting information all around the global.

Another turning point during the history of Landsat was the open-access policy implemented in 2008 when all existing and future Landsat data were made freely accessible to the general public (Wulder et al., 2008). The de-commercialization of Landsat data skyrocketed the number of Landsat images used in research worldwide, marking the transition between conventional scene-based processing to more pixel-based compositing approaches possible (Wulder et al., 2008).

This dissertation utilized data acquired from Landsat-5 TM and Landsat-7 TM/EMT+ from 1984 to 2013. Images captured using Landsat-1-3 were not considered due to limited spatial details and spectral bands. There was a distinct difference between algorithms used to process Landsat-8 images and Landsat-4–5 TM, and Landsat-7 ETM+ Surface Reflectance, known as the Landsat Ecosystem Disturbance Adaptive Processing System (LEADPS). However, LEADPS was not available at the time of commencing this project. Therefore, Landsat-8 data were not included in this dissertation.

2.3. DMSP-OLS nighttime lights time series

Originally designed as a meteorology sensor, the Operational Linescan System (OLS) initiate the acquisition of Nighttime lights (NTL), a collection of satellite images taken during the night. The earliest OLS flown by U.S. Air Force Meteorological Satellite Program (DMSP) started collecting data in the early 1970s. The DMSP satellites are orbiting in a near polar sun synchronous orbit with an altitude of approximately 830 km. Each satellite passes over any location on Earth twice a day, providing a complete global coverage in about six hours.

The Operational Linescan System (OLS) records images along a 3000 km scan, corresponding to a temperature range from 190 to 310 Kelvins in 256 equal intervals. Onboard calibration is performed in each scan. Final pixel values are shown as Digital Numbers (DN) rather than absolute values in Watts per m^2. A telescope pixel is approximately 500m at high resolution mode. The final product was distributed on a global latitude-longitude grid at a spatial resolution of 30 arcs second grid, approximately 1-km at the equator. Two composites were produced for years when data were acquired by two sensor spontaneously (Highlighted in Table 2.2).

Since 1992, the OLS data were archived and distributed digitally by the National Oceanic and Atmospheric Administration (NOAA) National Geophysical Data Center (NGDC). Compared to other remote sensing products such as Landsat, NTL is an exceptional geographic data that highlights human activities and reveals the “cultural footprint” of each individual settlement (Kyba et al., 2014). Artificial light during nighttime is undoubtable one of the most direct measurements of human activity available through remote sensing in a way that daylight data is not capable of (Kyba et al., 2014).

Shortly after its initial release in 1992, the DMSP-OLS has been collecting continuous images of the Earth at night for over 21 years, pushing remote sensing data into urbanization and socio-economic studies, a domain that was before dominated mostly by census data (Bennett & Smith, 2017). With its annual stable cloud-free composite of average brightness the flagship product, DMSP-OLS has been widely used proxy for variables that are difficult to assess and reproduce at a global scale, for example, economic activity, carbon emissions, poverty, impervious surface density, and energy and water use.

This dissertation utilized the DMSP version 4.0 stable lights time series which was pre-processed on an annual increment using methods described by Baugh, Elvidge, Ghosh, & Ziskin (2010), following a set of criteria (C. Elvidge, Hsu, Baugh, & Ghosh, 2014):

1. Center half of orbital swath for optimal image quality and reduced noise
2. No sunlight and moonlight present
3. No solar glare contamination
4. No cloud coverage
5. No auroral activities/emissions
6. Normal gain settings
7. No gas flaring contamination

Table 2.2 NTL DMSP-OLS Version 4 average visible stable cloud-free lights (Years highlighted contain data acquired by two sensors.

	Satellites					
Year	F10	F12	F14	F15	F16	F18
1992	F101992					
1993	F101993					
1994	**F101994**	**F121994**				
1995		F121995				
1996		F121996				
1997		**F121997**	**F141997**			
1998		**F121998**	**F141998**			
1999		**F121999**	**F141999**			
2000			**F142000**	**F152000**		
2001			**F142001**	**F152001**		
2002			**F142002**	**F152002**		
2003			**F142003**	**F152003**		
2004				**F152004**	**F162004**	
2005				**F152005**	**F162005**	
2006				**F152006**	**F162006**	
2007				**F152007**	**F162007**	
2008					F162008	
2009					F162009	
2010						F182010
2011						F182011
2012						F182012

2.4. Data overview

Landsat surface reflectance images were used throughout this dissertation. Particularly in Chapter 3 and 4, I utilized all surface reflectance data from 1984 to 2012 with less than 70% cloud cover. Chapter 5 used all images from DMSP-OLS version 4 images from 1992 to 2012. Images acquired by two sensors (Table 2.2) were all downloaded for calibration purposes. Chapter 6 used data from both Landsat and NTL time series. Thus, only images from 1992 and 2012 were used in Chapter 6 (Figure 2.2).

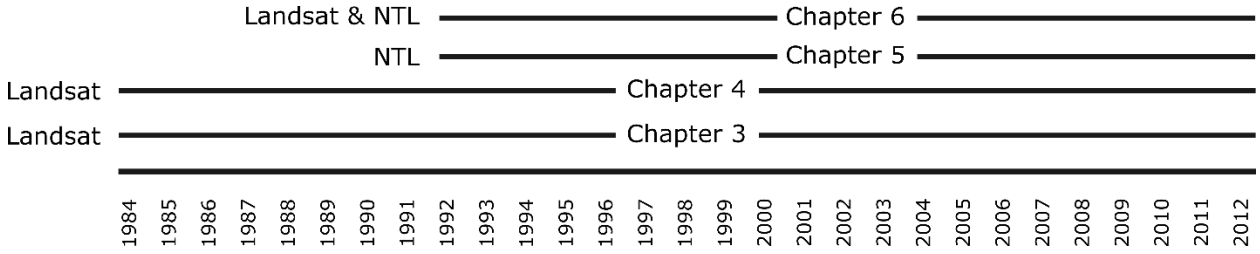

Figure 2.2 Time frame and sensors used for each research chapter.

Chapter 3

3. How can metrics derived from remotely sensed data inform environmental and socio-economic dynamics within and across cities in the pan Pacific region? Introduction

In the pan Pacific region, urbanization has become a major driver of local and regional development and is responsible for major vegetation loss from land clearing (Lo & Marcotullio, 2000b). Increasing numbers of people have migrated into urban environments over the last decade and by 2026 the urban growth rate is projected to exceed 50%, making the pan Pacific region the fastest urbanizing area in the world (UNESCAP, 2012). Large differences in socio-economic factors, such as population size and density, political system, and economic development cause the trend in mass migration to vary significantly among cities (Bagan & Yamagata, 2014). As a result, the urban environment is highly spatially complex, yet some common patterns exist (Marshall, 2013). Many cities are proximal to productive agricultural land and other natural assets such as forests and fresh water resources. Further outward from urban cores, cities often become less urbanized and more vegetated (Chen et al 2014), resulting in an inverse relationship between urban areas and vegetative conditions. As an urban area develops, outer rural areas often undergo more intense development and restructuring compared to urban core areas (Champion, 2001; Lo & Marcotullio, 2000a).

The concentric ring model has been a successful tool for investigating urban structure, even for cities with less regular concentric growth patterns (Dietzel, Herold, Hemphill, & Clarke, 2005; Handayani & Rudiarto, 2014). For cities located along coastlines or in mountainous areas, a concentric ring model can clearly differentiate the urban core from its more peripheral structures (Guérois & Pumain, 2008).

Detecting and analyzing the spatio-temporal dynamics of urban environments has, therefore, become an increasingly critical research topic with real management applications (Masek, Lindsay, & Goward, 2000; K. C. Seto & Fragkias, 2005; Sexton et al., 2013; X. Yang & Lo, 2002). A key element to developing an understanding of urbanization processes globally is the consistent monitoring of cities over space and time (Sexton et al., 2013). This complexity makes urban land monitoring a challenging task (Sexton et al., 2013). Remote sensing technology offers an exceptional resource that allows assessment of urban environments over time and space by collecting reflectance of urban land-cover characteristics (Masek et al., 2000; Woodcock et al., 2008). One common method of using remote

sensing in the urban environments is through land use classification (e.g., urban, vegetation, agriculture, etc.). However, the limitation of static categorical classifications is that they do not represent dynamics among different land-cover and land use types and therefore is insufficient for further statistical analysis given its categorical nature of measurement. Furthermore, categorical classification requires a set of pre-defined classes which might be incomparable for all selected cities.

An alternative method of monitoring urban environments using remote sensing is through spectral indices – numerical indicators primarily derived from spectral band combinations (Wentz et al., 2014). Spectral indices produce a continuous measurement of urban land-cover rather than classifying pixels into categorical classes (e.g. urban vs. non-urban; vegetation vs. non-vegetation). This minimizes the problems that arise from spectral mixing and inferential land-cover interpretation that result from the heterogeneity of urban environments (Barnsley & Barr, 1997; Wentz et al., 2014). Two common indices based on vegetation and urbanized area detection are, respectively, the Enhanced Vegetation Index (EVI) and the Normalized Built-up Index (NDBI), both of which have been used to assist in characterizing and quantifying vegetation condition and urbanization (Lyon, Yuan, Lunetta, & Elvidge, 1998; Varshney, 2013). (Huete, Jackson, & Post (1985) and Huete & Tucker (1991) suggested that EVI can be used as an alternative to other vegetation indices (e.g., Normalized Difference Vegetation Index) for minimizing the negative effects caused by canopy background and atmosphere interference, and thus enhance vegetation signals. Conversely, NDBI has been demonstrated to offer accurate and objective delineations of urban settlements (Zha et al., 2003). Combined, these two spectral indices provide a means to track the trends of urban and vegetation covers across cities over long time periods.

In general, for any land-cover observation and monitoring program, one of the most crucial components is a continuous archive of imagery (Wulder et al., 2008). However, the availability of cloud- and haze-free images relies heavily on variable local weather conditions and as a result regional investigations over long time periods at moderate spatial resolutions (i.e., 30m) are still rare. Data gaps are common for a given pixel in any particular year, which may limit the utility of images given most existing image processing algorithms (Hermosilla, Wulder, White, Coops, & Hobart, 2015). Thus, data gaps contribute to lost information for long term urban land-cover monitoring projects. Pixel-based compositing provides a solution to long term, seamless land monitoring challenges and enables a new paradigm of Earth observation programs due to the freely accessible Landsat image archive (White et al., 2014). These new compositing methods take full advantage of multiple decades of Landsat imagery

and are able to detect and in-fill missing pixel reflectance values based on the entire temporal trajectory of any given pixel (Hermosilla et al., 2015).

In this chapter I utilized a relatively simple urban expansion morphological model to compare and contrast a dense time series of moderate spatial resolution imagery and assess how urban and vegetation vary at regional scales in time and space. To do so annual gap-free Landsat imagery were created from 1984 - 2012 of 25 cities across 12 countries in the pan Pacific region. Two spectral indices—Enhanced Vegetation Index and Normalized Difference Built-up Index—were calculated at an annual basis and resampled using a hexagon-based ring model for all urban environments. Trajectories of the two spectral indices were then analyzed based on dynamic time warping and K-means clustering analysis to investigate intra- and inter-urban variations over time and space.

3.1. Materials and methods

This chapter used imagery from the entire Landsat Thematic Mapper (TM) Landsat Enhanced Thematic Mapper Plus (ETM+) archive from 1984 - 2012 (section 2.2) using a pixel-based compositing method (section 3.2.1) to generate annual gap-free image composites for 25 selected cities. I used previously defined Global Administrative Areas (GADM version 2.0, Areas, 2012) with a hexagon based ring model to assess urban vegetation and urban built-up conditions within each city (section 2.4) using a mask image to minimize seasonal variations and exclude water and snow cover from any subsequent analysis (section 2.5). I then clustered the performance of each urban environment based on its temporal and spatial characteristics (section 2.6) to allow inter- and intra city comparisons.

3.1.1. Landsat surface reflectance product

Surface reflectance images (L1T), including Landsat Thematic Mapper (TM) and Landsat Enhanced Thematic Mapper Plus (ETM+), were acquired for each urban environment through the United States Geological Survey (http://espa.cr.usgs.gov). I downloaded images with less than 70% cloud cover that were acquired within a specific temporal window, from May 1st to September 30th of the years 1985 to 2012. As I focused on differentiating urban land-cover from vegetation, winter imagery in Australia was more suitable given the high curing rate of vegetation and grasses in Australian urban areas in summer

(Keast, 2013). With mild winter temperature (Keast, 2013), and with much less deciduous vegetation in winter with no snow, vegetation is often very green in winter and in fact produces a much greater contrast with urban features than in summer. As a result, I applied the same uniform temporal window to Melbourne and Sydney as all other cities. Candidate images were all pre-processed using a mask function (Fmask) (Zhu & Woodcock, 2012) and the Landsat Ecosystem Disturbance Adaptive System (LEDAPS; Schmidt, Jenkerson, Masek, Vermote, & Gao, 2013).

Given the wide temporal window used for image selection, seasonal spectral variation due to agriculture practices can confuse the spectral indices (Hill & Donald, 2003). To minimize the impact caused by climate and phenological variations at each urban location, an agricultural mask was generated using a simple random forest classification. To do so the variables including the average, maximum, minimum, and standard deviation of the two spectral indices from 2008 – 2012 were used on the assumption that if a pixel was identified as agriculture in the last five-year period, it would likely to have been agriculture or non-urban land-cover in the earlier years. Training sites of agriculture, forest, and impervious surface were identified from the available Google Earth imagery.

3.1.2. Pixel-based image compositing

The best available pixel (BAP) approach was used to produce image composites to mitigate data gaps in the time series caused by cloud, cloud shadow, or haze. BAP scored every pixel using multiple Landsat images based on the following criteria: sensor, day-of-year, atmospheric opacity, and proximity to cloud or cloud shadow using the same criteria as White et al., (2014). Pixels identified by the Fmask algorithm (Zhu & Woodcock, 2012) as cloud or cloud shadows were masked from the composites. Additionally, a 50 pixel buffer was applied around clouds and cloud shadows to reduce misclassification errors (Griffiths et al., 2010). The Thematic Mapper (TM) sensor was scored higher than the Enhanced Thematic Mapper Plus (ETM+) sensor after 2003 to reduce the influence of the scan-line corrector malfunction. Day-of-year was scored according to a Gaussian function with a maximum score equivalent to the middle day-of-year of the temporal window. Pixels with atmospheric opacity higher than 10% were scored lower to avoid the selection of hazy observations. The pixels with the highest scores based on these criteria were then composited into annual images that were used in the disturbance mapping process (White et al., 2014). Finally, any remaining data gaps were infilled using linear interpolation of the values on the spectral trends. Two spectral indices, the EVI and NDBI, were calculated to assess urbanization and

vegetation changes (Equations 1 and 2). Urbanization and vegetation dynamics were then assessed by analyzing the temporal trajectories from 1985 – 2012 of a given spectral index (i.e. EVI or NDBI).

$$\mathrm{EVI} = 2.5 \times \frac{\mathrm{NIR} - \mathrm{Red}}{\mathrm{NIR} + 6\times\mathrm{Red} - 7.5\times\mathrm{Blue} + 1} \qquad Equation\ 1$$

$$\mathrm{NDBI} = \frac{\mathrm{SNIR} - \mathrm{NIR}}{\mathrm{SNIR} + \mathrm{NIR}} \qquad Equation\ 2$$

3.1.3. Concentric ring model

I used the Global Administrative Areas (GADM version 2.0, Areas, 2012) to define administrative borders (GADM version 2.0, Areas, 2012), which has also been used by a number of regional and global geospatial urban studies (Gaston, Duffy, & Bennie, 2015; Hawelka et al., 2014). Conventional urban ring models developed to monitor urban development often utilize absolute distances to define ring widths, and therefore cities with more variable forms and sizes can confound effective comparisons and cross-analysis. Given I am considering multiple cities, the distance between concentric rings was normalized to produce a normalized distance index (NDI) which represents how close a particular pixel is to the urban center (Equation 3). To produce general trends, and reduce high frequency noise, the indices were then summarised within a hexagon-based (~1km^2) concentric ring model which divides each urban environment into a lattice of rings which were defined using a normalized distance index (Figure 3.1). The distance of each hexagon to the urban centre is normalized to values between 0 (urban core) and 1 (urban edge). The central hexagon representing the urban core for each individual urban environment was located at the central business districts (CBD). Temporally, to simplify the subsequent statistical analysis and minimize the impact of any proxy outliers, I produced epoch images, which were five-year averaged image composite. Epoch images were then used in the clustering analysis.

$$\text{Normalized Distance Index (NDI)} = \sum_{i}^{\#\ of\ hexagons} \frac{d_i}{d_{max}} \qquad Equation\ 3$$

where $d = \sqrt{(x_m - x_n)^2 + (y_m - y_n)^2}$

$X_{m/n}$ is the x coordinate of hexagon m/n

$Y_{m/n}$ is the y coordinate of hexagon m/n

d_i is the distance between hexagon i to the central hexagon

d_{max} is the greatest distance among all hexagons

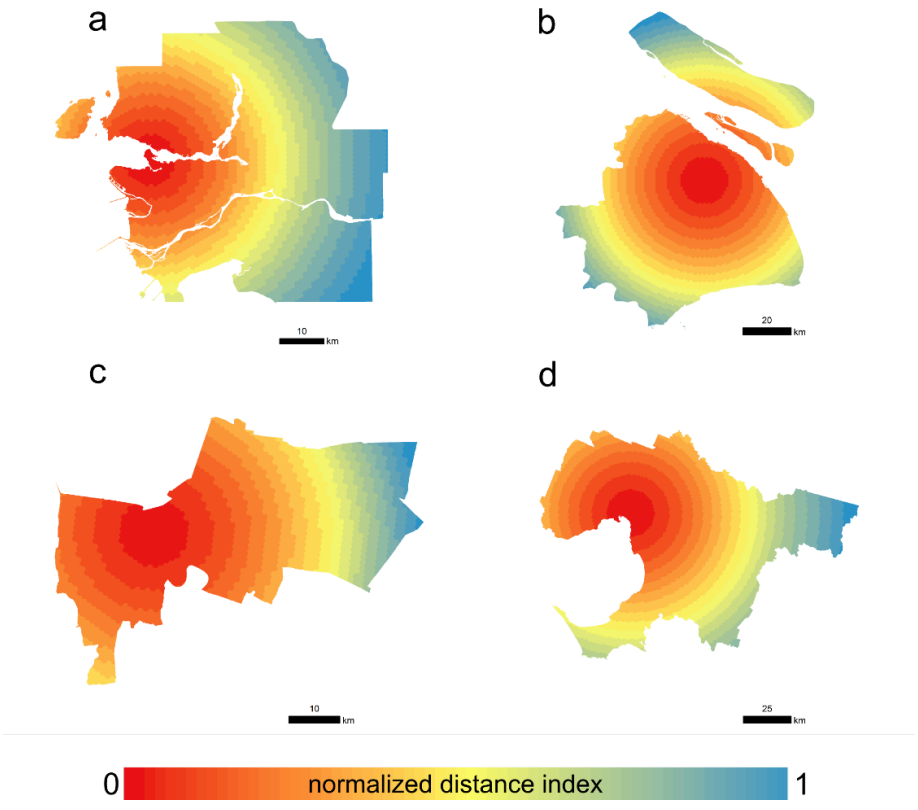

Figure 3.1 Examples of a hexagon based ring model; (a) Vancouver, Canada; (b) Shanghai, China; (c) Bangkok, Thailand; (d) Melbourne, Australia.

3.1.4. Dynamic time warping and cluster analysis

Once spectral trajectories of EVI and NDBI from 1985 – 2012 were developed, cities were clustered based on either the temporal changes or the spatial distribution of urban vegetation and urban built-ups using Dynamic time warping and K-means cluster analysis.

Dynamic time warping (DTW) is an approach originally developed to deal with sequential data was used to compare each epoch. DTW has been widely used in voice recognition (Müller 2007), pattern matching (Rath & Manmatha, 2003), and time series analysis (Bemdt & Clifford, 1994; Keogh & Ratanamahatana, 2005). Specifically, DTW identified the optimal alignment between two temporal sequences that may vary in time or rate (Bemdt & Clifford, 1994; Salvador & Chan, 2007). Although the approach was developed for time-dependent sequences, it could also be used to examine trends in any data stream presented as a linear sequence (Giorgino, 2009), such as in this case where trajectories along a distance index were compared. The approach computed the similarity of spectral indices through time by calculating the difference in the index between each epoch pair for each hexagon-based concentric ring from the centre to the edge of the urban environment.

The mean of the differences was then compared to contrast cities. Cities with similar trajectories through time were expected to have minimal differences and thus a low overall mean across the epochs. In contrast, if a city has been changing markedly the mean differences would appear greater. The magnitude of EVI and NDBI were also used to assess and compare the vegetation and urban dynamics, with an urban environment with more vegetation cover having a greater EVI and lower NDBI. In general, cities that were undergoing more rapid development were expected to have a greater NDBI and lower EVI.

Once temporal and spatial change were captured, a K-means cluster methodology was used to group the mean and standard deviations of the difference curves for both EVI and NDBI as well as the absolute spectral values across cities. I selected the k value based on the highest silhouette widths by iterating a K-means clustering analysis 25 times using k from 1 to 25.

I then applied K-means clustering four times using the four sets of variables representing the spatial and temporal changes of vegetation and urban conditions. The silhouette width provided an indication of the accuracy of the classification for each individual urban environment and was used to assess the

clustering performance (Bolshakova & Azuaje, 2003). As silhouette widths approached 1, it was indicative of a strong likelihood a given urban environment was assigned to the correct cluster (Bolshakova & Azuaje, 2003; Rousseeuw, 1987). I also computed the ratio of between (BSS) to total sum of square (TSS) to evaluate the K-means classifications, where BSS was the sum of squared distances per group means while TSS was the sum of squared distances to the global means.

All image processing in this paper was done in IDL 8.3, ENVI 5.2, and ArcMap 10.2.2 and statistical analysis in R 3.1.1 using the Cluster package (Maechler, Rousseeuw, Struyf, Hubert, & Hornik, 2012), and the DTW package (Giorgino, 2009).

3.2. Results

3.2.1. Spectral indices

Figure 3.2 demonstrated the hexagon based rings for four example cities' spatial distribution of vegetation (colored in green) and urban conditions (coloured in red). A high EVI value was indicative of marked vegetated cover whereas NDBI corresponded to greater urban expansion and/or urban densification. In general, EVI and NDBI showed contrasting patterns with urban cores having a much higher NDBI and lower EVI values than the outer areas.

As expected, regardless of the magnitude of the EVI and NDBI, all cities had undergone expansions and/or densifications over the epochs but at varying rates. For example, cities such as Vancouver and Melbourne experienced less urban expansion than Shanghai and Manila where EVI experienced a sustained reduction. Likewise, cities where substantial vegetation loss were observed to have a marked increase in the NDBI. Small satellite settlements around urban centers could also be detected in the epoch images, such as in Shanghai at epochs 3 and 4, which showed a number of small "cities" developing around the urban core.

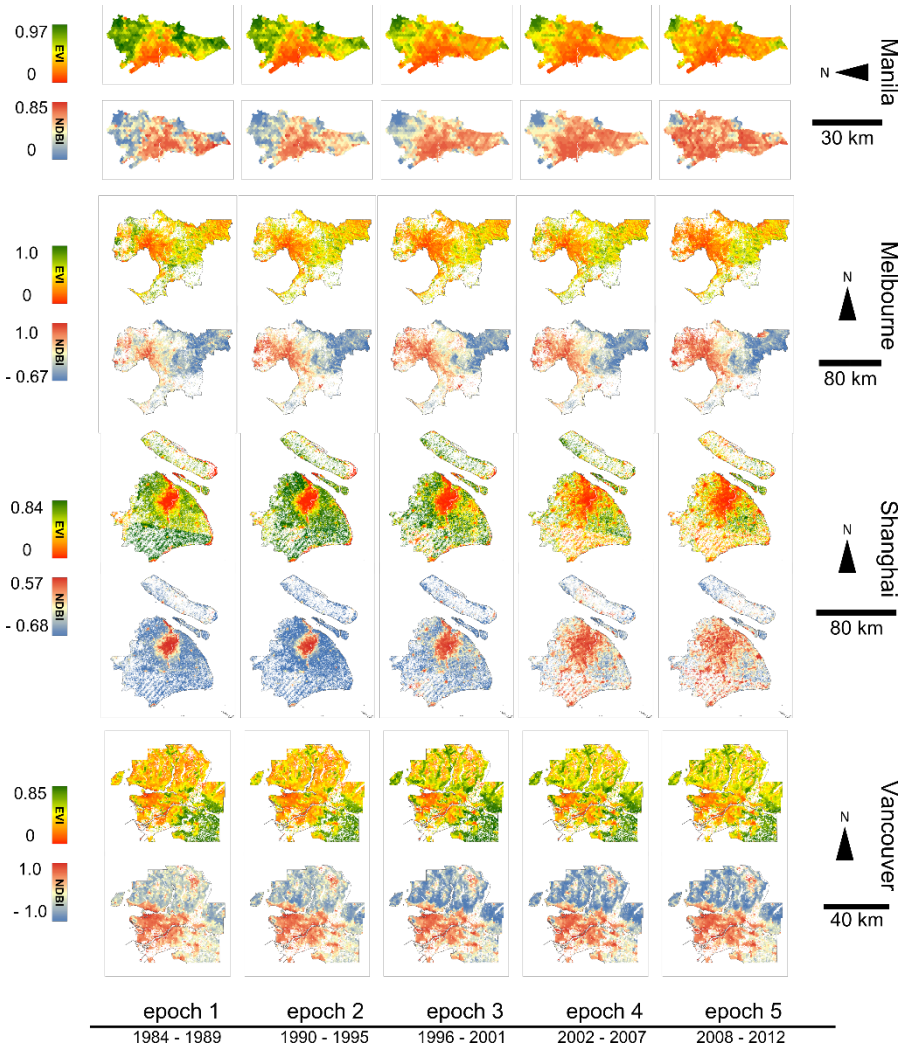

Figure 3.2 Temporal changes of EVI and NDBI of four studied urban environments.

Figure 3.3 showed that spatially consistent across all urban environments outer areas generally experienced the highest EVI value and the lowest NDBI value. Despite the varying differences among each trajectory, EVI values tended to decrease as the distance index increases from the urban center. A similar pattern can also be observed as NDBI decreases when moving towards outer area of the urban environment. However, exceptions can be found in cities such as Melbourne where the highest EVI value was located in the transition area between inner and outer urban areas.

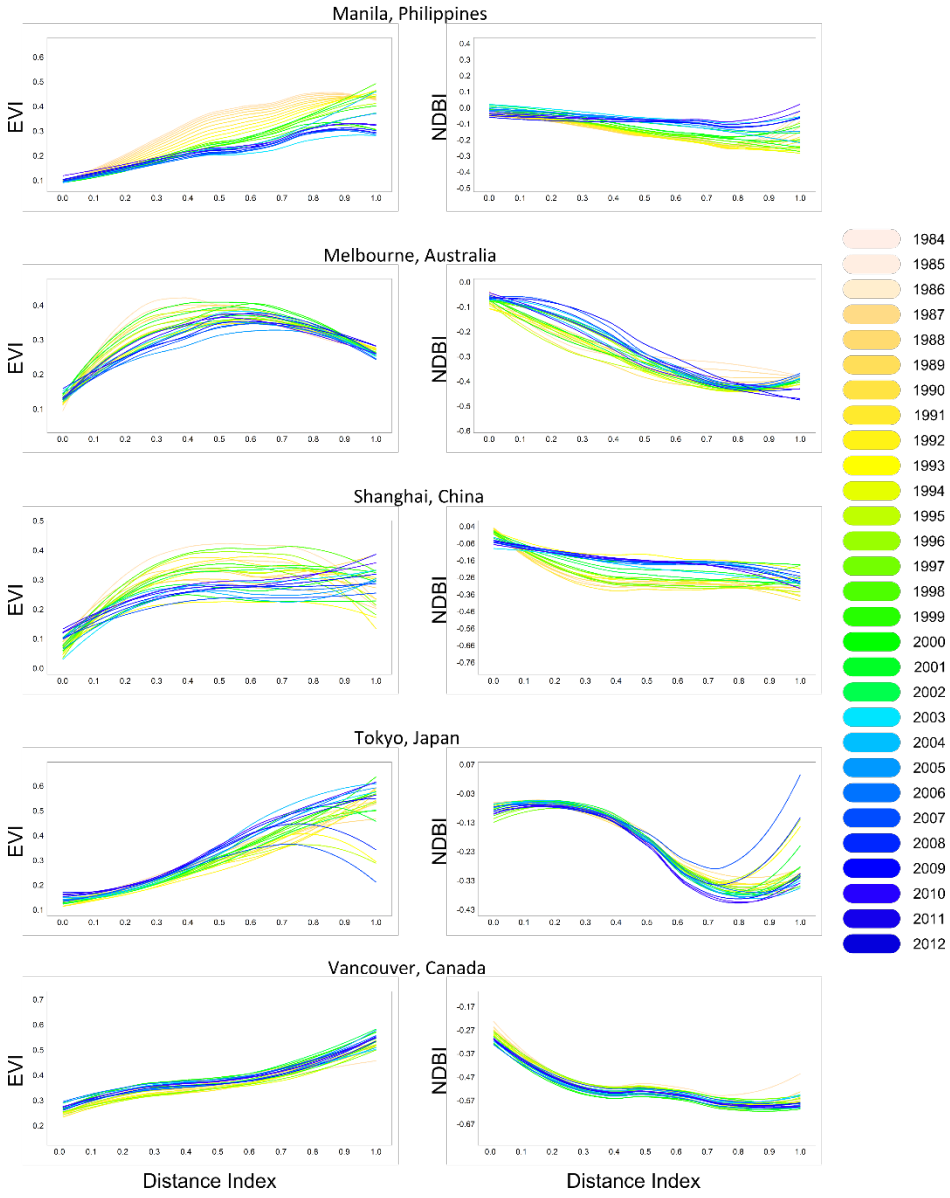

Figure 3.3 Example annual spectral trajectories of EVI (left column) and NDBI (right column). See Appendix 1 for all 25 cities.

Temporally, Figure 3.3 also demonstrated the overall change rates by comparing the differences between each temporal trajectory. For a given urban environment, a greater distance between trajectories was expected when there was a marked change in EVI and/or NDBI values. For example, Manila had much more notable EVI decrease and NDBI increase comparing to cities like Tokyo and Vancouver. Combined with the distance index, Figure 3.3 illustrated where and how rapidly different urban environments changed over time. For example, Melbourne and Shanghai experienced more changes in the transition areas than the centers and edges of the urban environments.

3.2.2. Dynamic time warping and cluster analysis

Figure 3.4 showed the spatial distribution of vegetation and urban built-up represented by their separability as derived from DTW analysis across all urban environments. Greater separability values were indicative of more different trajectory shapes hence dissimilar vegetation or urban spatial distribution. Overall, the results suggested that the separability was more apparent for the EVI trajectory than for NDBI as indicated by a slightly higher average separability of EVI (0.36). As DTW estimated the separability using only the spatial information which incorporated the absolute EVI and NDBI values for each of the concentric rings, Figure 3.4 highlighted urban environments that experienced a relatively unusual spatial distribution of vegetation and/or urban patterns. For example, Phoenix (phx) had a large separability in EVI compared to the other urban environments while Vancouver had an overall higher separability in terms of NDBI.

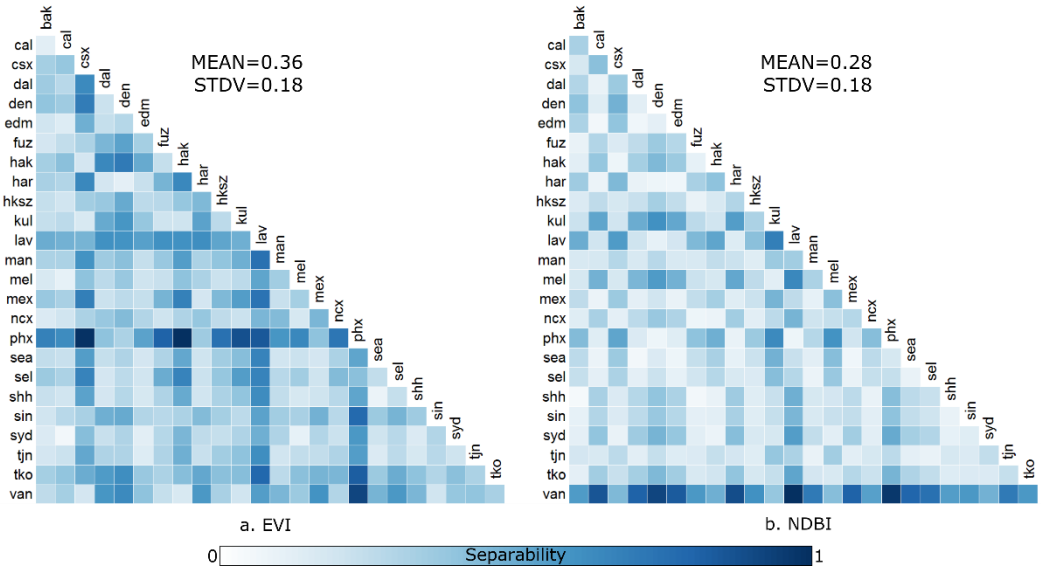

Figure 3.4 Separability metrics estimated by DTW for a. EVI and b. NDBI.

A K-means clustering analysis was then applied to group spatially similar urban environments. A K value (i.e. number of clusters) will be favored if it generated greater silhouette width (i.e. closer to 1) and a meaningful clustering analysis (i.e. k < 15). The results indicated 5 optimum clusters resulted in the highest silhouette width. The averaged trajectory of each cluster is shown in Figure 3.5 for both EVI and NDBI. Results show variations in EVI and NDBI values for each of the clusters. Cluster 5 showed the highest EVI and the lowest NDBI in the urban centre, suggesting a relatively greener and less urbanized environment core than other groups. Cluster 2 and 4 showed a much lower EVI and higher NDBI, indicating more developed and less vegetative urban environments. Interestingly, although cluster 3 had an overall higher EVI than cluster 1, 2, and 4, it also had a greater NDBI index, particularly in the sub-urban areas.

Figure 3.5 summarized the temporal changes for each epoch periods. Temporal changes were represented by DTW derived distances between pairs of epoch trajectories. Urban environments were ordered based on their averaged temporal changes (e.g. distances) between trajectories as shown in the last columns in Figure 3.5. Although the absolute order varied when comparing EVI or NDBI changes, more developed urban environments such as Vancouver (van), Seattle (sea), and Phoenix (phx) tended to have less temporal changes of both EVI and NDBI as indicated by relatively small distances between epoch trajectories. Urban environments located in less developed regions such South and South-east Asia tended to experience more temporal changes with varying change magnitudes over different epoch periods. For example, Dalian (dal) showed marked temporal changes of both EVI and NDBI. Nanchang

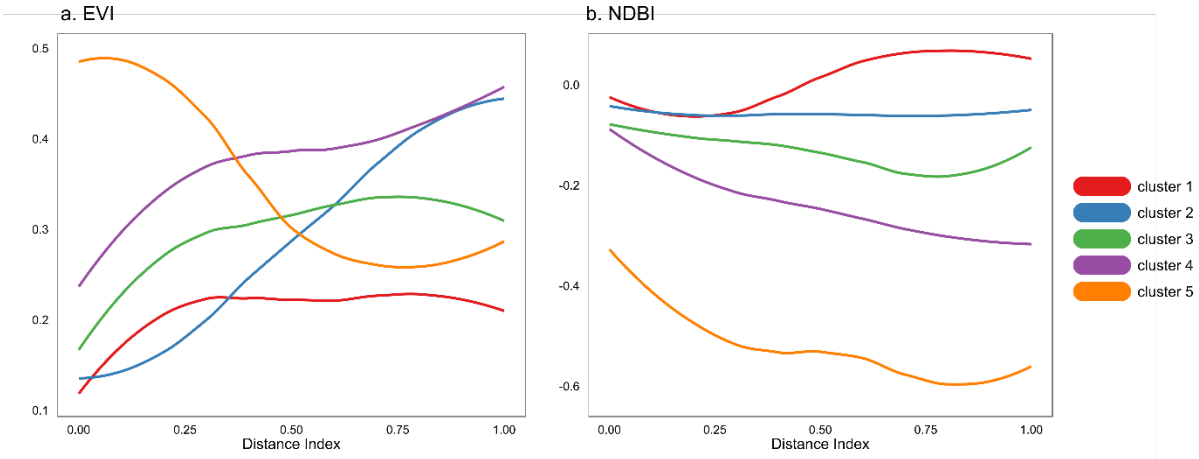

Figure 3.5 Average trajectories of a. EVI and b. NDBI for each cluster.

(ncx) showed more notable changes of EVI between epoch 1 and 2 and less change in NDBI. Interestingly, urban environments such Las Vegas experienced a relatively great temporal change of EVI yet remained constantly low in NDBI changes suggesting a marked change of vegetation and a constant stable trend in urban.

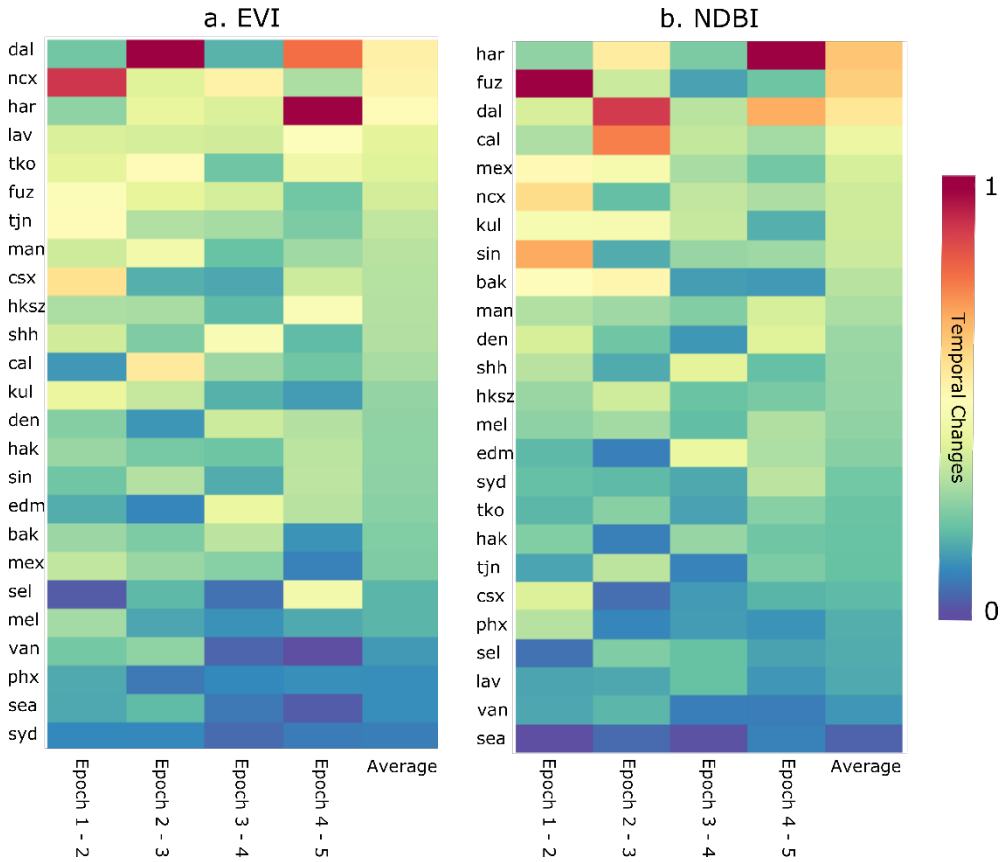

Figure 3.6 Temporal change metrics of a. EVI and b. NDBI.

A K-means clustering analysis was also applied to group temporally similar urban environments. Combined with the cluster results from Figure 3.5, the final results of K-means clustering were summarized in Figure 3.7 using the silhouette width of each individual urban environment. The average silhouette width ranged from 0.37 to 0.60, and the ratio of the between to the total sum of square (BSS/TSS) ranged from 69% to 92% (Table 3.1). Overall, using temporal changes in NDBI and EVI offered higher silhouette width and BSS/TSS ratio than spatial separability.

Table 3.1 Cluster analysis summary

	BSS/TSS ratio		**Silhouette width**	
	EVI	NDBI	EVI	NDBI
Spatial distribution	68.8%	89.2%	0.37	0.48
Temporal changes	91%	92.3%	0.60	0.50

Silhouette width of each individual urban environment indicated how well an urban environment fits its cluster (Figure 3.7). Urban environments with low silhouette width were likely to be assigned to the

incorrect cluster. Low silhouette widths were therefore useful as a measure of uniqueness of a given urban environment. For example Melbourne and Calgary had low silhouette width (< 0.1) and therefore had limited similarity in terms of spatial distribution of vegetation (Figure 3.7a). Dalian and Phoenix were also relatively unique in terms of their spatial distribution of urban vegetation and built-ups (Figure 3.7b). Temporal changes yielded slightly better overall clustering results with a number of urban environments such as Kuala Lumpur and Phoenix having a low silhouette width (Figure 3.7c-d).

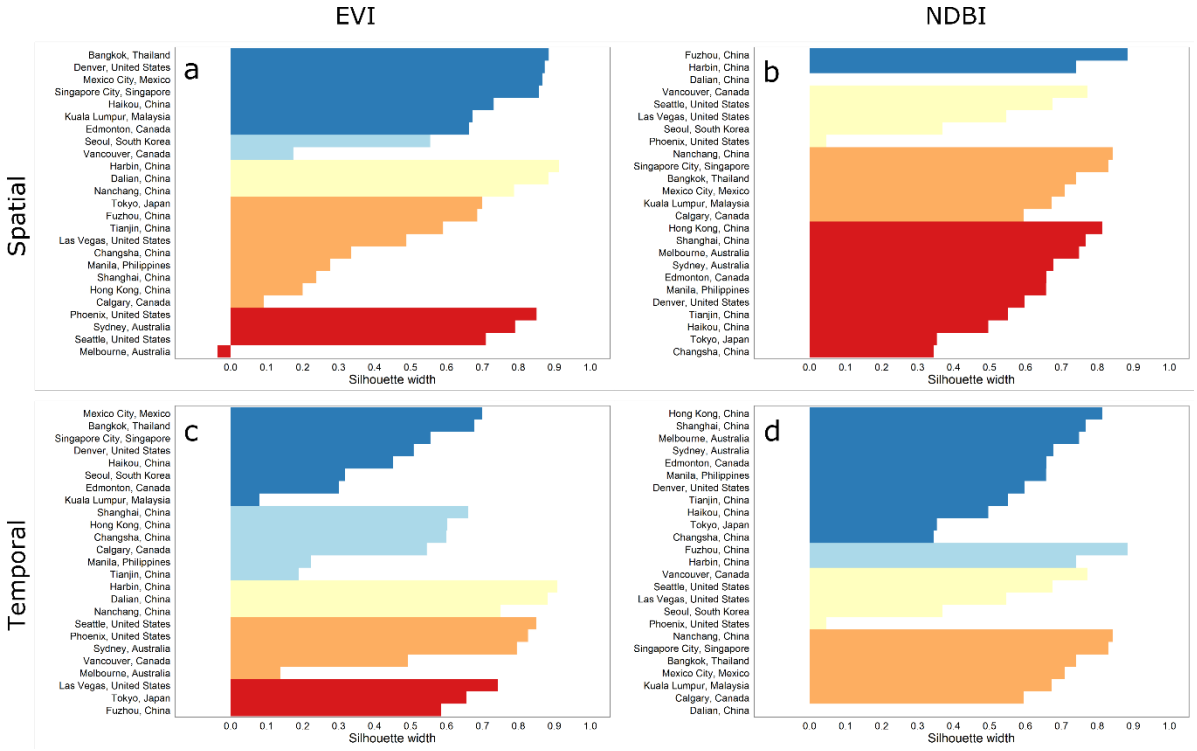

Figure 3.7 Silhouette width based on a. temporal vegetation changes, b. temporal built-up changes, c. spatial vegetation patterns, and d. spatial built-up patterns (groups are identified by colors).

Figure 3.8 summarized the degree of similarity both spatially and temporally across urban environments in the pan Pacific region. A likely strong connection (e.g., thicker lines in Figure 3.8) between two urban environments represented high spatio-temporal similarity. In total, there were three pairs of urban environments that were consistently being grouped together—Melbourne and Sydney; Tianjin with Manila; and Singapore City with Kuala Lumpur. In contract, cities such as Las Vegas and Vancouver demonstrated less similar features both spatially and temporally with any of the other urban environments.

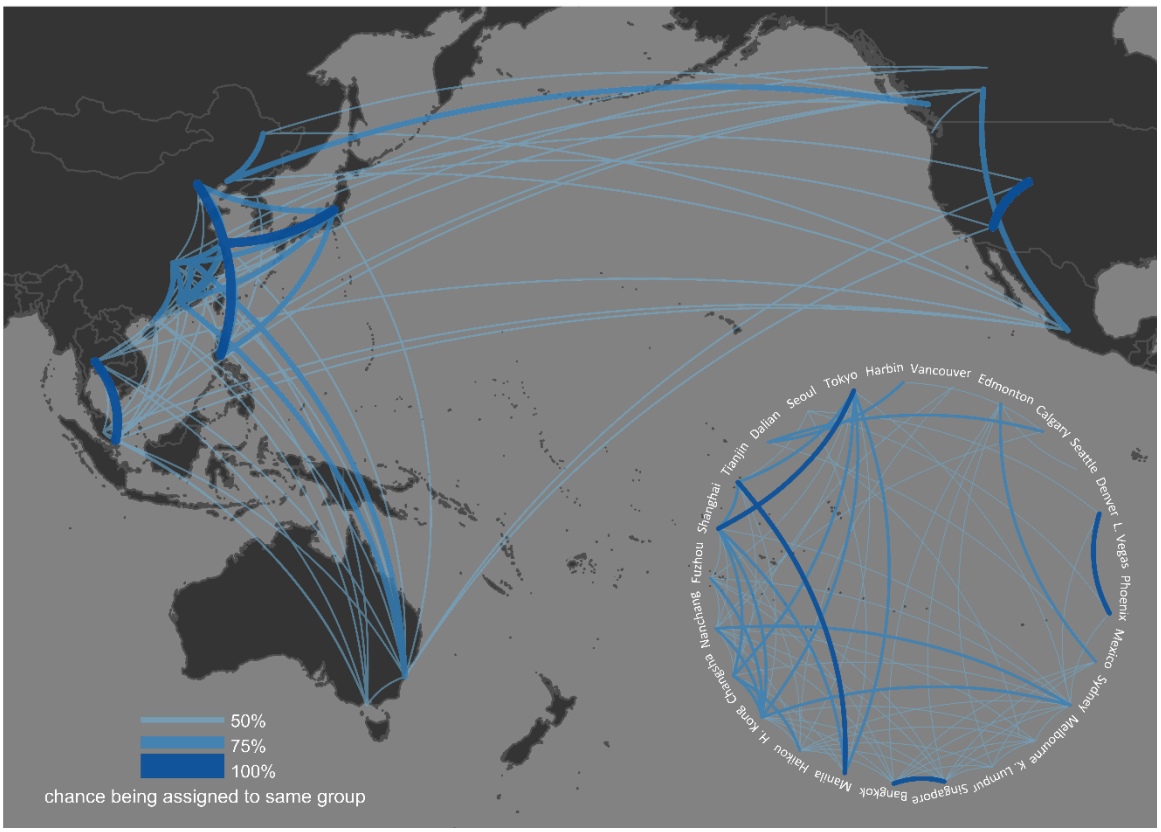

Figure 3.8 Number of times cities were grouped together during K-means classification based upon spatial and temporal variables. Number of groupings ranged from 2 to 4.

3.3. Discussion

3.3.1. Urbanization patterns in pan Pacific cities

This chapter integrated a hexagon based ring model with the pixel-based image compositing to investigate spatio-temporal changes of vegetation and urban built-up among 25 cities across the pan Pacific region. As anticipated, the majority of the cities in developing countries observed marked development rates compared to the urban environments in more developed regions. Still, exceptions existed where urban environments that were not geographically proximal could also be similar in terms of the vegetation and urban dynamics over time and space. This was likely due to the highly concentrated early urbanization of large cities in some of the developing nations, such as Hong Kong, Bangkok, and Shanghai, which may resemble the urbanization patterns of cities in a more developed regions (Henderson, Yeh, Gong, Elvidge, & Baugh, 2003). I concluded with a simple model which

generalizes the urbanization process as starting as a centralized landscape, then expanding radially (Figure 3.9). More mature urban environments, such as Vancouver, Melbourne, and Tokyo tended to decentralize over time, characterizing an evenly spread spatial pattern with less visible urban cores (e.g., Figure 3.8, Melbourne and Vancouver). A similar trend occurred on less developed urban environments where small and medium sized settlements started blending into each other, forming a more decentralized urban environment, such as Shanghai. Interestingly, although the trend seemed to be highly similar across majority of the urban environments, the time required to reach a similar level of urbanization magnitude was much shorter for developing than developed urban.

Remote sensing based assessment of urban environments also reflected some of the socio-economic pressures, particularly for cities that have undergone substantial development over the past few decades. For example, the population of Shanghai has a 95% growth rate with a population increase from 11.8 million to over 23.0 million since the 1980s (World Population Statistics, 2013). To accommodate such a massive population growth, as shown in Figure 3.9, Shanghai has massively expanded and already started decentralizing and in-filling gaps between the pre-existing urban core and the surrounded settlements. During the studied period of this work (i.e. 1984-2012), the population of greater Vancouver has only increased from 1.4 million to 2.3 million, which is about 48% slower than Shanghai (BC Statistics, 2012).

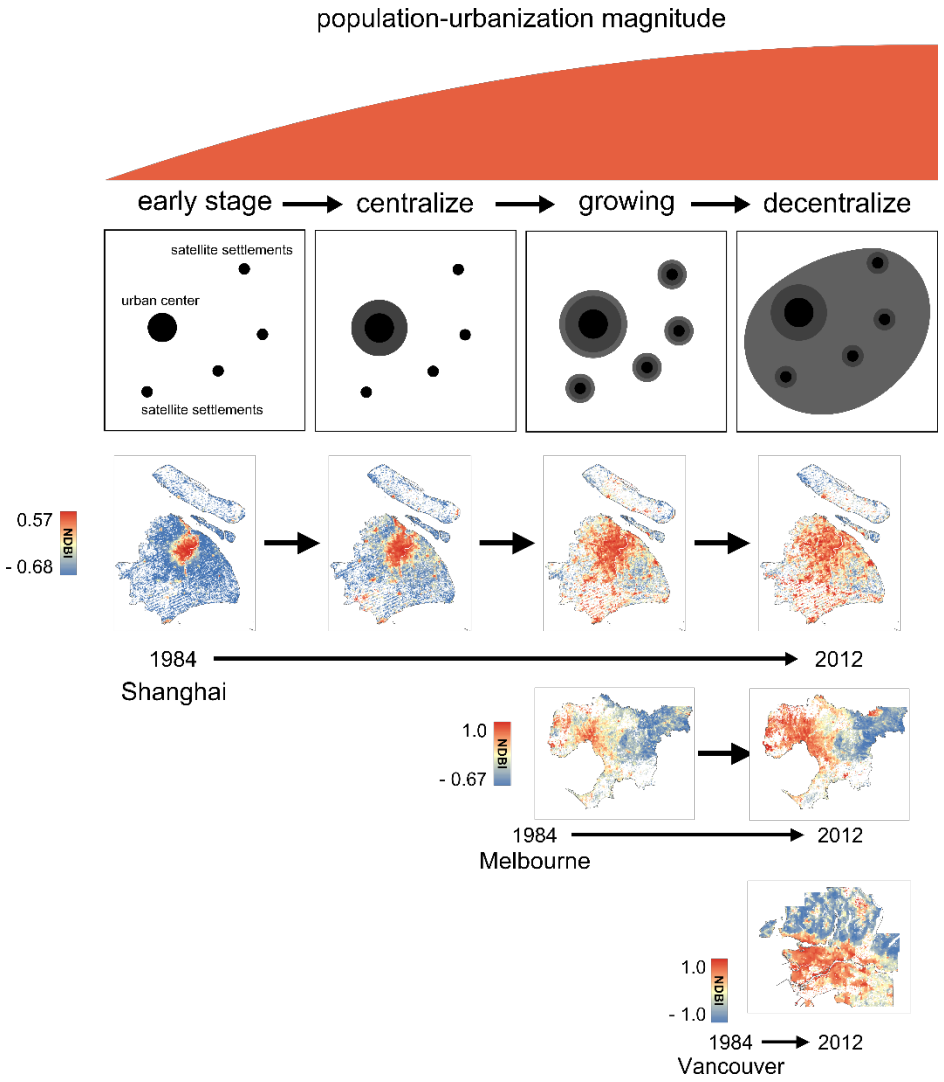

Figure 3.9 A conceptual representation of urbanization.

The uneven development rates were likely due to a number of geographical factors including the current urban areal extent, political system, and urban population distribution (Birch & Wachter, 2011). In addition, the historical development of each urban environment was also a critical variable. Regions such as North America and Australia were generally developed much earlier than urban environments in less developed countries and therefore were likely to be saturated and more stable in terms of urban expansion and vegetation conditions. Since all images were acquired after the mid-1980s, it was difficult to show patterns of urbanization in these developed regions.

An uneven developing rate could also be found among different sections (i.e. concentric rings) within the urban environments, suggesting an intra-urban developing variation. Understanding intra- urban variation is critical for urban planners to accomplish a balanced and sustainable urban development. By 2050, if all cities doubled their size, roughly 10 to 15% of the productive agricultural land would be converted into concrete to house the rapidly growing population (Birch & Wachter, 2011). Such a trend poses a major threat to sub-urban environments around agricultural and farm land as well as water pollution. Therefore quantitative information is needed for sustainable urban planning, crafting local developing polices, and setting land use priority to optimize both urban development and resources allocation.

3.3.2. Urban densification and expansion

However, urbanization is not only occurring in the form of physical expansion, but also densification. In most cases, expansion is occurring in rural or sub-urban areas, while intensification can often be seen in existing urban areas as well as the transition zones between urban core and urban edge. Maps are needed that are capable of representing urban land extent (i.e. expansion) as well as measuring the intensity of changes in both pre-existing and newly developed urban environments. Although mapping of the urban environments has been undertaken through a variety of perspectives and models, such as urban land-cover classification, urban population, urban heat island effect, etc., I chose an alternative method using urban and vegetation metrics, using two distinct features of the urban environment. Spectral indices (i.e., EVI and NDBI) avoid using hard land-cover classifications, and offer quantitative insights into the physical changes of the urban environments. Another key benefit of spectral indices over hard classifications is that a continuous numeric measurement provides more options for further statistical analysis which can help better reveal the relationships and patterns in a dataset.

Relatively small urban areas, in particular those in less developed countries, are often the subject of less research interest than larger urban environments and therefore have been often overlooked in many studies. Previous studies have indicated that about 2/3 of urban residents live in cities of less than 1 million people (Clancey, 2004). Even in United States, where almost 45 million people live in cities with a population of over 250,000, and another 40 million live in places of between 50,000 and 250,000 (Clancey, 2004). Assess changes in these urban environments using remote sensing offers a way to provide data to urban planners for closer examination of the dynamics in these urban areas. By including these smaller urban environments in this paper enables us to provide a more comprehensive picture of urbanization in the pan Pacific region.

This chapter used the traditional concentric ring model to quantify and compare vegetation and urban dynamics within and among different urban environments. Each urban environment was assigned with a single urban core, which is a monocentric model. Although polycentric or multi-nuclei models suggest that modern urban environments are likely to have more than one functional urban core, in this research I believe that using a single urban core was sufficient for meeting our key objective of analyzing changes to urban and vegetation cover over long time periods. First, although the concentric ring model assigns a single core to each urban environment, I are still able to quantify intra-urban growth by using the Normalized Distance Index (NDI). The NDI not only allows us to compare urban environment with varying physical sizes, it also provided a sense of urban development in the surrounding satellite settlements. For example, a decreasing EVI and increasing NDBI will likely to occur near NDI=0.5 which indicate some degree of development in the outer areas. Secondly, the major CBD is more likely to be the most developed area of an urban environment even in a multi-nuclei spatial organization (Wheaton 2004). Lastly, given the wide spectrum of urban environments I studied in this work, some less developed urban environments (e.g. Fuzhou and Nanchang) are still highly concentric and yet have not clearly shown evidences of forming additional urban cores. Thus, I decided to apply the concentric ring model with one major urban core.

In this chapter, I focused on examining the overall trends in vegetation and urban built up than the actual timing of the change. Using a combination of epoch images and linear interpolation was sufficient to capture overall EVI and NDBI trends over the study period. Secondly, image quality and availability varied dramatically across the globe (Wulder et al., 2015). The purpose of using epoch images and linear interpolation was to essentially further reduce unnecessary noises and outliers while still retain the trend of land-cover changes.

Yet, there were two key caveats to be addressed in the next chapter. Firstly, spectral saturation is known to cause inaccurate descriptions of urban vegetation (Van Der Meer & De Jong, 2000). Studies have proven the superiority of spectral unmixing compared to spectral indices for quantitatively estimating vegetation (Elmore, Mustard, Manning, & Lobell, 2000; Hostert, Röder, & Hill, 2003). Vegetation estimated from spectral indices is not compatible particularly across a heterogeneous region such as an urbanized environment (C. D. Elvidge & Lyon, 1985; Huete et al., 1985; Huete & Tucker, 1991; Major, Baret, & Guyot, 1990; Todd & Hoffer, 1998). Additionally, many spectral indices derived from multispectral images (e.g. NDVI, EVI, and NDBI) are typically constrained to two or three spectral bands, leaving other spectral information under utilized (Lyon et al., 1998). In this chapter, certain land-cover types such as snow and ice also showed similar EVI and NDBI values to urban dominated pixels. Thus, by spectrally unmixing vegetation the influence of these other land-cover types is minimised. Since EVI and NDBI both use the Near Infrared part of the spectra, information overlapping and redundancy might be expected when comparing EVI directly against NDBI.

In Chapter 4, an alternative approach, Spectral Mixture Analysis (SMA) was used to spectrally unmix each pixel using a linear unmixing algorithm. A vegetation fraction value (VF) was then derived to represent how vegetated each pixel is relative to the most spectrally pure pixel (i.e. endmember) within each city over the study period.

Chapter 4

4. How to can urban vegetation be mapped at the sub-pixel scale?

4.1. Introduction

In the previous chapter, I discussed the benefit of using remote sensing to chronologically monitor urbanization in terms of urban expansion and urban densification (Chapter 3, Section 3.4.2). In this chapter, I focus on investigating an alternative approach to measure temporal change in vegetation using spectral unmixing analysis and a Theil-Sen slope estimator. The combination of these two processing techniques aims to minimize the possible saturation issues from spectral indices (e.g. EVI in Chapter 3) and data outliers.

Urbanization can be defined as a gradual land-cover change in the form of urban sprawl and densification (Sexton et al., 2013). Urban sprawl, or urban expansion is the physical growth of a city, primarily through conversion from non-urban land-cover (e.g. vegetation) to the presence of urban land-cover (e.g. impervious surfaces). Urban densification most often occurs adjacent to existing urban areas where the natural land-cover has already been disturbed to some extent. The interplay between urban sprawl and densification is consistently re-shaping the local geometric and ecological properties of urban environments, increasing the density of anthropogenic infrastructure while replacing local vegetation, interrupting micro climate, habitat loss, energy fluxes, and modifying the water and carbon cycles (Groffman et al., 2014; Kahn, 2000; Ziter, 2016). Previous studies have suggested that urbanization has a direct association with a series of environmental issues, such as urban heat island (UHI, Oke, 1982), habitat loss (McKinney, 2002, 2006), and water shortage (Gober, 2010; Kummu, Ward, De Moel, & Varis, 2010; Wu & Tan, 2012).

An effective way of mitigating the negative impacts brought about by urbanization is through urban vegetation (Escobedo, Kroeger, & Wagner, 2011; Nowak & Dwyer, 2007). Urban vegetation is a term that collectively describes urban greenspaces, including parks, wetland, grassland, and patches of urban gardens (Kumagai, n.d.; Ridd, 1995; Tooke et al., 2009). The presence of urban vegetation is known to be beneficial to modifying the local climate, and thus the social, and physical environments through temperature control (Oke, 1982), air pollution reduction (Nowak et al., 2006), noise and storm water control (Glass & Singer, 1972), and habitat preservation (Nowak & Dwyer, 2007). Studies have also

indicated the significant social (Grahn & Stigsdotter, 2003), economic (Tyrväinen et al., 2005), and aesthetic values (Jim & Chen, 2006; Tyrväinen et al., 2005) associated with urban vegetation. As a result, urban vegetation has been utilized as an effective tool to achieve sustainable and functional urban environments. Efforts towards preserving healthy urban vegetation can therefore be found worldwide, particularly in developed regions, such as in North America and Europe (Nowak, 2002).

In less developed areas, despite the benefits and services offered by urban vegetation, economic growth and urbanization often receive higher prioritization than preserving and maintaining urban vegetation (Grimm et al., 2008). Vegetation in these urban environments often grows in more isolated and fragmented patches compared to vegetation grown in more novel and well-managed urban environments, making it more challenging to manage for local urban planners. Another concern associated with poorly managed and fragmented urban vegetation is ecological inequity (N. Heynen et al., 2006), causing uneven access for local residents to quality urban green space. With the majority of new urban residents located in less developed regions (Grimm et al., 2008), there is a strong need for data and methodological approaches that are capable of quantifying and tracking vegetation changes over space and time (Clancey, 2004).

Remote sensing is an exceptional data source to urban planners and researchers (Jensen & Cowen, 1999). Although studies using fine spatial resolution imagery (Benz, Hofmann, Willhauck, Lingenfelder, & Heynen, 2004), hyperspectral data (Heiden, Segl, Roessner, & Kaufmann, 2007; Roberts et al., 1998), and aerial photography (Hodgson, Jensen, Tullis, Riordan, & Archer, 2003) have shown promising results all have limited spatial and temporal coverage limiting their global application. A recent review by (Schneider, 2012)highlighted the potential value of multi-temporal dense image stacks generated from moderate spatial resolution (e.g. 30meters) remote sensing platforms such as the Landsat series of satellites to urban remote sensing research. Recently, increased accessibility of the Landsat data archives (Schneider & Woodcock, 2008; Wulder & Coops, 2013) with more sophisticated image processing procedures (Griffiths et al., 2010; White et al., 2014) and compositing techniques (Hermosilla et al., 2015) have allowed mapping of urban land-cover as well as quantitatively describing urban physical features and patterns at regional scales over 30 years.

However, with a 30-meter pixel size, spectral information collected by the Landsat Thematic Mapper (TM), and Enhanced Thematic Mapper (ETM+) are more likely to contain a mixture of surface materials (Small, Elvidge, Balk, & Montgomery, 2011). Spectrally mixed pixels are commonly seen in Landsat images where multiple surface materials jointly occupy one pixel (Keshava & Mustard, 2002). Sub-pixel

analysis or spectral unmixing has been developed to determine the areal amount of pure, distinct, surface materials within a single pixel. Spectral unmixing is well established in the remote sensing literature and has applied in a large number of studies across a broad range of spatial resolutions (Asner & Heidebrecht, 2002; Van Der Meer & De Jong, 2000; Vikhamar & Solberg, 2003).

While urban environments are highly heterogeneous, there are some common land-cover properties consistent across all cities, such as vegetation, impervious surfaces, and soil (e.g. the V-I-S model) (Ridd, 1995) and as a result systematic unmixing models can be generated. Spectral unmixing involves two critical steps, identifying pure surface materials (i.e. endmember) followed by decomposing mixed pixels (Shi and Wang 2014). Theoretically, the selected endmembers should represent all spectral variations in the image. Based on previous work (Van Der Meer & De Jong, 2000), although endmembers derived directly from the image are relatively less divergent compared to laboratory measured spectra, they have the advantage of sharing a more similar atmospheric conditions which is essential for unmixing Landsat time series.

The majority of previous research has focused on unmixing single images with less research on unmixing multi-temporal time series data. Building upon previous urban spectral unmixing research (Ridd, 1995; Tooke et al., 2009), this chapter aims to further contribute to this field by i) incorporating pixel based compositing (PBC) techniques to produce seamless annual image composites, ii) examine the capacity of spectral unmixing approaches to be applied to dense annual Landsat composites from 1984 to 2012 to determine vegetation cover of 25 urban environments in the pan Pacific region; and iii) generate temporal and spatial information on urban vegetation features based on the distance and orientation from urban centers and boundaries. Such information is valuable for local urban planners as it offers insights into the within-urban spatial and temporal dynamics of urban vegetation change, and importantly, it has potential to assist regional cross-urban study in areas such as the pan Pacific region, one of the most diverse and fastest growing areas in terms of urbanization (Lo & Marcotullio, 2000b).

4.2. Materials and methods

The opening of Landsat archive has allowed the chronicling of land-cover changes over a large spatial area with longer and denser temporal dimensions than previously available. The amount of vegetation in each pixel and year was determined by applying spectral unmixing analysis to each multi-temporal urban image stack (section 4.2.1). The temporal trends in urban vegetation were then estimated using

the Theil–Sen estimator (Sen, 1968; Theil, 1992) on the estimated vegetation fraction (section 4.2.1). Image processing in this paper was done in IDL 8.3, ENVI 5.2, and ArcMap 10.2.2 and statistical analysis in R 3.1.1.

4.2.1. Spectral unmixing

Conventionally, spectral indices have been widely used to extract and monitor vegetation dynamics. However, spectral indices can saturate in area s of high canopy cover and leaf area index (Jackson et al., 2004). Alternatively, spectral unmixing approaches allows users to pre-define endmembers and compute a fraction score representing the abundance of a given endmember (i.e. vegetation). The classic unmixing process can be summarized in three major steps: (1) identify endmembers (i.e. spectrally pure pixels); (2) build spectral library; and (3) apply unmixing algorithm (Singer and McCord 1979; Ridd 1995). I used the pixel based compositing (PBC) image stack for each city for endmember selection and followed the same procedure as Small and Lu (2006) and Tooke et al. (2009) who incorporated a three endmember model, including a vegetation, a high albedo (i.e. reflected brightness)

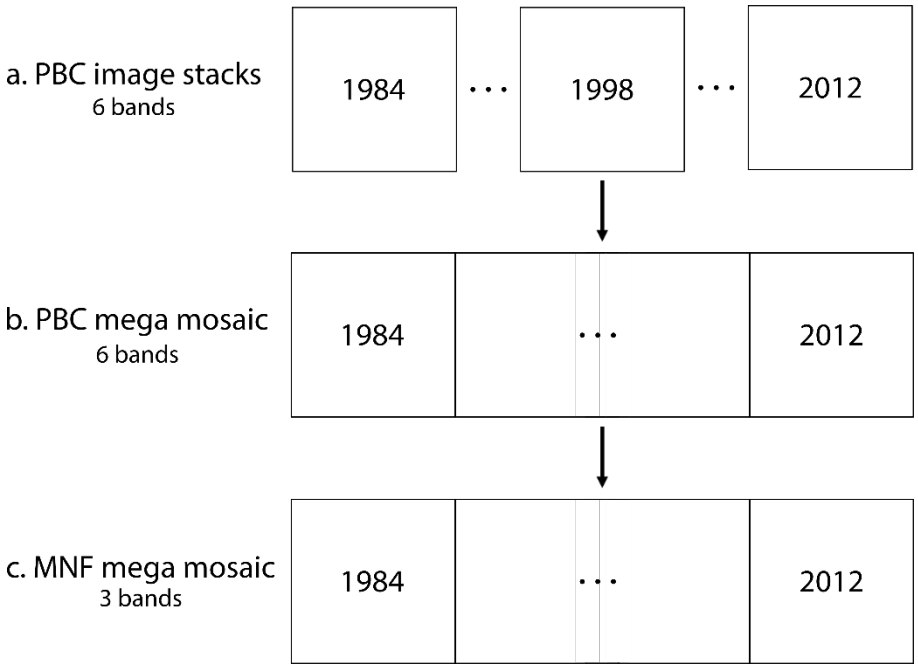

Figure 4.1 Image mosaicking and transformation process using a). Pixel based compositing (PBC) multispectral images (6 spectral bands); b). Mosaicked PBC image (6 spectral bands) and c). Minimal Noise Fraction transformed PBC mega (3 components bands).

and dark endmember. As suggested by others (Wu and Murray 2003), I also included a water mask and undertook a Minimal Fraction Noise transformation (Green, Berman, Switzer, & Craig, 1988) prior to the unmixing (Figure 4.1). I selected the first 3 components for collecting endmembers as they explained over 98% of the variance in all sample urban environments.

A spectral library of the selected endmembers was then developed for each MNF transformed proxy image based on the following two assumptions (Equation 1). First was linearity where the spectra of each mixed pixel is a linear combination of the endmembers as recorded in the spectral library. Second was unity which implies that for each mixed pixel, the sum of fractions (*f*), should equal to one. Fraction images with values indicating fractions of each endmember for mixed pixels were generated for each urban environment and used for the subsequent trend analysis.

$$R = \sum_{i=1}^{n} f_i e_i + \varepsilon \qquad Equation\ 1$$

Where *R* is the unmixed surface reflectance; f_i is the fraction or the fraction of the surface reflectance value of endmember e_i; ε is the root mean square error; n is the total number of endmembers.

4.2.2. Validation

Unmixed vegetation fractions were validated using high spatial resolution Google Earth images for the corresponding year. As quality and availability of cloud free Google Earth images varied greatly from region to region, I chose the best available images for the following city, Vancouver (year 2009), Tokyo (year 2006), Las Vegas (year 2011) and Shenzhen-Hong Kong area (year 2009). The reference vegetation fraction was determined by defining a random sample of 100 pixels stratified across 10 vegetation fraction classes. Each pixel was then divided into a 6x6 m grid (i.e. 25 grids per pixel). Each grid was interpreted as either having a presence or absence of vegetation. The reference vegetation fraction value was calculated by counting the number of vegetated grids within each pixel (e.g. 20 vegetated grids equal to 80% vegetation fraction). Spectrally unmixed vegetation fraction was then compared against the interpreted reference vegetation fraction using correlation analysis.

4.2.3. Vegetation trend analysis

When using annual vegetation fraction images, cities located in high latitudes (e.g. Harbin) and particularly mountainous regions (e.g. Vancouver) may require extra caution. In those cases, pixels with low vegetation fraction may not necessarily indicate intense urbanization, but rather low vegetated land-cover types, such as bare rock and snow. One major benefit of utilizing the entire time series is that it allows changes in vegetation fraction over time to be easily assessed rather than classifying images into discrete land-cover types based on limited temporal snapshots of the city.

I applied a non-parametric Mann-Kendall test for each pixel to determine whether or not the trend was significantly monotonic (Mann, 1945). I then applied the Theil-Sen estimator (TS; Sen, 1968; Theil, 1992) to fit only significant vegetation change trends identified by the Mann-Kendall test. Given its robustness and computational efficiency with distribution-free, non-normal input data requirements (Wilcox, 2010), the TS estimator has been widely used in remote sensing trend analysis (Fernandes & G. Leblanc, 2005; Hansen, M. C., Roy, D. P., Lindquist, E., Adusei, B., Justice, C. O., Alstatt, 2008). The TS estimator provided a slope value by taking the median slope of all pairwise time series data points. This procedure was repeated for every non-water pixel of all 25 cities. An alpha level of 0.05 was used for all statistical tests.

To derive the spatial and temporal patterns of urban vegetation changes I analyzed the trend results using concentric rings which have been widely applied in previous urban studies (Handayani & Rudiarto, 2014) and chapter 3 to demonstrate the spatial distribution of urban vegetation changes. I divided the 60-km radius circular study area into 100 concentric rings (i.e. 600-meter per ring) to summarize vegetation trends from urban core to urban edge. The 60-km radius circle was also divided into 360 slices (i.e. 1-degree per slice) to generate a directional circular histogram to examine how vegetation changes based on its direction to urban core. I summarized the median of the direction and slope of the change trends for each concentric ring and slice.

4.3. Results

4.3.1. Vegetation fraction

Vegetation fraction was estimated for each urban environment (examples in Figure 4.2). Pixels with high vegetation fraction were largely located outside urban centers. Low vegetation fraction pixels also successfully delineated small satellite settlements as well as urban corridors that connect existing urban centers and developing sub-urban settlements (Figure 4.2 a-b). Exceptions can be found in cities located in dry and deserted regions such as Las Vegas (Figure 4.2 e) where opposite vegetation patterns occur as urbanized area was relatively much greener than rural and undeveloped areas.

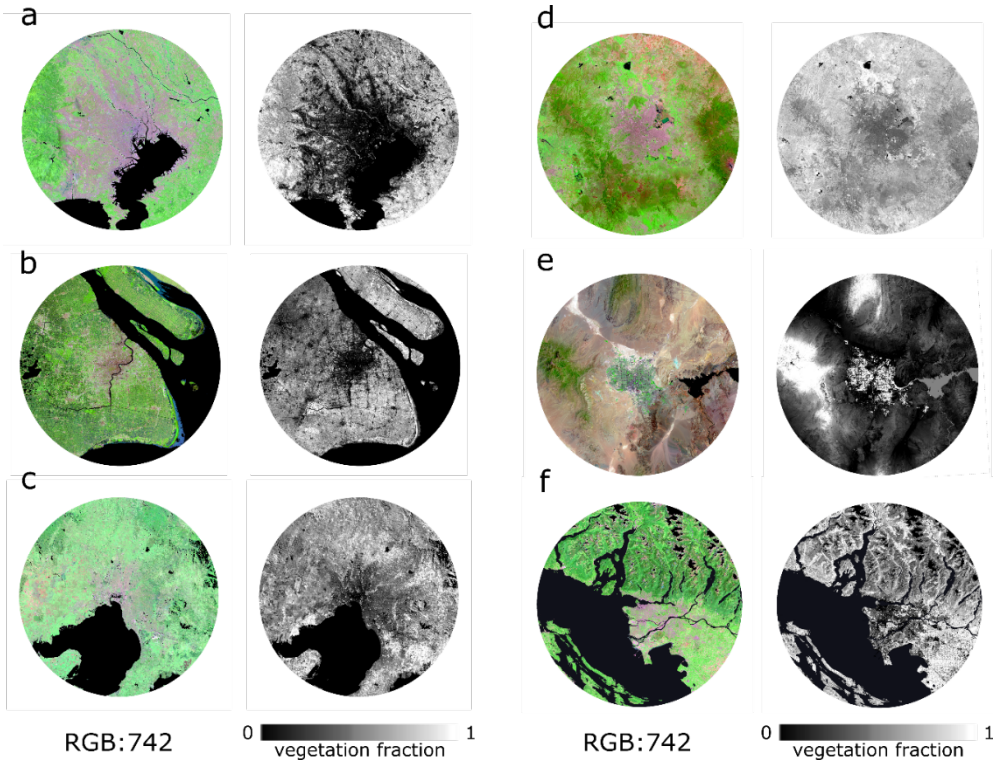

Figure 4.2 Landsat proxy image (left panel) and unmixed vegetation fraction results (right panel) in year 2000 of a). Tokyo, b). Shanghai, c). Melbourne, d). Mexico City e). Las Vegas, and f). Vancouver (scale 1: 800,000).

Validation using high spatial resolution Google Earth images showed a correlation coefficient of 0.66, 0.72, 0.72, and 0.77 for Vancouver, Las Vegas, Tokyo, and Shenzhen-Hong Kong area, respectively (Table

4.1). As shown by the median values in Table 4.1, I found that overall in Shenzhen-Hong Kong and Vancouver, the estimated vegetation fraction were lower than the reference vegetation fraction values while in Las Vegas and Tokyo, the estimated vegetation fraction was slightly higher than the interpreted one.

Table 4.1 . Correlations of interpreted versus estimated vegetation fractions with median values.

	Correlation coefficient	Median (Interpreted)	Median (Estimated)
Shenzhen-Hong Kong	0.77	0.62	0.50
Las Vegas	0.72	0.36	0.49
Tokyo	0.72	0.48	0.50
Vancouver	0.66	0.88	0.51

Figure 4.3 shows the median value between interpreted and estimated vegetation fraction for every 20% increment. The interpreted vegetation fraction from Google Earth images showed greater variations than Landsat estimated vegetation fraction as indicated by a wider standard deviation error bar (Figure 4.3). The estimated vegetation fractions were higher for 0-20% stratum while the interpreted

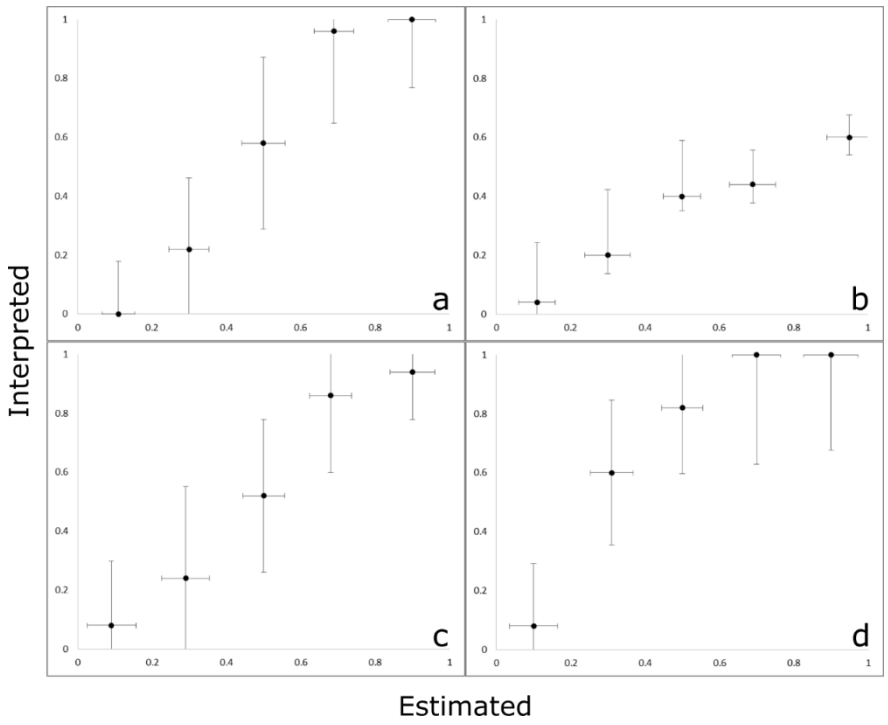

Figure 4.3 Comparison between estimated and interpreted vegetation fraction of a) Shenzhen-Hong Kong, b) Las Vegas, c) Tokyo, and d) Vancouver. Error bars represented the standard deviation of all sample points within each 20% increment.

vegetation fractions exceeded the estimated values for the higher vegetation fraction samples (Figure 4.3a, 4.3c, and 4.3d). Las Vegas, however, showed an opposite pattern where the interpreted values were lower than the estimated vegetation fraction for all strata (Figure 4.3b).

Figure 4.4 illustrates an annual vegetation fraction time series in Las Vegas. Unlike other urban environments, as urbanization develops in Las Vegas, vegetation fraction gradually increases particularly near the sub-urban and the small satellite urban areas. Urban densification can also be seen through time as vegetation fraction decreased in urban center.

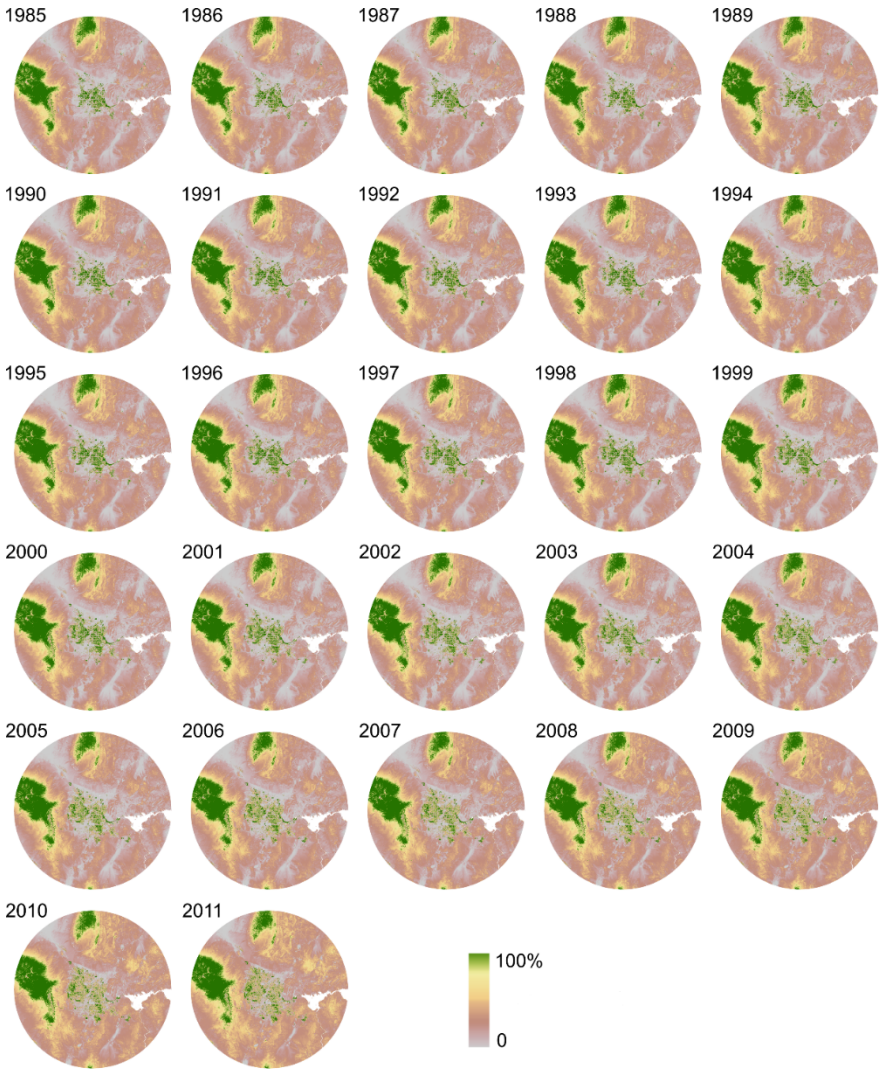

Figure 4.4 Annual vegetation fraction (0 – 100%) results of Las Vegas.

4.3.2. Temporal characteristics of vegetation fraction

As shown in Figure 4.5, for a given pixel, a negative trend slope indicates a decreasing vegetation fraction while a positive slope indicates an increasing vegetation fraction during the study period (i.e. 1984-2012). By comparing all 25 urban environments, it was apparent that each urban environment was highly variable in terms of temporal vegetation changes. To capture only the statistically significant trend, slope values with a Man-Kendall p-value greater than 0.05 were not included in the subsequent analysis hence masked out in Figure 4.5. The absolute value of the trend slope (refer to as vegetation slope) represented the magnitude of vegetation loss and/or gains. In general, most vegetation loss

occurred outside the existing urban core, except in Las Vegas where urbanization caused vegetation gains in sub-urban areas and the urban core only experienced a slight vegetation fraction decrease.

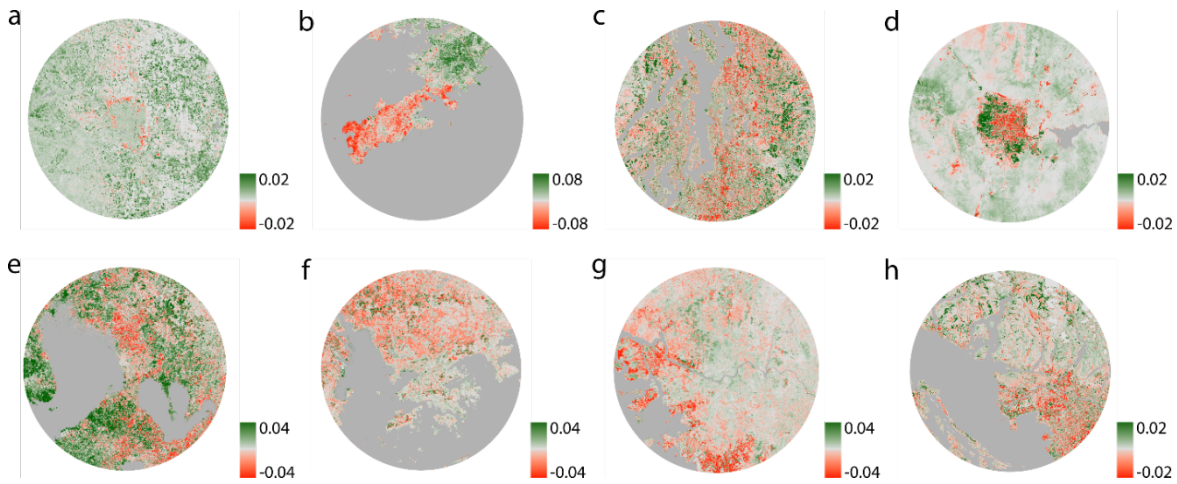

Figure 4.5 Theil-Sen estimated vegetation trend slope ($p < 0.05$) of a). Calgary, b). Dalian, c). Seattle, d). Las Vegas, e). Manila, f). Shenzhen-Hong Kong, g). Seoul, and h). Vancouver (scale: 1:700,000). Water is colored as grey.

4.3.3. Spatial dynamics of vegetation fraction

Median vegetation trend slope value per ring was extracted and plotted for all 25 urban environments (Figure 4.6). In general, in terms of spatial distribution of the trends, there were four main types of urban environment trends. The first includes cities such as Shenzhen-Hong Kong area (Figure 4.6a) which exhibited a gradual decline in vegetation from the urban center through to the outer areas. Second set of cities included cities such as Las Vegas that had consistently increasing vegetation slope as the distance from urban center increases (out to 20-km in the case of Las Vegas) (Figure 4.6b). The third type contains cities such as Shanghai (Figure 4.6c) where vegetation slope was mostly negative across the 60km radius circle. These types of cities were mostly located in China, including Dalian, and Nanchang. The last type of cities such as Vancouver (Figure 4.6d), Tokyo, Sydney, Edmonton, and Calgary, where vegetation changes were relatively minimal as indicated by a near zero vegetation change trend. These types of cities were mostly located in developed regions.

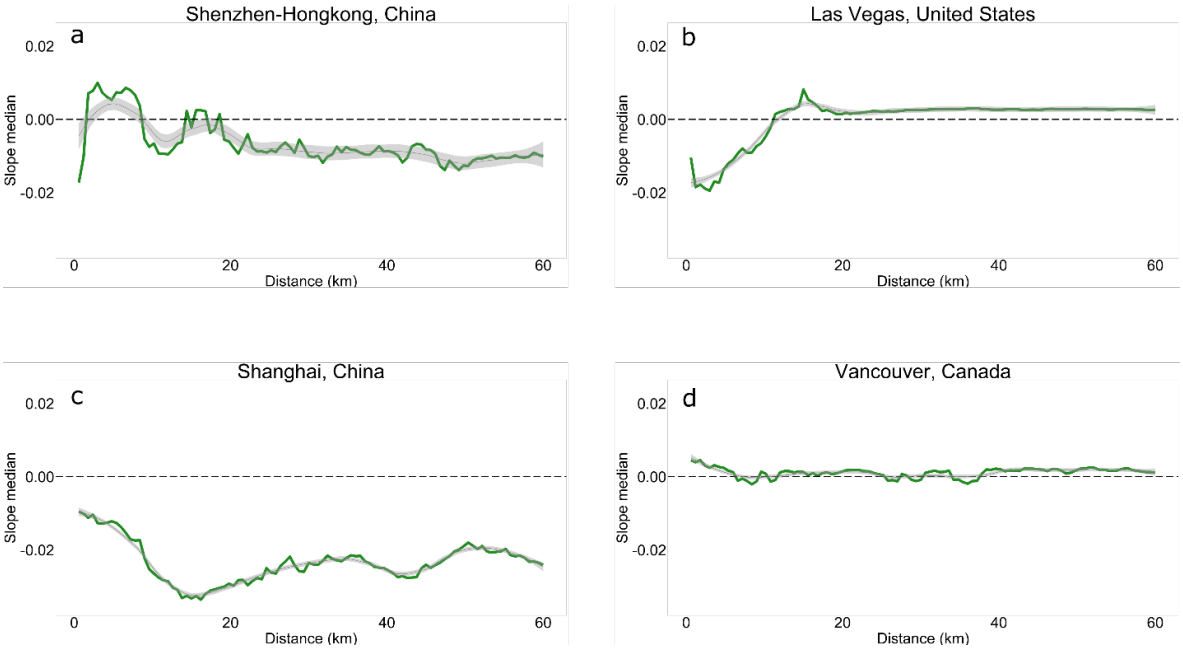

Figure 4.6 Vegetation trend slope median per ring (600-meter per ring). Green represents median slope value. Grey represents confidence interval of smoothed slope value (black). Appendix 2 shows circular histogram of all 25 cities.

Figure 4.7 exhibits the temporal vegetation trend in terms of vegetation loss or gain with respect to its direction from the urban center between 1984 and 2012. The results reflected the variability across cities with each city having varying magnitudes and spatial distribution of vegetation. Dalian, for example, had a great amount of vegetation decrease in the west of the city (Figure 4.7a) while Shenzhen-Hong Kong area experienced more intense vegetation loss in the north (Figure 4.7b). Most inland cities such as Nanchang and Changsha have a greater spread of vegetation loss (Figure 4.7c and 4.7e). More developed cities such as Vancouver (Figure 4.7d), although not showing as much vegetation loss as other less developed urban environments, it still showed some degree of vegetation decrease (e.g. the northern and south-eastern part of the Vancouver).

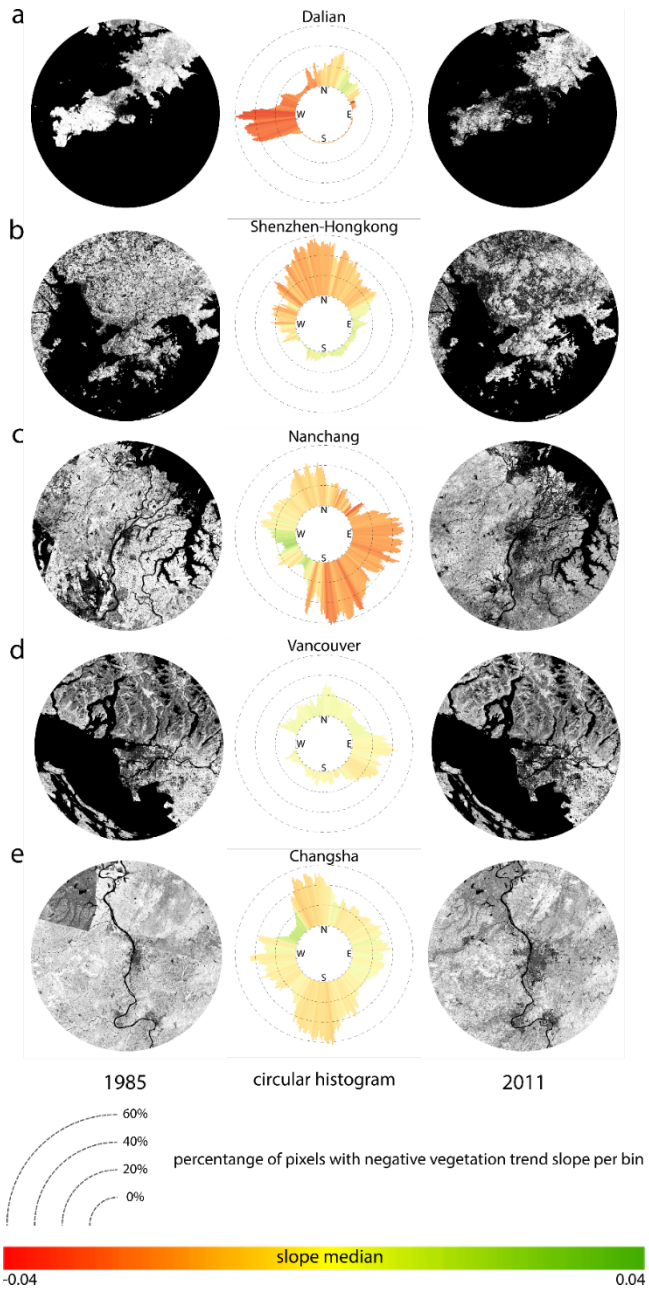

Figure 4.7 Circular histogram of vegetation trend with slope median value per bin (1-degree per bin). The bar length indicated the percentage of pixels with a decreasing vegetation trend. The median slope value was colored with a red-yellow-green scheme with red representing the most negative slope, green representing the most positive slope, and yellow represent stable vegetation fraction. Water is colored as black. Appendix 3 shows circular histogram of all 25 cities.

4.1. Discussion

4.1.1. Urban boundaries

This chapter demonstrated advances in previous chapter. These include more appropriate definitions of city limits, using advanced image processing approaches to extract the vegetation of pixels and updated validation approaches. Compared to chapter 1, I defined urban boundaries using a 60-km radius buffer from the city center, rather than using an inconsistent global database of administrative borders. Although radius buffers are an unconventional and less intuitive way to define urban boundaries, it minimizes issues associated with finding temporally consistent administrative boundaries across multiple different jurisdictions (e.g. China vs United States). Global Administrative Areas (GADM) is an exceptional data source that provides urban boundaries of individual countries and is often used in defining urban boundaries however it is apparent that the boundaries are at a spatial scale not compatible with the 30-meter spatial resolution of Landsat imagery. For example, rapidly expanding cities such as Changsha, which comprises a number of urban centers was not well captured as they fall outside Changsha's administrative border (Figure 4.7e). The dimension of the radius buffer is however dependent on the location (i.e. coastal vs inland) and the physical footprint of the city. The larger the radius buffer, the more image data that is required to be downloaded and processed. For very large megacities such Shanghai and Tokyo, a 60-km radius buffer may not be sufficient cover all of the vegetation changes associated with urban development as opposed to cities such as Las Vegas and Calgary where the majority of the urban environments easily reside within the 60-km radius buffer. I acknowledge that a fixed radius buffer is likely less optimal for coastal cities such Dalian (Figure 4.5b) as most of the area within the 60-km buffer is water with limited land mass for investigating vegetation changes at the further distances.

4.1.2. Spectral unmixing vs spectral index

Secondly, compared to the traditional spectral indices, the integration of spectral unmixing and Theil-Sen (TS) estimated trend slopes offers increased ability to compare and contrast vegetation across urban environments. A spectral index for a given pixel can be difficult to compare across different urban environment over time. A number of studies have discussed the ecological meaning of vegetation index values compared to vegetation fraction estimates (Pettorelli et al., 2005). In this chapter I observed

similar vegetation fraction values from natural forest, wetland, and agricultural vegetation across the 25 cities (e.g. Figure 4.2). The absolute score of an unmixed vegetation fraction pixel can be interpreted as the quantity and/or the quality of different types of vegetation. Using the vegetation fraction of a single pixel at a single snapshot can be prone to a range of errors and distortions as discussed as discussed through-out this paper resulting in potential confusion especially in heterogonous urban environments. Therefore, the slope of change in vegetation fractions derived from a time series of spectrally unmixed vegetation fractions is likely to be a more robust representation of the relative vegetation change at a sub-pixel level which is less sensitive to individual data outliers caused by factors such as phenological variations and vegetation types. Another well-known challenge in urban remote sensing is separating bare ground and soil due to their spectral similarity (Weng, 2012). Therefore, I reduced reliance on the urban built up index (e.g. Normalized Difference Built-up Index in chapter 3) and assumed vegetation loss was primarily caused by urban growth within the 60-km radius buffer.

4.1.3. Google Earth as a validation tool

Lastly, I included a validation procedure to examine the vegetation fractions using Google Earth Desktop. Google released Google Earth in 2005 allowing users to seamlessly examine any location on the globe by streaming the best available imagery. With up to 10 petabytes of data and sophisticated built-in images pre-processing such as geo-referencing and image mosaicking, Google Earth is a reliable data source for visual assessment and interpretation has previously been unavailable to remote sensing researchers (Bey et al., 2016). I found that for two of the Asian megacities, namely, Bangkok and Manila, the results confirm those of Murakami, Medrial Zain, Takeuchi, Tsunekawa, & Yokota (2005) who detected a decreasing population density from the urban center to urban boundaries indicating a less active urban development in the rural and suburban area. Although, the administrative boundaries were used in Murakami, Medrial Zain, Takeuchi, Tsunekawa, & Yokota (2005) they concluded that the urban growth had continued beyond the city limits. Similarly, I detected that vegetation condition was less disturbed as the distance from the urban center increases, likely causing by less urban activity in such areas. Xian & Crane (2006) also reported the reverse trend between vegetation and urban impervious area in Las Vegas, indicating urbanization can potentially increase the vegetation cover. Practically, Google Earth is an ideal alternative for validation purposes. Compared to conventional high spatial resolution aerial photography and satellite imagery, Google Earth imagery has two main advantages.

First, Google Earth imagery is freely accessible. To date, most of high spatial resolution remote sensing data is expensive with limited access. Second, Google Earth images offers a rich temporal record of locations worldwide. The timeline option in Google Earth enables easily navigate through time allowing users to select the highest possible quality, cloud free imagery, for validation purpose. However, the validation process also exposed uncertainties and new challenges. Compared to previous studies (Small et al., 2011; Small & Lu, 2006), our correlation coefficients between 0.66 and 0.77 were relatively low. This is partially due to challenges associated with human interpretation of vegetation fraction scores in highly vegetated locations. In spectral mixture analysis, a common validation process often involves applying spectral unmixing on high resolution aerial photography or satellite imagery. Given digital high spatial resolution imagery was not readily available for all of the cities of interest I believe visual interpretation approaches were appropriate recognizing the benefit of Google Earth (Dorais & Cardille, 2011) as a reliable source of validation images that match the scale of this work.

4.1.4. Potential drivers of urban vegetation change

Previous studies (N. C. Heynen & Lindsey, 2003; J. Liu, Zhan, & Deng, 2005; Luck, Smallbone, & O'Brien, 2009) have summarized a list of potential physical drivers behind urban vegetation change, including topography, proximity to water, climate, as well as vegetation type. As a result common patterns across a number of cities are evident. Cities such as Mexico City and Edmonton developed in flat terrains are more likely to expand evenly around urban center hence vegetation loss in all directions. Cities such as Dalian and Shenzhen-Hong Kong exhibited a typical linear urbanization pattern, which is often seen in coastal cities. In such cases, urbanization is largely restricted by water bodies. Although, due to the poor accessibility, mountainous topography can also be a limiting factor in spatial urbanization, it does not restrict urbanization as much as large water bodies. Climate and vegetation type, have more absolute effects on the amount and condition of vegetation within an urban area. Cities located in dry and desert regions such as Las Vegas and Phoenix shown opposite vegetation change patterns compared to more temperate or tropical urban environments. In such cities, urbanization often brings with it increases in vegetation, replacing inhabitable landscapes with vegetated human settlements such as manicured gardens, parks, golf courses and public spaces. Such vegetation gains are not always viewed positively and be harmful for local environments by disturbing underground water tables (Gober, 2010) and introducing invasive species (McKinney, 2002).

Besides the aforementioned physical factors, there are a number of other social and cultural factors that are likely to contribute to the observed vegetation changes and their spatial distribution. Drivers such as the increasing demand of single-family housing (Kestens, Thériault, & Des Rosiers, 2004) and advanced fast transportation systems (Janelle & Beuthe, 1997) not only boost people's desire to live further away from the urban center, but also increase the inequality within urban environments in terms of accessing quality urban vegetation (Lu & Chen, 2004).

Recent efforts by urban researchers and local managers have focused on the relationships between social and cultural drivers with urban related land-cover changes (Swetnam et al., 2011). Next chapter, another remote sensing derived metric, nighttime lights (NTL) was introduced and compared against conventional census date to examine the casual relationship between population and GDP on urban brightness.

Chapter 5

5. Are bright cities big cities ?

5.1. Introduction

In this chapter, I first intercalibrated Nighttime lights (NTL) data using a localized modelling approach to ensure temporal consistency and minimize effect caused by saturated NTL pixels (Small & Elvidge, 2013). Second, I spatially delineated and track urbanization patterns using the Theil-Sen estimator for 25 urban environments across the pan Pacific region. Then, I examined the causality of two common socio-economic variables (population and GDP) on NTL using panel Granger causality procedures. This approach allows a statistical verification of the possible drivers of urban development, by examining the effect of exogenous macro-level socio-economic factors on physical city growth. This chapter demonstrates new ways of investigating relationships between NTL data and socio-economic development.

Cities have multi-faceted definitions, including the permanent areas of heavily human-induced infrastructure and the socio-economic entities that facilitate industrial development and population growth (Lo & Marcotullio, 2000a; Montgomery, 2008). City growth, commonly known as urbanization, is thus the interplay between its physical and socio-economic environments. Reliable assessment and quantification of urbanization is critical to better allocate resources and optimize developing efficiency.

Sustainable city growths rely primarily on reliable and consistent measurements of urbanization. The key metrics that have been utilized to examine such activity and its associated variations fall into two main categories. First are demographic metrics such as births and deaths, immigration and emigration, leading to estimates of population size and density. The second set of metrics are associated with the wealth of a city such as regional gross domestic product (GDP). These data can be acquired in a number of ways. Population data are often recorded through censuses where the resident population is polled locally using forms and interviews. Alternatively, economic data are most often complied directly by state government or local administrative units.

Census and economic data are often in tabular format with limited value for monitoring spatially explicit changes that are much needed in urban studies (Jensen & Cowen, 1999). It was not until the 1970s that remote sensing satellite imagery become an alternative data source for monitoring city

growth in a more repeatable and comprehensive manner and offers a much richer source of information than conventional survey data (Schneider, Friedl, & Potere, 2009). However, most urban remote sensing applications mainly focused on extracting physical features such as delineating city boundaries (Henderson et al., 2003) or mapping and quantifying land-cover changes (Venter et al., 2016). Characterizing the socio-economic nature of cities has still primarily remained the domain of census data.

Early studies such as (Welch, 1980) uses lights to model urban population and energy, while Croft (1973) uses the nighttime space photographs to map burning waste in oil fields. More recently, digital NTL data have been increasingly used on mapping urban and urbanization related human activities such as delineating urban expansion (Small et al., 2005), modelling economic activities (Ebener et al., 2005), and CO_2 emissions (Ghosh et al., 2010). Yet, the interpretation of NTL brightness, also known as digital number values (DN), is highly subjective and varies from study to study (Donaldson & Storeygard, 2016). In this chapter, I interpreted NTL values in a more general fashion to represent overall human activities. Thus, I assume that an increasing NTL value is indicative of growing human activities rather than one specific variable in previous studies.

Much of the existing research has shown encouraging results correlating NTL with other ancillary variables such as GDP and population size. However, few have investigated the causal interaction between NTL and socio-economic development. Analyzing the causal relationships between NTL and socio-economic variables can be more valuable than traditional correlation approaches for understanding the drivers of city growth, and prioritizing long-term policy drafting and practical urban planning.

5.2. Materials and methods

In 1992, the first digital NTL acquired by the Defense Meteorological Satellite Program's Operational Linescan System (DMDP/OLS) was released by NOAA's National Geographical Data Center (NGDC). NTL has been used extensively to track urban activity and its associated temporal characteristics, enabling researchers and urban planners to quantitatively compare and contrast spatio-temporal patterns. The full NTL temporal record enables us to chronicle the development of urban patterns and produce spatially explicit estimates that reflect a city's growth or decline (Ma et al., 2012). However, in most years, DMSP-OLS operates a dual-sensor system, meaning that there are two sensors recording

spontaneously. Thus, an intercalibration was needed (section 5.2.1) to build a robust time series of NTL (section 5.2.2). Using a panel version of Granger causality test (section 5.2.3), census data were then compared against NTL time series.

5.2.1. Intercalibrate nighttime lights time series

Annual average visible cloud-free nighttime lights composites (Version 4) were acquired from NOAA (http://ngdc.noaa.gov/eog/dmsp.html) covering 1992 - 2013. Images were formatted as Digital Numbers (DNs) ranging from 0 to 63 with a higher DN representing higher illumination or brightness of lights.

Due to the lack of an onboard calibration mechanism, robust intercalibration is a critical step to allow images from different years or sensors to be directly comparable. Recently, Pandey, Zhang, & Seto (2017) quantitatively evaluated nine most commonly used intercalibration techniques using a Summed Normalized Difference Index (SNDI, Equation 1). Similar to Zhang et al. (2016) and Elvidge et al. (2014) I built a 3rd degree polynomial model to calibrate each image to a reference year. A reference year was selected based on maximal DN values across the selected cites, an approach which has been used previously (Bennie et al., 2015; C. Elvidge et al., 2014; Li et al., 2013; Z. Liu, He, Zhang, Huang, & Yang, 2012; Pandey, Joshi, & Seto, 2013). Rather than using one single model for all cities, I fitted a polynomial model for each individual city to account for local NTL variations.

I evaluated the calibration results for each city using SNDI, which quantified the level of convergence in NTL temporal series of a given city. SNDI is the total of Normalized Difference Index (NDI, Equation 2) which assessed the absolute difference of total DN values (TDN, Equation 3) between two sensors in the same year between two different sensors. As suggested by Zhang et al. (2016) and Pandey et al. (2017) an effective intercalibration should yield a much lower SNDI than the raw images. My intercalibration SNDI was then compared against raw data, Zhang et al. (2016), and Elvidge et al. (2014).

$$SNDI = \sum_{i=1}^{11} NDI_t \qquad Equation\ 1$$

$$NDI_t = \frac{|TDN_{1t} - TDN_{2t}|}{TDN_{1t} + TDN_{2t}} \qquad Equation\ 2$$

$$TDN = \sum_{i=1}^{n} DN_{\ i} \qquad Equation\ 3$$

$t \epsilon (1997, 1998, 1999, 2000, 2001, 2002, 2003, 2004, 2005, 2006, 2007)$

A challenge associated with NTL data was a pixel saturation issue which can occur due to the limited radiometric range of NTL sensors. Recently Zhang et al. (2013) incorporated a series of vegetation images to desaturate NTL data on the assumption that there is an inverse relationship between vegetation abundance and NTL brightness. However, since our goal of this chapter was to investigate the casual relationship between NTL, GDP and population, the inclusion of another input variable (e.g. vegetation) would complicate the process of interpreting statistic analysis. In addition, Zhang et al. (2013) suggested a limited improvement of NTL variability for fast growing cities compared to more established legacy cities. The inverse relationship between NTL and vegetation may not hold for developing cities in this chapter. As a result, NTL images used in this chapter were calibrated but not alerted to accommodate potential saturation issues.

5.2.2. Generate NTL temporal trend

As indicated by previous studies, a "lit" pixel did not necessarily coincide with human activities due to the potential "blooming" effect caused by diffused or scattered light from neighboring pixels (Small & Elvidge, 2013). I therefore used a threshold of DN = 12 as a threshold between lit and non-lit or dimed pixels (Small et al. 2011). I then generated NTL trends for all 25 urban environments over the 21 years. In order to capture any development in initially low-lit area, NTL trends were generated for all non-water pixels, including the ones with a DN value below 12. A Mann-Kendall non-parametric test (Mann, 1945) was used to determine the significance of the monotonic trend in NTL. The TS estimator, which has been widely used with time series data (Hansen, M. C., Roy, D. P., Lindquist, E., Adusei, B., Justice, C. O., Alstatt, 2008) to describe temporal change in intensity, was applied to pixels identified by Mann-

Kendall as statistically significant ($p < 0.05$). Those pixels were then used to calculate the trend slope values based on the median of pairwise data points from 1992 to 2013.

Based on the slope values, I then grouped the 25 cities into two classes. The first class contained cities which have experienced rapid NTL growth over the 21-year period. The second class represented cities with much lower or no slope in trend in NTL, indicative of little urban growth over the time. Specifically, cities in rapid NTL growth group needed to have at least 20% of pixels experience significant changes. In addition to the slope values I also examined the NTL with a predefined threshold (e.g. DN=12) to determine for which year a given pixel exceeded the threshold value, indicating the year urban establishment in that pixel passed the brightness threshold.

5.2.3. Granger causality test

Although NTL has been extensively used as a proxy to anthropogenic activities, many econometric theories and tools have rarely been applied with the NTL time series. The most notable challenge is that econometric tools often require decadal or even centurial time series as input in order to capture the often weak relationship between two given economic variables (Levin, Lin, & Chu, 2002). NTL imagery collected by DMSP/OSL has a relatively short time span (i.e. 1992-2013) and therefore are often not well suited to econometric tools. Recent studies (Hsiao, 2007) however have shown encouraging results for utilizing relatively short time series for causation testing through panel data that are a collection of entities (e.g. cities) where the variables are observed across time.

Statistically, the Granger causality test (Granger, 1969) describes the strength of association between two time series by testing whether or not the inclusion of one time series (x_t) can improve the forecasting of future values in another time series (y_t). If the addition of xt significantly improves a model's explanatory power in predicting y_t, I could conclude that x_t "granger causes" y_t.

In this chapter, the panel version of the Granger causality test combined individual short-time series data in a form of cross-sectional structures that increased the test efficiency and power by raising the number of observations and degrees of freedom (Hoffmann, Lee, Ramasamy, & Yeung, 2005). In this chapter, a total of three panel data sets were generated for causality test, namely, total DN (T_{DN}), total population (T_{POP_Total}), and total GDP (T_{GDP_Total}) for each of the 25 cities. As a result, each panel data set had a total of 25 cross-sections (N=25 cities) and 22 temporal units (T=22 years). Total DN was

calculated as the sum of DN values of all lit pixels for each year to represent both the area and intensity of the NTL. I also examined the differences between cities which are rapidly developing (N=13) versus those which are more established (N=12).

Granger causality tests required all panel data to be stationary and co-integrated based on two panel unit root tests; the Levin & Lin (Levin et al., 2002), known hereafter as the LLC test and Im & Pesaran (2003), known hereafter as IPS. The panel co-integration test of Johansen (Johansen, 1988) was applied to examine co-integration among all pairs of temporal variables (test results in Appendix 4).

The rejection of Granger causality tests H_0 ($p < 0.01$) indicated a unidirectional causal relationship from one input variable to the other. I employed the panel Granger causality test proposed by Dumitrescu & Hurlin (2012), thereafter DH, which respected the heterogeneity within relatively small panel data sets.

5.3. Results

5.3.1. Intercalibrating NTL time series

Overall, all calibration methods successfully reduced the systematic biases in the NTL images with a lower SNDI than for the raw data across most of the cities (Figure 5.1). Although Zhang et al. (2016) and Elvidge et al. (2014) yield lower SNDI at the global scale, our city level calibration shows a marginally better calibration result in terms of minimizing systematic biases. Haikou (HAK), Nanchang (NCX), and Vancouver (VAN) all have a relatively higher SNDI value compared to the other cities tested.

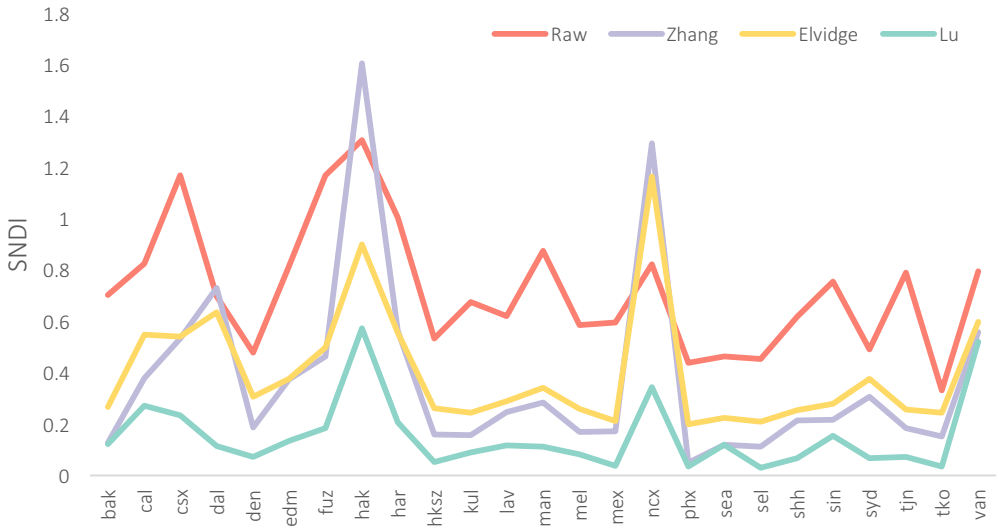

Figure 5.1 Sum of normalized difference index (SNDI) derived from raw image, Zhang et al., (2016), Elvidge et al., (2014), and Lu (this chapter).

5.3.2. Quantifying spatio-temporal changes

Large inter- and intra-city variations were apparent. For example, in Denver (DEN), steeper slopes were clustered in the north and east side of the city while in Kuala Lumpur (KUL), intensive NTL changes were located in the south (Figure 5.2). The majority of pixels with rapid change were found in less developed cities (e.g. HAR) while more developed cities exhibited more stable NTL trends (e.g. CAL). Variations occurring within the same city also clearly exposed NTL change hotspots and the growth of surrounding satellite cities during the study period (e.g. BAK, SHH).

Figure 5.2 NTL change rate represented by Theil-Sen slope values showing the rate of change from 1992 to 2013. Water is colored as white. Cities were grouped based on its growth intensity. Left panel contains cities with fast and more dynamic urban growth while the right panel include cities with more stable and less development.

Spatially, the recent urban development generally occurred on the outer rings of each urban area (Figure 5.3; e.g. FUZ and CSX). Timing of urban development was also variable with cities such as Seoul and Kalua Lumpur dominated by land-cover changes in the early stage of the time series while changes in Changsha and Dalian were relatively more recent.

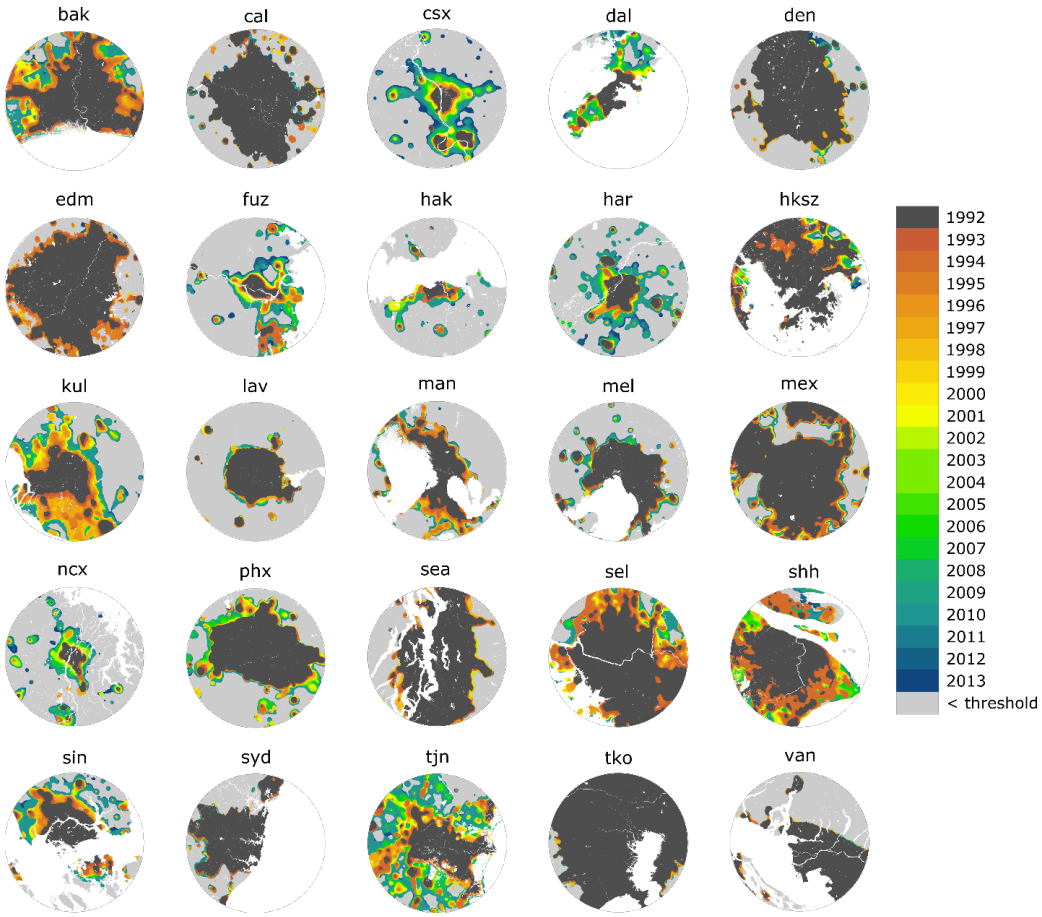

Figure 5.3 . The year when a given pixel within each urban environment exceeded the pre-defined DN value. Dark grey pixels represent existing urban areas prior to 1992 while light grey indicating areas with no sufficient light sources in 2013.

I observed a wide range of variation within and across all 25 cities in urban development (Figure 5.4). For example, Tokyo (TKO) and Hong Kong (HKSZ) have over 75% of land urbanized prior to 1992 while most cities in China had less than 10%. Cities such as Shanghai (SHH) and Tianjin (TJN) experienced substantial growth over the period studied with nearly 50% of the land crossing the pre-defined threshold value. A few cities, however, had less growth with approximately 75% of land remaining undeveloped.

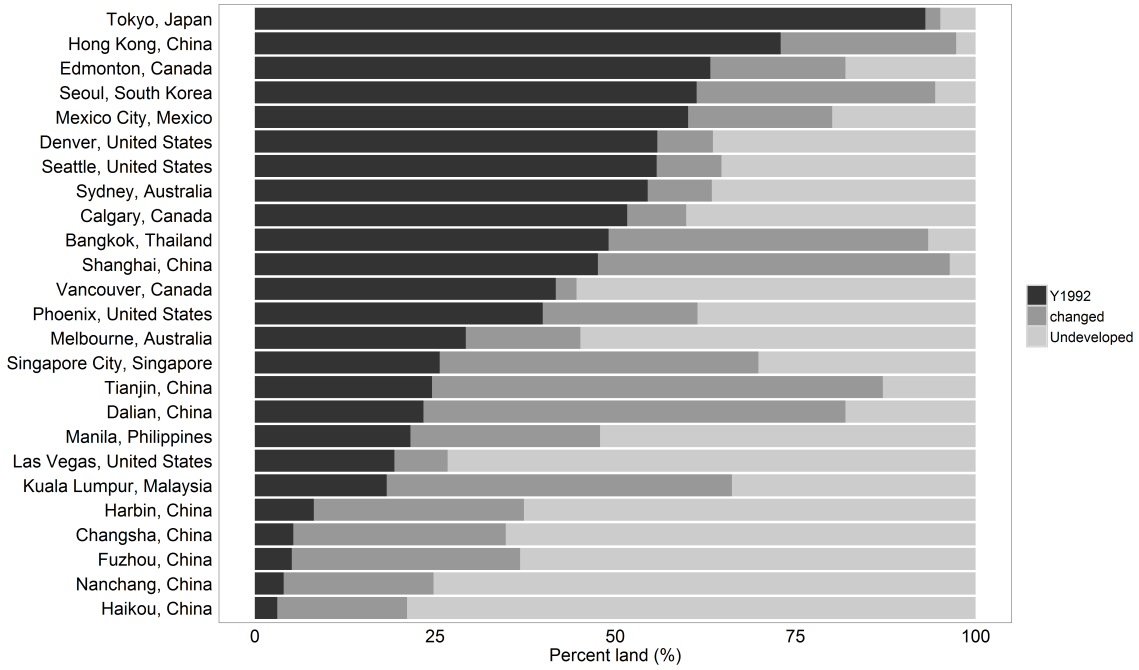

Figure 5.4 Urban land breakdown of changed, undeveloped, and existing urban areas, ranking the 25 cities from the highest proportion of lit pixels (i.e. TKO) to the least (i.e. HAK).

5.3.3. Granger causality test

The Causality test results differ depending on the cities analyzed (Figure 5.5). Expectedly, across all cities, both population and GDP played a major role in directing changes of NTL. Additionally GDP and NTL also "granger caused" changes in population ($p < 0.01$, Figure 5.5a). This implied that the brightness of cities follows increases in both population and GDP equally and that neither population nor GDP alone is responsible for increasing the NTL. Unexpectedly, the test also suggested GDP and NTL "granger cause" population growth suggesting that population change was the outcome rather than the cause of urban development (Figure 5a).

Stratifying the cities by development stage I found contrasting and unexpected results. In the case of more established cities with few NTL changes over the analysis period, the causal relationship from NTL to population was no longer significant yet changes in population "granger caused" both GDP and NTL (Figure 5.5b). This suggested that in cities with relatively stable NTL, population and GDP were likely the key driver of local economic and urban development but not the other way around.

For fast changing and more dynamic cities, there were only two significant casual relationships – growth in NTL and GDP leading to an increase in population. Unexpectedly, there was no significant causal association between GDP and NTL (dash lines in Figure 5.5c). This suggested that in rapidly changing cities population increases were driven by brighter and more economically active urbanization.

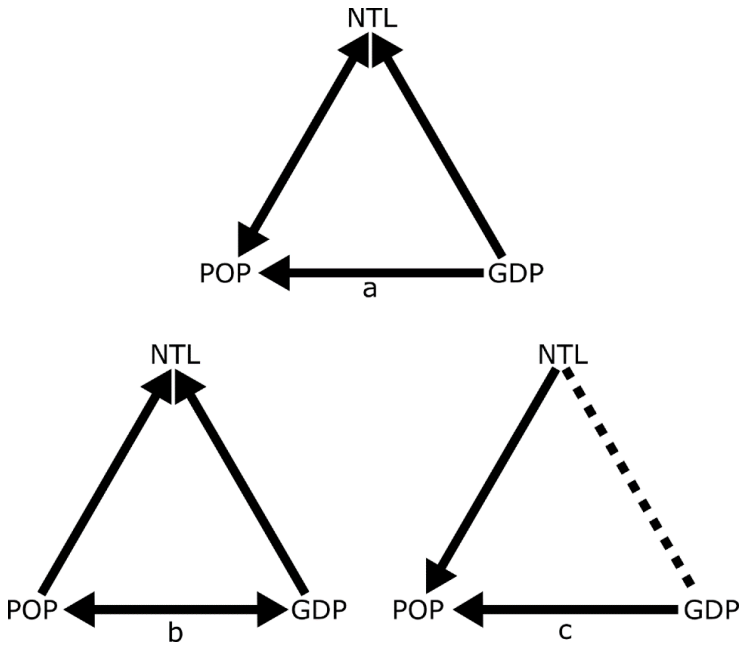

Figure 5.5 Causal interactions among NTL (nighttime lights), POP (population size), and GDP (Gross Domestic Product) of a) all cities, b) established cities, and c) dynamic cities. A solid line represents a statistically significant causal relationship while a dotted line indicates no significant causality. Arrow head indicates the direction of causal relationship and a double-headed arrow represents a bi-directional causal relationship.

5.4. Discussion

5.4.1. NTL calibration

The calibration method in this chapter successfully minimized the systematic biases at the city scale, enabling direct comparisons among images taken by different sensors (Figure 5.1). Pandey et al. (2017) suggested that a global calibration (i.e. national level) could outperform regional models which does not appear to be the case in this study. I found that intercalibrated models at city scale achieved relatively lower SNDI across all 25 cities than using calibration parameters from previous studies (Figure 5.1). One rationale was that the majority of the pixels used in the calibration process were brightly lit (i.e. pixels

located in urban area) which had a much higher contribution to the overall SNDI statistics than dimly lit pixels (Pandey et al., 2017). It was also noticeable that the calibration performance varies across cites. Images with large portion of dimly lit pixels were more likely to suffer from less optimal calibration due to existence of random noises and the skewed radiometric DN values. Island cities or cities surrounded by large green spaces may have a relatively less even distribution of DN values, which may explain our inconsistent calibration performance in Figure 5.1. Cities with higher SNDI values were either located in developing regions (e.g. Changsha and Haikou) or cities with higher cover of vegetation cover (e.g. Vancouver). Generally, those cities had fewer brightly lit pixels than cities such as Tokyo. Therefore, I concluded that a locally fitted intercalibration model will likely work better in areas dominated by high DN pixels.

5.4.2. Is 60-km buffer ideal

It was unsurprising to see that cities with more dynamic and fast changing rates were located in Asia. According to United Nation's review in 2001, on average, Asian cities were at least 50 years behind Europe and North America in terms of urbanization level (United Nations, 2002). Mega-cities in Asia on the other hand showed highly dominating and disproportional impact on regional and national economic development. Studies (Jones, 2002) have suggested that urban dwellers have an overall better living standard such as education and consumption level, hence attracting substantial amount of in-migration from rural areas. Understanding the spatial pattern and the timing of urban development in those fast changing cities could offer valuable information on efficient land resources allocation which can further reduce the per capita cost of infrastructure and basic services (Cohen, 2006). In contrast, urbanization tended to be less concentrated in more developed cities due to their advanced urban network (Cohen, 2006). As a result I noticed that while a 60-km radius buffer was sufficient for fast changing and more dynamic cities, it was clearly not large enough to capture recent urbanization activities in more developed cities (Figure 5.2 & 5.3). Other alternatives such as algorithmically derived urban extent have been used in previous literatures, focusing on primarily tracking urban land-cover and land use over time. This approach however, still required a fixed boundary to define where the city ends.

Although this chapter used a ground distance of 60 km to delineate urban boundary, other distance measuring approaches such as travel time ratio (Dijst & Vidakovic, 2000) or Manhattan distance (Apparicio, Abdelmajid, Riva, & Shearmur, 2008) may affect the casualty tests. One limitation regarding

to the boundaries of selected cities was the spatial scale difference between remote sensing data and census record which was often collected using administrative units. The scale inconsistency between these two data sets may alter the final results. Yet, since the census data used in this chapter represented metropolitan area which in general covers a relative larger area than normal administrative units, the results were still able to offer valuable insights on decoupling the relationship between NTL and socio-economic development.

5.4.3. Chicken or the egg: causal relationship between NTL and socio-economic factors

A large number of econometric studies have reported inconsistent results when examining interactions between socio-economic and environmental variables. Mozumder and Marathe (2007) summarized a number of studies and found mixed causal relationship results depending on the study location, types of variables, and duration of time series used. Knapp & Mookerjee (1996) tested the underlying interaction between population growth and global CO_2 and concluded a weak long-term equilibrium but strong short-term relationships between population and CO_2. Seto & Kaufmann (2003) also employed panel causality procedures with remotely sensed images to estimate the economic drivers of land conversion in urban areas and concluded that investment in capital construction is driving urban land conversion.

It has long been thought that population was the primary driver of urban brightness while economic development was rather a form of outcome of urbanization. In this chapter, I found that population and GDP revealed contrasting effects on NTL trends between stable and more dynamic cities. Statistically, changes in NTL were significantly driven by both population and GDP growth in more established, slow changing cities. Previous work (Dietz, Rosa, & York, 2007; Satterthwaite, 2009) has indicated that rather than growing population alone, it was the high consumption lifestyle, economic and political decisions that lead to urban growth. My results showed that in more developed cities, it was in fact both the population and economic development that drives urban NTL changes.

However, in fast changing, yet often less developed cities, the growth of NTL brightness and GDP were driving population changes rather than the other way around. In those cities, a major source of population increase was through large in-migration from rural and neighboring areas and involves densification and conversion of existing farm, forest or barren land to urban land-cover types (Jones,

2002). My results implied that migration was more attracted to cities with promising economic conditions and undergoing fast urbanization paces.

In the following chapter, vegetation fraction (chapter 3) and NTL time series (chapter 4-5) were compared against each other using three candidate relationships, namely, linear, quadratic, and cubic models, in order to confirm the Environmental Kuznets Curve (EKC) theory.

Chapter 6

6. Testing EKC theory: What is the relationship between urban vegetation and nighttime brightness across pan Pacific cites?

6.1. Introduction

My goal in this chapter is to evaluate the relationship between human development and environmental quality within, and across, cities at a pixel level using results from previous chapters. I used vegetation fraction value (Chapter 3) to represent urban vegetation cover while NTL time series (Chapter 4) was used as a proxy to urban economic development.

Cities worldwide strive to grow not only economically strong but also environmentally sustainable. Understanding relationships between urban activity and the environment has critical implications for achieving long-term sustainability and evaluating policy decisions (Panayotou, 1997). Declines in environment conditions such as the loss of vegetation (Chapter 3), highlight the need for stricter regulations and government efforts that prioritize environmental recovery over economic development. Conversely, improvements in the environmental conditions within cities suggest sustainable and planned development.

Despite the fact that the relationship between urban economic development and the impact on environment has been widely debated (Schaltegger & Synnestvedt, 2002), there is no consistent framework from both theoretical and empirical studies that provide suggestions as to how cities can develop in a sustainable and environmentally friendly manner. Many studies conclude an irreversible and monotonic impact on the environment brought about by human development primarily as a consequence of economic activities (Akbostanci, Türüt-Aşik, & Tunç, 2009; Stern, 2004). High rates of economic activity such as extraction of natural resources typically produce large quantities of waste and pollution (Hoornweg, Bhada-Tata, & Kennedy, 2013). For example, Fodha & Zaghdoud (2010) found a linear trend between per capita CO_2 emissions versus per capita GDP in Tunisia. Similarly, Akbostanci, Türüt-Aşik, & Tunç (2009) showed that per capita CO_2 emissions increased monotonically with per capita income in Turkey.

Others argue that the negative impact of human development in cities decreases over time in response to more efficient production (Bartlett, 1994; Beckerman, 1992). These studies suggested that urban environments ultimately reduce the impact of environmental degradation through increased wealth and education. For example, Panayotou (1997) found across 30 countries the level of ambient SO2 (a key indicator of pollution) decreased as GDP per capita increased. A more recent study (Aldy, 2005) investigated the relationship between the consumption of CO_2 per capita versus income per capita in the United States, and suggested a similar trend where CO_2 levels reduced with increasing income.

Schaltegger & Synnestvedt (2002) suggested one hypothesis for the often conflicting conclusions of these previous studies. First, a lack of consistent and compatible data, with which to assess both environmental degradation and economic activity, largely complicates the process of comparing cities across time and space. Common datasets on economic development include statistics on local Gross Domestic Production (GDP) and income level. However, these were commonly compiled by local census departments, which often do not share similar scales and resolutions in terms of temporal updates and spatial details. Various measurements of airborne and water pollutions were frequently used as the basis of environmental performance (Grossman & Krueger, 1991; Selden & Song, 1994; Shafik, 1994). However, using pollution emissions as an indictor of environmental performance received criticism (Stern, 1998). For example, the Hecksher-Ohlin hypothesis (Heckscher, 1919; Ohlin, 1952) suggested that developing countries are more likely to produce goods that are labour- and resources-intensive given their inexpensive and abundant resources. More developed countries tend to focus on tertiary goods and services and human capital development with a relatively small environmental footprint. Additionally, it is difficult to compare spatially and temporally inconsistent measurements over time that are exclusively recorded for a specific production or industry type and are not representative of other environmental issues over the entire cityscape (Cadenasso, Pickett, & Schwarz, 2007).

Environmental Kuznets Curve (EKC) theory hypothesizes a U-shaped relationship where environmental performance decreases at the early stage of economic development and recovers as the economy reaches a certain turning point (Kuznets, 1955). Indicators such as income levels and measurements of certain pollutants are often used to represent economic development and environmental performance, respectively. Appling EKC based approaches at both inter- and intra- city scales provides insights into the balance between human activity and environmental sustainability. For example, at the urban core, downtown or city centre there may be low vegetation cover and high levels

of human development and density, whereas outer suburban areas may be more likely to exhibit an opposing pattern with increased vegetation cover and lower human activities. As a result, the relationship between human development and environment performance is not a simple linear decline and will likely vary within and across cities.

Indicators of both the economic and environmental conditions within city environments range from simple tabular data to more complex spatially explicit predictions. In comparison to statistics on airborne and water pollution, or industrial output that have commonly been used for EKC analysis, changes in urban vegetation cover is a relatively direct measurement of the environmental conditions within a city with urban greenspace being shown to be indicative of effective environmental management and government regulation (Zhao et al., 2016). Conversely declining urban vegetation cover has been linked to intensification of human development and increases in impervious surfaces (Quigley, 2002, 2004). Conventionally, information on urban vegetation cover has been generated from land use or land use maps, both of which represent vegetation cover as a categorical variable (e.g. vegetation vs. non-vegetation). Vegetation cover can also be effectively observed from satellite imagery due to the reflective properties of foliage in the visible and near infrared regions of electromagnetic spectrum.

Changes in satellite-derived nighttime light (NTL) intensity has also been shown to be a good indicator of economic activity particularly in cities (Bennett & Smith, 2017; Small & Elvidge, 2013; Small et al., 2005). The most common and perhaps the earliest interpretation of NTL is as a proxy to economic development, on the assumption that a brighter city is a wealthier city (Doll, Muller, & Morley, 2006). The main benefits of NTL compared to conventional socio-economic data is its compatibility and consistency over time and its capability of providing reliable estimates especially for undocumented regions or areas with poor census data. Although the use of remote sensing data has been demonstrated in urban studies (e.g. Seto & Kaufmann 2003; Zhang, Pandey, & Seto 2016), uncoupling the relationship between human development and the environment has not been fully articulated. There is also a need to examine whether trends in these metrics are generalizable across and within different cities.

In this chapter, I statistically tested the relationship between economic and environmental conditions on fine spatial detail (30-meter spatial resolution) of 25 cities across the pan Pacific region from 1992 to 2012.

6.2. Materials and methods

Two sets of variables were needed for testing the EKC theory. Firstly, intercalibrated NTL time series (section 6.2.1) were used as a proxy for urban economic development (x-axis on EKC). Secondly, vegetation fraction values (section 6.2.2) were used as an indicator for environmental conditions (y-axis on EKC). A pixel-based model fitting procedure was used to find the optimal relationship based on Akaike Information Criteria (section 6.2.3). Parameters of the optimal model were then used to determine the directionality and magnitude of the relationship between VF and NTL (section 6.2.4). Lastly, a join-count statistics was used to examine the spatial autocorrelation of each individual models (section 6.2.5).

6.2.1. Human development and economic indicator—Nighttime lights

I used NTL images acquired by the Defense Meteorological Satellite Program (DMSP) from 1992 to 2012 (https://ngdc.noaa.gov/eog/viirs/download_dnb_composites.html). Cloud-free NTL composites measured the brightness level of the target and have been widely used to represent human activities. In order to capture changes in the relationship between NTL and vegetation cover, I excluded pixels that I re already bright at the beginning of the time series (i.e. 1992) on the assumption that they would not undergo any more significant brightness changes for the analysis period. To be defined as a bright pixel, it had to exceed the 95-brightness percentile of the entire time series of a given pixel.

6.2.2. Environment condition indicator – Vegetation fraction

I used the annual vegetation fraction (VF) images derived from spectrally unmixed Landsat composites as proxies to environmental condition for the 25 cities from 1992 and 2012. VF images I re developed using spectral unmixing analysis (SMA) which assumes each pixel contains multiple pure land-cover materials, known as endmembers, and decomposes each pixel into fractions of those endmembers. Chapter 4 developed an annual VF layer at a 30m resolution for all 25 selected cities using annual Landsat composites.

6.2.3. Model fitting

Common approaches of examining EKC theory generally utilise two sets of time series variables, one representing economic development and the other indicating the environmental performance. Various forms of statistical fits have assessed the validity of the EKC framework (Figure 6.1) and three common relationships from previous literature, namely, linear, quadratic, and cubic models. I then attempted to identify the most appropriate model for each qualified pixel within each city by comparing those three relationships (Figure 6.2). In theory, a linear model represents monotonic and irreversible relationship while a quadric model is likely indicative of the EKC theory. A cubic model is more complicated than linear and quadratic relationships, suggesting a rather more modulating relationship between vegetation fraction and nighttime lights.

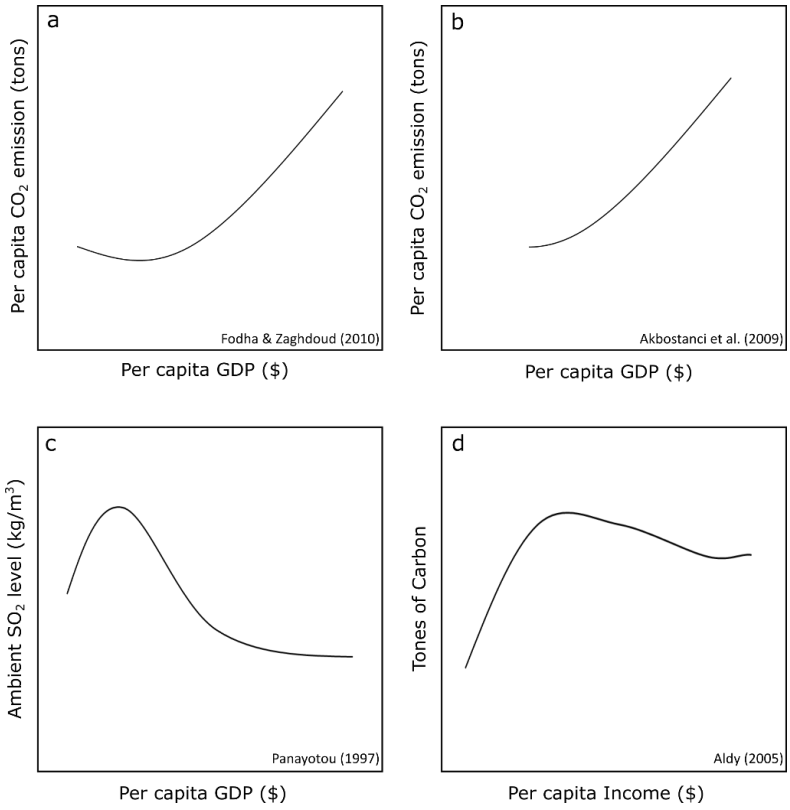

Figure 6.1 An Illustration of previous studies attempting to quantify the relationship between economic indicators versus an environmental variable. (Note that all figures have been simplified to only highlight the relationship between the corresponding variables.

Specifically, I applied model-fittings for each of the pixels within the city limits using the three models and selected the best model based on two criteria. First, the best model must have an AIC score (Akaike Information Criteria) that is at least two units lower than other two competing models (i.e. $\Delta AIC \geq 2$)

(Burnham & Anderson, 2003; Gergel et al., 2004). The second criteria relied on *F* tests ($p < 0.05$) to eliminate statistically insignificant models that may score a low AIC value (Gergel et al., 2004). A water mask (Chapter 3) was applied to exclude water bodies from model fitting processing.

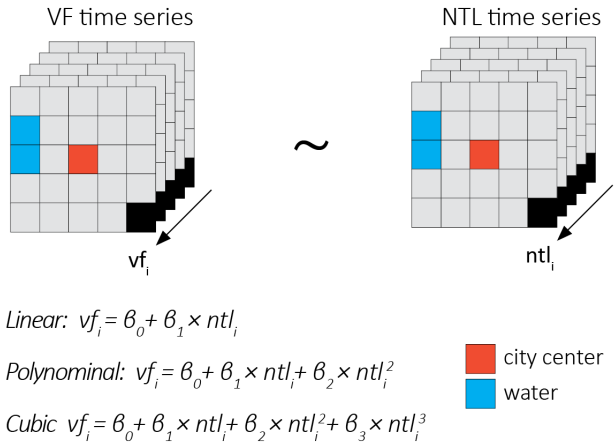

Figure 6.2 Vegetation fraction (VF) time series regresses against Nighttime time light (NTL) time series pixel by pixel. Three candidate models (linear, quadratic, and cubic) I re used to determine the most appropriate model based on AIC score and statistics significance. The red pixel symbolizes where the city center is while the blue pixel represents water which was excluded from all subsequent model fitting.

6.2.4. Directionality and magnitude

Once the best model form was identified, I extract the leading coefficient (i.e. the parameter of the variable with the highest exponent) and its associated t test. For each pixel with a statistical ($p < 0.05$) trend, I then determined both the direction and magnitude of the trend (i.e. a positive vs negative leading coefficient). A positive leading coefficient can be interpreted as a growing vegetation with a booming economic development.

6.2.5. Join-count statistics

In order to examine the spatial patterns of the trends within individual cities I computed the global spatial autocorrelation index using join-count statistics (Cliff & Ord, 1970). Join-count statistics are widely used to measure spatial association for categorical data (Getis & Ord, 1992). This chapter used

the Queen case contiguity to define neighbouring focal cells and three possible combinations of neighbouring cell components, typically known as BB (black-black), WW (white-black), and BW (black-white) joins. A BB join indicated that the neighbouring cells have been assigned to the same model while a WW join indicated that none of the adjacent cells had a statistically significant relationship. The BW join indicated that neighbouring cells have been assigned different trends.

Once assigned join-counts I re examined in comparison to a random distribution to establish if any trends within cities were clustered. I calculated the ratio between total join counts for each individual model and values from a random spatial pattern (refer to as $R_{j/r}$ thereafter). Theoretically, with a higher ratio, I would expect a stronger spatial association.

Lastly I divided the classic EKC figure into 4 quadrants to compare and contrast differences across cities through time representing (i) initial development with rapid environment degradation, (ii) slowing environmental degradation with a more mature economy, (iii) economic prosperity with a recovering environment and finally (iv) a prosperous economy and sustainable environment.

6.3. Results

6.3.1. Model selection

Only pixels with statistically significant trend were qualified for model fitting. Eight cities had more than 70% of their area consisting of statistically significant ($p < 0.05$) relationships. More than half of the cities (i.e. 19 out of 25) had over 50% of pixels successfully fitted to one of the three relationships (i.e. linear, quadratic, or cubic). Overall, coastal cities (e.g. Shenzhen-Hong Kong, Vancouver etc.) had a relatively fewer qualified pixels compared to inland cities.

6.3.2. Goodness of fit

A linear relationship indicates a monotonic trend between VF and NTL while quadratic or cubic models were indicative of at least one directional change between urban VF and NTL with the correlation coefficient providing an indication of goodness of fit (Figure 6.3). Overall, despite the fact that linear models were the most popular candidate relationship (Figure 6.4), they explained the least of the variation between NTL and VF compared to quadratic and cubic models. Four cities from China (i.e.

Changsha, Shenzhen, Shanghai, and Tianjin) exhibited cubic patterns rather than quadratic. Phoenix and Tokyo had almost an equal proportion of linear and quadratic models comparing to the rest of the cities.

The majority of Asian cities showed a dominating pattern of cubic relationships when compared to North American cities (Figure 6.4). Cities from high income countries were more dominated by linear models. It was also apparent that cities located in tropical and temperate climate schemes were more likely to have more quadratic and cubic models than cities from continental and arid climate schemes.

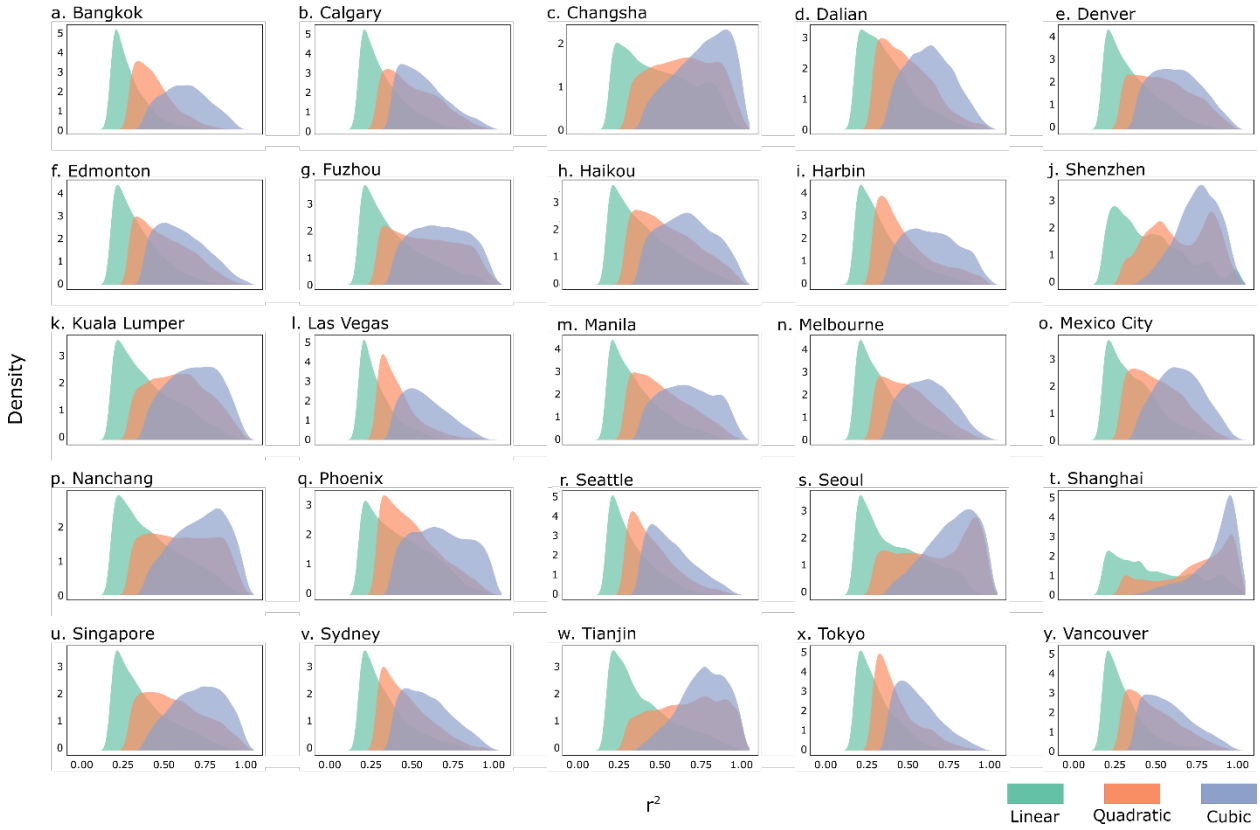

Figure 6.3 Histograms of r^2 values for each selected model.

6.3.3. Spatial distribution of fitted models

Pixel-based model fitting allowed visualization and investigation of the spatial distribution of all fitted models. Cities showed varying patterns of model distribution. For example, linear relationships dominated the urban centers of Tokyo and Shenzhen (Figure 6.5a-b) while in Manila and Shanghai, city centers were characterised by more quadratic models (Figure 6.5d-e). Another noticeable difference among cities were the varying range of leading coefficients for each model. Cities such as Calgary (Figure

6.5c) had a narrower range of coefficient values (i.e. from -0.31 to 0.27) compared to cities such as Shanghai (i.e. range from -3.23 to 2.79).

Although clusters of pixels within each city were apparent, the spatial distribution of these clusters varied from city to city. Figure 6.6 shows how strong the spatial association was for each model within a city. Quadratic relationships tended to have a similar or slightly lower spatial association than cubic models except for Vancouver and Tokyo. Interestingly, I also noticed that coastal cities had an overall higher spatial association than inland cities.

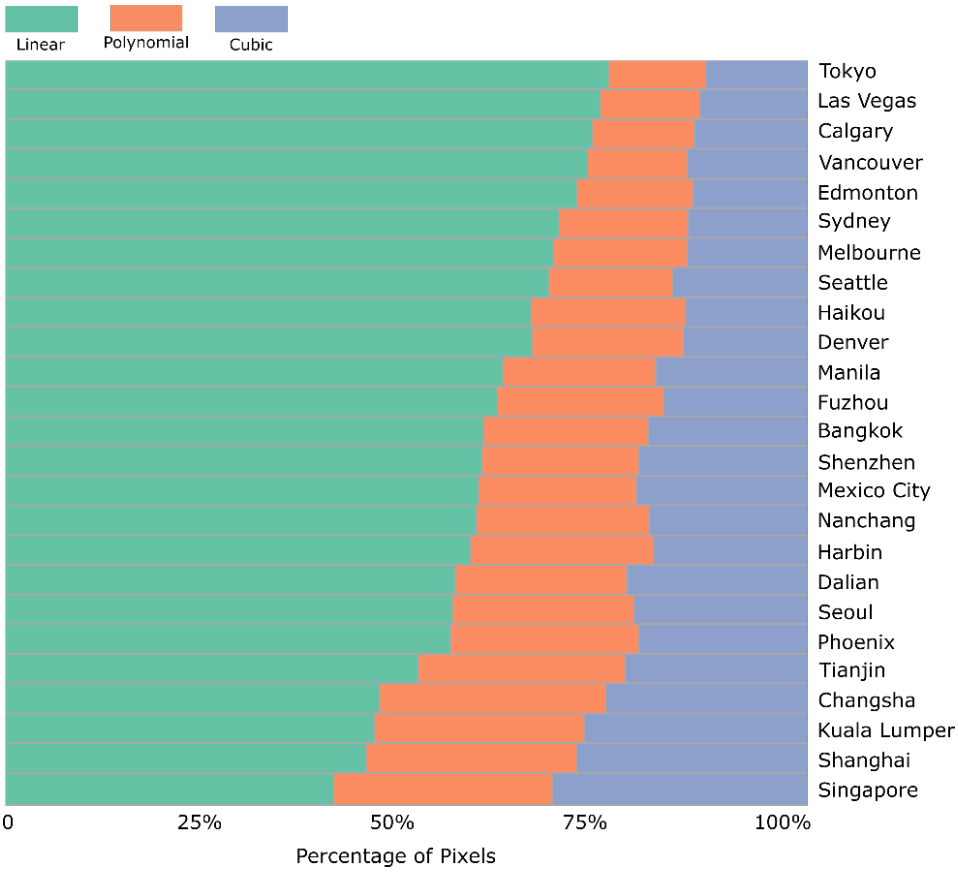

Figure 6.4 Percentage of pixels for each selected best model type at a city level. Only pixels with significant changes were used for calculating the percentage of each model. Pixels that did not fit any of the three functions were not concluded.

6.3.4. Locations of cities on an EKC

I found no cities located in quadrant i, confirming that all 25 cities have likely passed the stage where environmental degradation drastically outpaces economic growth (Figure 6.7). Overall, four out

of six cities positioned in quadrant ii were located in Asia, with the exception of Las Vegas (lav) and Phoenix (phx). Interestingly, other cities from Asia such as Shanghai, Seoul, and Bangkok have been grouped with cities from high income North American cities. The majority of quadrant iv cities were located in relatively more developed regions with a minimal increment on brightness but noticeable increases in vegetation. Cities that experienced noticeable vegetation fraction decrease were mostly from Arid or Continental climate schemes.

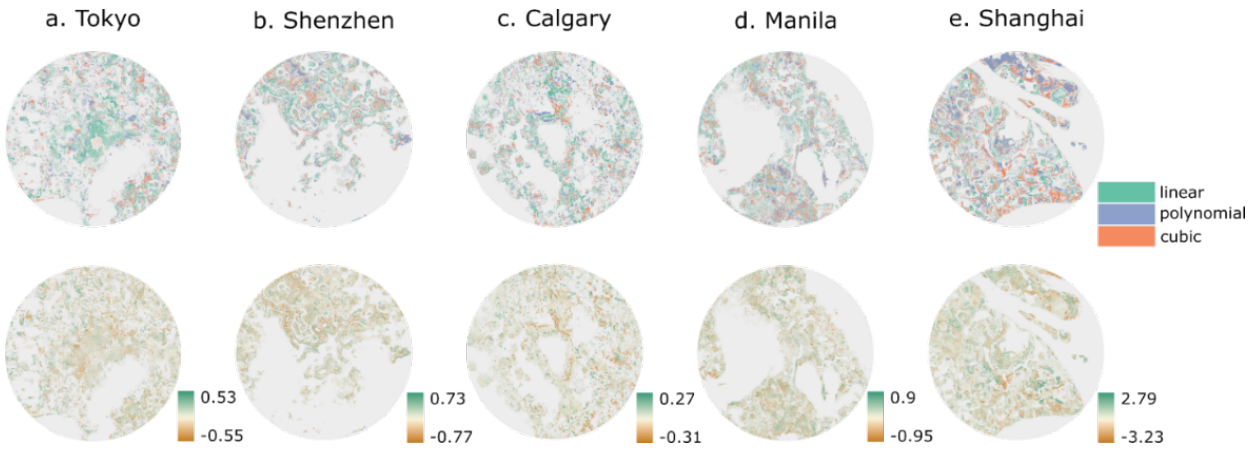

Figure 6.5 The top panel represents the best model selected based on AIC score and F-test at pixel level. Coefficients of leading variables for each selected model were shown in the bottom panel. The sign of each coefficient determines the directionality of the relationship while the absolute value of the coefficient indicates the magnitude of impact of NTL on VF.

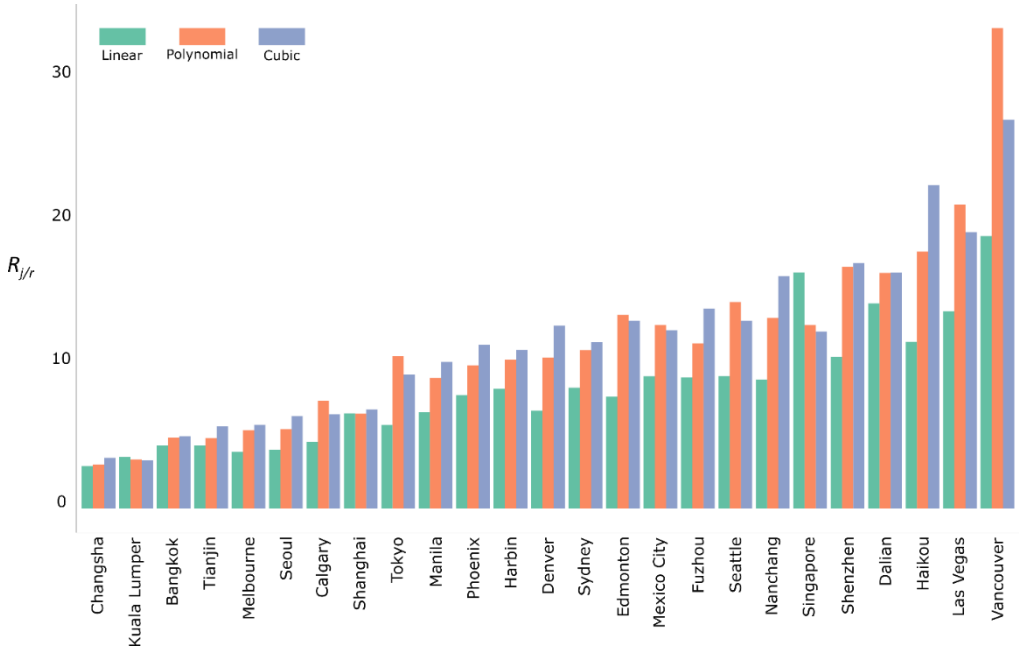

Figure 6.7 Spatial autocorrelation represented by the ratio between total counts of joins and a random spatial pattern calculated by Join-count statistics for each model. Theoretically, with a higher $R_{j/r}$, I would expect a stronger spatial association.

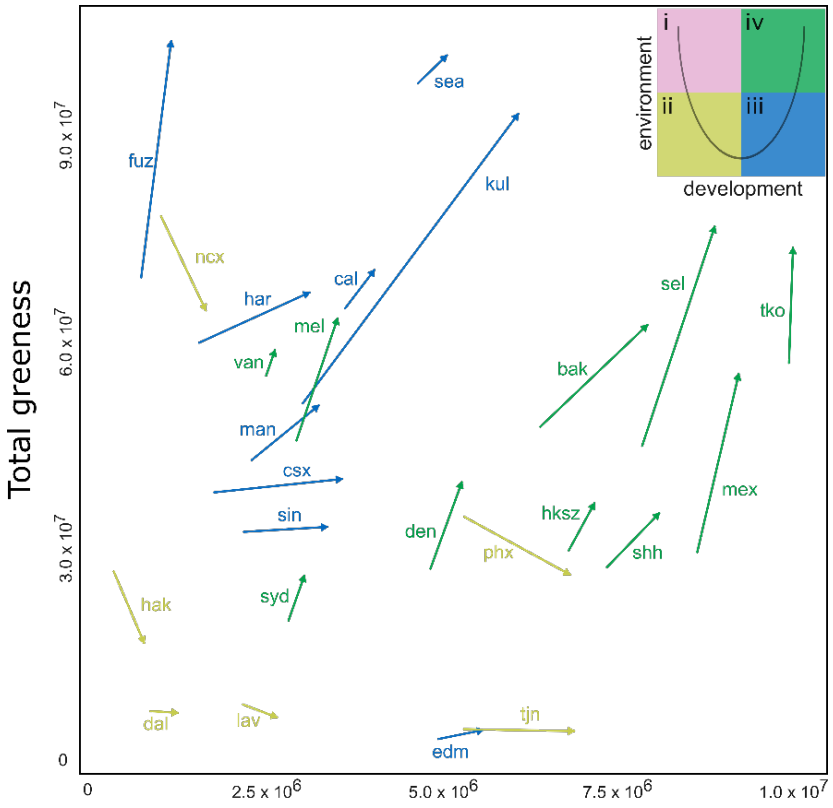

Figure 6.6 Positions of the examined cities on the EKC curve. It classifies the 25 cities using the summed value of NTL and VF pixels excluding water.

6.4. Discussion

Questions as to whether EKC trends exist were examined using various socio-economic and environmental indicators yet with a variety of contradictory conclusions. I examined the validity of the EKC hypothesis at both inter and intra urban scales. To do so I examined the relationship between human development and the environment represented by nighttime lights (NTL) and vegetation fraction (VF) by fitting a variety of model forms.

I found that linear models were the most dominating relationship across the wide range of examined cities, particularly in high-income cities from North America and Oceania. On the other hand, the pattern was less obvious for middle and low-income cities. For example, the city of Haikou in China is a middle high-income city but it was also dominated by linear models. In terms of spatial-temporal pattern, I found that in general, sub-urban in Asian cities experienced more temporal changes of VF and NTL comparing to high income cities. I also noticed dramatic differences of spatial autocorrelations (Figure 6.6). Across the pan Pacific cities, there was little evidence of quadratic or cubic relationships (Figure 6.4). Although quadratic models were not the most dominating among all three tested models, I still found certain hotspots or clusters of areas displaying a typical EKC theory. These hotspots of quadratic models also demonstrated a stronger spatial association comparing to other two candidate models (i.e. Tokyo, Vancouver). Together, these two results indicated that the hypothesized EKC likely exists within city confines and is likely highly clustered. For example, in spite of a general vegetation decrease in Shanghai's metropolitan area, a substantial vegetation increase was observed on Chongming Island located to the north of Shanghai city centre. The integration of both within, and across, city comparisons furthers the discussion of the existence of EKC trends and avoids generalizing entire cities using measurements from a single dataset. Both positive and negative parameters were present in all three tested model by examining the parameter with the highest order. Overall, our findings, using vegetation fraction and artificial light brightness at a pixel level, suggest that at least in certain part of the cityscape, the environment recovers with a growing economy.

Clean energy supplies, urban greenspaces, and efficient public transportation systems are being aggressively built in many cities worldwide. Evidences suggest that wealthier and more developed cities place a higher value on environmentally conscious policies. For example, despite its strikingly high urban density, the city of Hong Kong reserves much of its landmass for parks and nature reserves (Corlett, 1999; Ng, 2010). Since 1976, the government of Hong Kong enacted the Country Park Ordinance to

initialize, monitor, and manage Hong Kong's urban parks and reserves. In 2011, approximately 40% of Hong Kong was forested (Ng, 2010).

There were a few potential caveats in interpreting the patterns that I found in this chapter. First of all, even with correction and calibration, the well-known saturation issue of NTL data could cause total brightness values to plateau, particularly in more developed high income cities (Zhang, Schaaf, & Seto, 2013). Secondly, the prevalence of more efficient lighting technology could potentially lead to a decrease in total brightness value with a growing economy, explaining the minimal increase or even a decrease in total brightness. However, I found limited literature on how exactly the shift in lighting source affects the brightness values observed by VIIRS sensors. Thirdly, according to previous research, cities that were historically green were more likely to recover from environmental degradation. The results suggested that the majority of vegetation decreases occurred in Arid and continental climate schemes where vegetation grows expectedly slower than temperate and tropic areas.

Much of the current research uses data with a relatively short time span that is unlikely to capture the full time frame over which the Kuznets curve is based upon. As a result, cities are undergoing transitions across different stages of the curve in terms of economic development and environment recovery. Although in this chapter, I found that every city exhibited some degree of vegetation recovery, the presence of EKC does not guarantee that economic development is able to automatically resolve environmental degradation issues. One of the key assumptions of EKC is that the economy does not suffer from a declining environmental quality. EKC assumes that economy and production will remain growing regardless of the environmental performance (Stern, Common, & Barbier, 1996). There is a chance that, even with the existence of statistically significant EKC, vegetation loss occurred at the take-off stage of the economy has crossed the ecological capacity threshold irreversibly. Many vegetation-related ecological properties such as biodiversity were not as easy as pure "vegetation" to capture using satellites. As a result, it is challenging to quantitatively test the robustness of this assumption. Ultimately, human development is believed to be highly relevant to environmental performance (Arrow et al., 1995). Extending from current chapter, future research could incorporate additional quantitative and spatially classified climate and economic schemes to further verify the existence of EKC theory and even potentially identify list of drivers causing the varying developing patterns observed in this chapter.

Chapter 7

7. Conclusion

Contemporary cities are collectively more dynamic, multi-dimensional, and complex than ever before. Cities worldwide strive to grow not only economically strong but also environmentally sustainable. The balance between the economy and environment has been challenging particularly for cities in the pan Pacific region, which is seeing some of the most rapid urban growth rates globally. Urbanization and its associated physical and socio-economic characteristics are interacting at a much faster pace and occurring at a range of spatial and temporal scales.

This work applied time series of satellite images, chronically monitoring the relationship between urban environment and economics. From pixel to cityscape scale, this approach has the advantage of being intuitively appealing, simple to reproduce and implementable in practical urban planning and management. The derived information is useful for planners to compare and visualize land use patterns as well as for policy-makers to better understand inter-and intra- city development in polycentric and highly connected global urban systems.

7.1. Research innovation

This dissertation provides key innovations for characterizing regional urbanization dynamics using open access remotely sensed images:

- The integration of the classic concentric ring model and gap-free time series of satellite data unlocked new ways to informing urban environment and socio-economics dynamics (Chapter 3).
- Urban vegetation was derived using an innovative spectral unmixing approach on an entire time series image stack, allowing an improved understandings of vegetation in urban environments across the pan Pacific region (Chapter 4).
- A classic econometric model was used to examine the casual relationship between conventionally collected census information and advanced remote sensing nighttime lights data (Chapter 5).

- Relationships between urban environment and economic development were tested using remote sensing derived proxies. The results advanced our understanding of changing environment and socio-economic characteristics from pixel to regional scales (Chapter 6).

7.2. Answers to proposed research questions

7.2.1. How can remotely sensed derived metrics inform urban environment and socio-economics dynamics within and across cities in pan Pacific region?

Remote sensing data, particularly Landsat and NTL time series demonstrated advantages over conventional tabular formatted census data. Varying political and cultural backgrounds within the pan Pacific region limited and complicated inter- and intra city comparisons. Remote sensing derived metrics offered measurements that were not only spatio-temporally consistent but also comparable across different cities, unlocking new ways for regional and global scale urban studies.

Two spectral indices (i.e. EVI and NDBI) group 25 pan Pacific cities into 5 classes. The average silhouette width ranged from 0.37 to 0.60, while the ratio of the between to the total sum of square (BSS/TSS) ranged from 69% to 92% for EVI and NDBI respectively. Dynamic Time Warping (DTW) derived separability metrics showed an averaged distance of 0.36 (EVI) and 0.28 (NDBI) among all cities. Spectral unmixing analysis successfully estimated vegetation fraction at a sub-pixel level. Validation using high spatial resolution Google Earth images showed a correlation coefficient ranging from 0.66 to 0.77.

Comparing to categorically dividing the cities into land use or land-cover classes, spectral indices and vegetation fraction images offered continuous measurements of the urban environments and socio-economic dynamics that were valuable for further modelling processes.

7.2.2. What models exist to examine the relationship between urban environment and socio-economic develop over time and space?

Linear trends between urban environment and economic development are assessed to be the most dominating among all three tested relationship (i.e. linear, quadratic, and cubic). Remote sensing derived metrics, namely vegetation fraction (VF) and nighttime lights (NTL) time series were used as a proxy to urban environment and economic respectively.

The result implied that the vegetation changes within cities in pan Pacific regions were monotonic and irreversible. Despite the dominance of linear models, EKC-like quadratic models also existed within all examine cities. In majority of the cities, quadratic models tended to be more spatially clustered compared to linear and cubic models. The results statistically quantified the behaviour of how vegetation responses to city brightness changes, furthering the discussion of EKC theory by integrating remote sensing observations as means of measuring environmental performance and human development, bridging the gap between conventional econometric theories with Earth observation platform.

7.2.3. What similarities and differences exist across cities in the pan Pacific region both spatially and temporally?

Cities showed both inter- and intra variations in terms of spatial and temporal changes of vegetation and nighttime lights brightness. Regional similarities were found (Chapter 3) particularly in Asian countries where the relationship between vegetation fraction values and NTL brightness was less linear than North American cities. Climatically, vegetation dynamics tended to be more alike within the same climate scheme (Chapter 6) among different cities.

In terms of spatio-temporal patterns of urban environment and economic development, I found three pairs of urban environments that were strongly similar to each other namely, Melbourne with Sydney; Tianjin with Manila; and Singapore City with Kuala Lumpur.

Characterizing the relationships between VF and NTL revealed new patterns. Mostly, Asian cities showed a dominating pattern of cubic relationships when compared to North American cities. While cities with higher economic activity level were more dominated by linear models yet patterns were less obvious for middle and low-income cities.

7.2.4. Characterizing urban built-up and greenspace over time and space

A key element of developing an understanding of urbanization processes globally is the consistent monitoring of cities over space and time (Sexton et al., 2013). Detecting and analyzing the spatio-temporal patterns of urban environments have become an increasingly critical research topic with practical management applications. Early studies indicated that a city can be divided into a series of

expanding rings, also known as the concentric ring model (Burgess, 1925). This model has been used widely even for cities with less regular concentric growth patterns.

In Chapter 2, built upon the classic concentric ring model, I used remote sensing derived spectral indices, namely the Enhanced Vegetation Index (EVI) and the Normalized Difference Built-up Index (NDBI). As expected, patterns from these two indices illustrated opposing trends. Spatially, urban cores had a much higher NDBI and lower EVI than outer areas. I also observed the existence of a developing multi-core pattern in cities where both EVI and NDBI did not follow a simple linear trend. Temporally, urban vegetation showed much greater variation than built-up marked by results from Dynamic Time Warping (DTW) where the separability among each trajectory was much greater for the EVI trajectories than for NDBI's.

Commonality can still be found among the 25 cities however. Two sets of K-means cluster analyses were applied to group spatially and temporally similar cities. K-means clustering analysis indicated an optimal number of five classes. As anticipated, the majority of the urban environments in developing countries experienced noticeable development rates compared to the urban environments in more developed regions. I summarize the degree of similarity both spatially and temporally across urban environments in the pan Pacific region. In total, there are three pairs of urban environments consistently being grouped together, namely, Melbourne with Sydney; Tianjin with Manila; and Singapore City with Kuala Lumpur. In contrast, cities such as Las Vegas and Vancouver had less similar features both spatially and temporally with any of the other urban environments.

Compared to the traditional spectral indices the integration of spectral unmixing and Theil-Sen (TS) estimated trend slopes offers increased ability to compare and contrast vegetation across urban environments (Chapter 3). Spectral indices for given pixels can be difficult to compare across different urban environments over time. Spectral unmixing analysis (SMA) demonstrated new ways to study urban greenspace dynamics. A spectral library of spatially and temporally pure pixels successfully estimated vegetation fraction value at a sub-pixel scale for all cities. When using annual vegetation fraction images, cities located in high latitudes (e.g. Harbin) and particularly mountainous regions (e.g. Vancouver) may require extra caution. In those cases, pixels with low vegetation fraction may not necessarily indicate intense urbanization, but rather low vegetated land-cover types, such as bare rock, ice, and snow.

Temporally, there were four types of urban vegetation changing patterns. The first included cities such as Shenzhen-Hong Kong area which exhibited a gradual decline in vegetation from the urban center through to the outer areas. The second set of cities includes cities such as Las Vegas that had consistently increasing vegetation slope as the distance from urban center increases. The third type contains cities including Shanghai where vegetation mostly decreased over time. And lastly cities such as Vancouver, Tokyo, Sydney, Edmonton, and Calgary, where vegetation changes were relatively minimal as indicated by a near zero vegetation change trend. These types of cities were mostly located in developed regions.

7.2.5. Characterizing social-economic dynamics over time and space

Contemporary cities are collectively dynamic, multi-dimensional, and complex. Urbanization and its associated physical and socio-economic characteristics are interacting at a much faster pace and occurring much beyond local level. In this work, such characteristics were reflected by inter- and intra-city variations derived from the nighttime lights imagery for 25 cities in pan Pacific region.

7.2.6. Contrasting effects of GDP and population on NTL

Large inter- and intra-city variations of urban economic activities were apparent as indicated by nighttime lights (NTL) time series (Chapter 4). Tokyo and Shen Zhen-Hong Kong had over 75% of land with active brightness prior to 1992 while most cities in China had less than 10%. Cities such as Shanghai and Tianjin experienced substantial growth in their economies over the study period with over 50% growth. Other cities, however, experienced less economic growth with approximately 75% of land remaining undeveloped.

Across all cities, both population and GDP played a major role in directing changes of NTL. According to the Granger causality test, the brightness of cities followed increases in both population and GDP equally and neither population nor GDP alone is responsible for increasing the NTL. Unexpectedly, I found that GDP and NTL "granger caused" population growth suggesting that population change was the outcome rather than the cause of GDP and NTL growth. A wealthier and more economically active city would likely to attract more population.

Population and GDP revealed contrasting effects on NTL trends between stable and more dynamic cities. It has long been thought that population was the primary driver of urban growth while economic development was an outcome of booming populations. For cities with minimal NTL changes over the analysis period, the causal relationship from NTL to population was not statistically significant yet changes in population "granger caused" both GDP and NTL. This implied that in cities with relatively stable NTL, population and GDP were likely to the key drivers of NTL changes but not the other way around. Previous work (Dietzel et al., 2005; Satterthwaite, 2009) found that rather than growing population alone, it was the high consumption lifestyle, economic and political decisions that led to urbanization.

In fast changing cities however, growth in NTL and GDP unexpectedly led to an increase in population. There was no significant causal association between GDP and NTL, suggesting that in rapidly changing populations the increases were driven by the economic development. In those cities, the main source of population increase was through immigration from rural and neighboring areas, involving densification and conversion of existing farm, forest or barren land to urban land-cover types. Chapter 4 demonstrated that migration was more likely to be attracted to cities with promising economic conditions and undergoing fast urbanization paces.

7.3. Testing the EKC theory

The relationship between urban development and environment appeared to be linear in the majority of the cities (Chapter 5). There was little evidence of quadratic or cubic relationships. A linear relationship indicated a monotonic irreversible relationship between urban vegetation fraction (VF) and NTL.

In general, I demonstrated that within the study period (i.e. 1992-2012), the hypothesized Environmental Kuznets Curve (EKC) was not the dominating relationship among all three tested models (i.e. linear, quadratic, and cubic). Linear models were the most dominating model yet explained the least amount of variation of all marked by an overall relatively low r^2 value.

The hypothesized EKC likely existed within city limits and was highly clustered. Our findings, using vegetation fraction and artificial light brightness at a pixel level, suggested that at least in certain part of the cityscape, the environment recovered with a growing economy. Cities that showed a dominating

vegetation decreasing trend could also contained substantial vegetation recovery particularly in wealthy cities where clean energy supplies, urban greenspaces, and efficient public transportation systems have been aggressively built.

The majority of Asian cities showed a dominating pattern of cubic relationships when compared to North American cities. While higher income level cities were relatively more dominated by linear models, such patterns were less obvious for middle and low-income cities. Chapter 5 also showed that cities located in tropical and temperate climate schemes had more quadratic and cubic models than cities from continental and arid climate schemes likely due to varying phenological responses to local climate conditions.

7.4. Research challenges

7.4.1. Urban boundary

Like other ecosystems, urban environments rarely have definitive boundaries. Attempts to use two sets of urban boundaries, namely, conventional administrative boundary (Chapter 3) and a 60-km circular buffer (Chapter 4, 5, and 6) posted one of the main challenges for urban research in this thesis. The integration and connectivity among today's urban environments had outpaced the conventionally defined city administrative boundaries. The trade-off however was the ease of integrating census-based data with remotely sensed data when using administratively defined boundaries. The key factors determining how to define urban boundaries in remote sensing studies include the consistency, availability, and the quality of local census data. Administrative boundaries can be considered when high quality census data were available. While an artificially drawn circular buffer boundary was free from the local jurisdiction systems, offering a unique alternative for urban studies that focused less on social and economic aspects and more towards ecological and environmental dynamics.

7.4.2. Urban heterogeneity

Another major challenge was a function of urban environmental heterogeneity where each medium resolution pixel (i.e. 30m) can contain more than one land-cover or land use types. Although spectral unmixing analysis (Chapter 4) showed potential in time series urban vegetation studies, the process of

selecting spectrally pure endmembers could be improved using a more systematic procedure. Regional and global scale studies would likely to involve cities located in varying climate and ecologically complex locations, causing difficulties in collecting spectrally consistent yet global comparable endmembers. Given that, this dissertation does not directly compare the absolute vegetation fraction values. Rather I computed the rate of vegetation for each individual city at a pixel level using Theil-Sen slope, a metric that was more comparable both within and across cities. Such a comparison however limited my ability to compare and contrast cities on an annual basis.

Additionally, spectral responses from non-forested vegetation (e.g. agriculture, golf courses) were likely to be mixed with more ecologically functional vegetation (e.g. parks, grassland). Highly responsive pixels such as snow and ice on the other hand are spectrally similar to pixels within cities, both of which had a high reflectance throughout the Landsat spectral bands.

7.4.3. NTL Saturation

Due to the limited radiometric range of NTL sensors, NTL data were often saturated in bright areas such as at the city centre. Zhang et al. (2013) incorporates a series of vegetation images to de-saturate NTL data on the assumption that there is an inverse relationship between vegetation fraction values and NTL brightness. However, the inclusion of another input variable (e.g. vegetation) complicated the process of interpreting statistic analysis particularly in Chapter 6 where vegetation was compared directly against NTL. The use of saturated NTL data potentially could hinder our ability to capture to full temporal profile in brightly lit areas.

7.4.4. High quality census data

Characterizing the socio-economic nature of cities was still primarily remained the domain of census data. Local census and economic data used in Chapter 4 had varying collecting intervals and qualities. In many developing regions, census data were collected infrequently with questionable qualities. The scarcity of well maintained census data was one of the main obstacles when comparing against remotely sensed derived information that was derived using an institutionally different collecting approach and scale.

However, local census data still play an important role in urbanization researches. One of the main challenges of this dissertation, or remote sensing derived model in general, was the lack of reliable validating data. High quality census data can not only be used in the model fitting process but also provide an alternative sources for model validation and ground-truthing purposes.

7.4.5. Future research opportunities

Real-time accurate information derived from remote sensing devices offers wall-to-wall evaluations of new policies and regulations. Previous literature highlighted the gap between on-ground initiatives and the associated spectral responses from remote sensing sensors (Liu et al., 2005). With new remote sensing sensors being designed to continuously image the Earth, it is possible for future research that quantifies such delays as a measurement of local policy effectiveness.

Beyond the local scale, many global remote sensing products focused on urbanization are now available (e.g. Román et al., 2018). Regional to global scale, temporally informed, urban research is starting to emerge. However, a more comparable metric is needed for comparing and contrasting cities on an annual basis, particularly for characterising vegetation and other ecological dynamics. Given the diverse climate and ecological conditions, future research should focus on developing metrics integrated with climate variables to account for local climate variations.

Landscape metrics (e.g. measurements of area, density, and edge) have been used widely with remote sensing data. The spatial configuration of each city offers a unique perspective of the current land use patterns, effectively informing future plans. However, the relationship between the landscape configuration and urban temporal changes is less explored (K. C. Seto & Fragkias, 2005). Relating time series data with landscape metrics will be critical to better understand the rate of landuse changes in a language that is more familiar to urban planners.

An even less charted topic is the marriage between advanced remote sensing data and conventional econometric theories and models at regional and global scales. Many classic econometric theories such as Environmental Kuznets Curve were developed and tested using spotted and discontinuous data, often before the era of advanced Earth observation data. The integration of remote sensing derived variables will greatly minimize the uncertainties, allowing a more systematic and repeatable test.

Reference

Akbostanci, Elif, Türüt-Aşik, Serap, & Tunç, G.Ipek. (2009). The relationship between income and environment in Turkey: Is there an environmental Kuznets curve? *Energy Policy*, *37*(3), 861–867. https://doi.org/10.1016/j.enpol.2008.09.088

Aldy, J. E. (2005). An Environmental Kuznets Curve Analysis of U.S. State-Level Carbon Dioxide Emissions. *The Journal of Environment & Development*, *14*(1), 48–72. https://doi.org/10.1177/1070496504273514

Apparicio, Philippe, Abdelmajid, Mohamed, Riva, Mylène, & Shearmur, Richard. (2008). Comparing alternative approaches to measuring the geographical accessibility of urban health services: Distance types and aggregation-error issues. *International Journal of Health Geographics*, *7*(1), 7. https://doi.org/10.1186/1476-072X-7-7

Arrow, Kenneth, Bolin, Bert, Costanza, Robert, Dasgupta, Partha, Folke, Carl, Holling, C. S., Jansson, Bengt-Owe, Levin, Simon, M~iler, Karl-Gsran, Perrings, Charles, & Pimentel, David. (1995). Economic growth, carrying capacity, and the environment 1. *Ecological Economics*, *268*(2), 520–521. https://doi.org/10.1016/0921-8009(95)00059-3

Ash, Caroline, Jasny, Barbara R., Roberts, Leslie, Stone, Richard, & Sugden, Andrew M. (2008). Reimagining cities. *Science*, *319*(5864), 739. https://doi.org/10.1126/science.319.5864.739

Asner, G. P., & Heidebrecht, K. B. (2002). Spectral unmixing of vegetation, soil and dry carbon cover in arid regions: Comparing multispectral and hyperspectral observations. *International Journal of Remote Sensing*, *23*(19), 3939–3958. https://doi.org/10.1080/01431160110115960

Bagan, Hasi, & Yamagata, Yoshiki. (2014). Land-cover change analysis in 50 global cities by using a combination of Landsat data and analysis of grid cells. *Environmental Research Letters*, *9*(6), 64015. https://doi.org/10.1088/1748-9326/9/6/064015

Balbo, Marcello, & Navez-Bouchanine, Françoise. (1995). Urban fragmentation as a research hypothesis: Rabat-Salé case study. *Habitat International*, *19*(4), 571–582. https://doi.org/10.1016/0197-3975(95)00008-4

Barnsley, Michael J., & Barr, Stuart L. (1997). Distinguishing urban land-use categories in fine spatial resolution land-cover data using a graph-based, structural pattern recognition system. *Computers, Environment and Urban Systems*, *21*(3–4), 209–225. https://doi.org/10.1016/S0198-9715(97)10001-1

Bartlett, Bruce. (1994). The high cost of turning green. *The Wall Street Journal*, *14*(0).

Baugh, Kimberly, Elvidge, Christopher D., Ghosh, Tilottama, & Ziskin, Daniel. (2010). Development of a 2009 Stable Lights Product using DMSP-OLS data. *Proceedings of the Asia-Pacific Advanced Network*, *30*, 114–130. https://doi.org/10.7125/APAN.30.17

BC Statistics. (2012). Population estimates. Retrieved from https://www2.gov.bc.ca/gov/content/data/statistics/people-population-community/population

Beckerman, Wilfred. (1992). Economic growth and the environment: Whose growth? whose environment? *World Development*, *20*(4), 481–496. https://doi.org/https://doi.org/10.1016/0305-

750X(92)90038-W

Bell, David, & Jayne, Mark. (2009). Small cities? Towards a research agenda. *International Journal of Urban and Regional Research*, *33*(3), 683–699. https://doi.org/10.1111/j.1468-2427.2009.00886.x

Bemdt, Donald J., & Clifford, James. (1994). Using Dynamic Time Warping to FindPatterns in Time Series. Retrieved from https://www.aaai.org/Papers/Workshops/1994/WS-94-03/WS94-03-031.pdf

Bennett, Mia M., & Smith, Laurence C. (2017). Advances in using multitemporal night-time lights satellite imagery to detect, estimate, and monitor socioeconomic dynamics. *Remote Sensing of Environment*, *192*, 176–197. https://doi.org/10.1016/j.rse.2017.01.005

Bennie, Jonathan, Davies, Thomas W., Duffy, James P., Inger, Richard, & Gaston, Kevin J. (2015). Contrasting trends in light pollution across Europe based on satellite observed night time lights. *Scientific Reports*, *4*(1), 3789. https://doi.org/10.1038/srep03789

Benz, Ursula C., Hofmann, Peter, Willhauck, Gregor, Lingenfelder, Iris, & Heynen, Markus. (2004). Multi-resolution, object-oriented fuzzy analysis of remote sensing data for GIS-ready information. *ISPRS Journal of Photogrammetry and Remote Sensing*, *58*(3–4), 239–258. https://doi.org/10.1016/J.ISPRSJPRS.2003.10.002

Bey, Adia, Sánchez-Paus Díaz, Alfonso, Maniatis, Danae, Marchi, Giulio, Mollicone, Danilo, Ricci, Stefano, Bastin, Jean-François, Moore, Rebecca, Federici, Sandro, Rezende, Marcelo, Patriarca, Chiara, Turia, Ruth, Gamoga, Gewa, Abe, Hitofumi, Kaidong, Elizabeth, & Miceli, Gino. (2016). Collect Earth: Land Use and Land-cover Assessment through Augmented Visual Interpretation. *Remote Sensing*, *8*(10), 807. https://doi.org/10.3390/rs8100807

Birch, Eugenie L., & Wachter, Susan M. (2011). *Global urbanization*. University of Pennsylvania Press.

Bolshakova, N., & Azuaje, F. (2003). Cluster validation techniques for genome expression data. *Signal Processing*, *83*(4), 825–833. https://doi.org/10.1016/S0165-1684(02)00475-9

Boone, Christopher G., & Fragkias, Michail. (2012). *Urbanization and Sustainability: Linking Urban Ecology, Environmental Justice and Global Environmental Change*. https://doi.org/10.1007/978-94-007-5666-3

Burgess, E. W. (1925). The growth of the city. In *The City* (pp. 47–62).

Burnham, Kenneth P., & Anderson, David R. (2003). *Model selection and multimodel inference: a practical information-theoretic approach*. Springer Science & Business Media.

Cadenasso, Mary L., Pickett, Steward T. A., & Schwarz, Kirsten. (2007). Spatial heterogeneity in urban ecosystems: reconceptualizing land-cover and a framework for classification. *Frontiers in Ecology and the Environment*, *5*(2), 80–88.

Castrence, Miguel, Nong, Duong, Tran, Chinh, Young, Luisa, & Fox, Jefferson. (2014). Mapping Urban Transitions Using Multi-Temporal Landsat and DMSP-OLS Night-Time Lights Imagery of the Red River Delta in Vietnam. *Land*, *3*(1), 148–166. https://doi.org/10.3390/land3010148

Champion, A. G. A. (2001). Changing Demographic Regime and Evolving Polycentric Urban Regions: Consequences for the Size, Composition and Distribution of City Population. *Urban Studies*, *4*(38), 657–677.

Chen, S. S., Yan, Yue, Gao, Qun, & Liu, Dene. (2014). Quantifying circular urban expansion patterns of

compact Chinese cities: the case of Yangtze River Delta, China. *Environment and Planning B: Planning and Design*, *41*(1963). https://doi.org/10.1068/b120004p

Cheng, Xiaoyun, Wei, Bensheng, Chen, Guojian, Li, Junxiang, & Song, Conghe. (2007). Influence of Park Size and Its Surrounding Urban Landscape Patterns on the Park Cooling Effect, 1–10. https://doi.org/10.1061/(ASCE)UP.1943-5444.0000256.

Clancey, Gregory. (2004). Local memory and worldly narrative: The remote city in America and Japan. *Urban Studies*, *41*(12), 2335–2355. https://doi.org/10.1080/00420980412331297564

Cliff, Andrew D., & Ord, Keith. (1970). Spatial autocorrelation: a review of existing and new measures with applications. *Economic Geography*, *46*(sup1), 269–292.

Cohen, Barney. (2006). Urbanization in developing countries: Current trends, future projections, and key challenges for sustainability. *Technology in Society*. https://doi.org/10.1016/j.techsoc.2005.10.005

Corlett, Richard T. (1999). Environmental forestry in Hong Kong: 1871--1997. *Forest Ecology and Management*, *116*(1–3), 93–105.

Croft, Thomas. (1973). Burning Waste Gas in Oil Fields. *Nature*, *245*, 375–376.

Dietz, Thomas, Rosa, EA, & York, Richard. (2007). Driving the human ecological footprint. *Frontiers in Ecology and the Environment in Ecology and the Environment*, *5*(1), 13–18.

Dietzel, Charles, Herold, Martin, Hemphill, Jeffrey J., & Clarke, Keith C. (2005). Spatio-temporal dynamics in California's Central Valley: Empirical links to urban theory. *International Journal of Geographical Information Science*, *19*(2), 175–195. https://doi.org/10.1080/13658810410001713407

Dijst, Martin, & Vidakovic, Velibor. (2000). Travel time ratio: the key factor of spatial reach. *Transportation*, *27*(2), 179–199. https://doi.org/10.1023/A:1005293330869

Doll, Christopher N. H., Muller, Jan-Peter, & Morley, Jeremy G. (2006). Mapping regional economic activity from night-time light satellite imagery. *Ecological Economics*, *57*(1), 75–92. https://doi.org/10.1016/j.ecolecon.2005.03.007

Donaldson, Dave, & Storeygard, Adam. (2016). The View from Above: Applications of Satellite Data in Economics. *Journal of Economic Perspectives*, *30*(4—Fall), 171–198. https://doi.org/10.1257/jep.30.4.171

Dorais, Alexis, & Cardille, Jeffrey. (2011). Strategies for Incorporating High-Resolution Google Earth Databases to Guide and Validate Classifications: Understanding Deforestation in Borneo. *Remote Sensing*, *3*(6), 1157–1176. https://doi.org/10.3390/rs3061157

Dumitrescu, Elena Ivona, & Hurlin, Christophe. (2012). Testing for Granger non-causality in heterogeneous panels. *Economic Modelling*, *29*(4), 1450–1460. https://doi.org/10.1016/j.econmod.2012.02.014

Ebener, Steeve, Murray, Christopher, Tandon, Ajay, & Elvidge, Christopher C. (2005). From wealth to health: modelling the distribution of income per capita at the sub-national level using night-time light imagery. *International Journal of Health Geographics*, *4*(1), 5. https://doi.org/10.1186/1476-072X-4-5

Egli, Hannes, & Steger, Thomas M. (2007). A dynamic model of the environmental Kuznets curve: Turning point and public policy. *Environmental and Resource Economics*, *36*(1), 15–34.

https://doi.org/10.1007/s10640-006-9044-9

Elmore, Andrew J., Mustard, John F., Manning, Sara J., & Lobell, David B. (2000). Quantifying vegetation change in semiarid environments: precision and accuracy of spectral mixture analysis and the normalized difference vegetation index. *Remote Sensing of Environment*, *73*(1), 87–102.

Elvidge, Christopher D., & Lyon, Ronald J. P. (1985). Influence of rock-soil spectral variation on the assessment of green biomass. *Remote Sensing of Environment*, *17*(3), 265–279.

Elvidge, Christopher, Hsu, Feng-Chi, Baugh, KimberlyE, & Ghosh, Tilottama. (2014). National Trends in Satellite-Observed Lighting: 1992-2012. In *Global Urban Monitoring and Assessment through Earth Observation* (pp. 97–120). CRC Press. https://doi.org/doi:10.1201/b17012-9

Escobedo, Francisco J., Kroeger, Timm, & Wagner, John E. (2011). Urban forests and pollution mitigation: Analyzing ecosystem services and disservices. *Environmental Pollution*, *159*(8–9), 2078–2087. https://doi.org/10.1016/J.ENVPOL.2011.01.010

Fan, Fenglei, & Fan, Wei. (2014). Understanding spatial-temporal urban expansion pattern (1990–2009) using impervious surface data and landscape indexes: a case study in Guangzhou (China). *Journal of Applied Remote Sensing*, *8*(1), 83609. https://doi.org/10.1117/1.JRS.8.083609

Fauvel, M., & Benediktsson, Ja. (2008). Spectral and Spatial Classification of Hyperspectral Data Using SVMs and Morphological Profile. *… and Remote Sensing …*, *46*(11), 3804–3814. https://doi.org/10.1109/TGRS.2008.922034

Fernandes, Richard, & G. Leblanc, Sylvain. (2005). Parametric (modified least squares) and non-parametric (Theil–Sen) linear regressions for predicting biophysical parameters in the presence of measurement errors. *Remote Sensing of Environment*, *95*(3), 303–316. https://doi.org/10.1016/J.RSE.2005.01.005

Fodha, Mouez, & Zaghdoud, Oussama. (2010). Economic growth and pollutant emissions in Tunisia: An empirical analysis of the environmental Kuznets curve. *Energy Policy*, *38*(2), 1150–1156. https://doi.org/10.1016/j.enpol.2009.11.002

Gaston, Kevin J., Duffy, James P., & Bennie, Jonathan. (2015). Quantifying the erosion of natural darkness in the global protected area system. *Conservation Biology*, *29*(4), 1132–1141. https://doi.org/10.1111/cobi.12462

Gergel, Sarah E., Bennett, Elena M., Greenfield, Ben K., King, Susan, Overdevest, Christine A., & Stumborg, Basil. (2004). A TEST OF THE ENVIRONMENTAL KUZNETS CURVE USING LONG-TERM WATERSHED INPUTS. *Ecological Applications*, *14*(2), 555–570.

Getis, Arthur, & Ord, J.Keith. (1992). The analysis of spatial association by use of distance statistics. *Geographical Analysis*, *24*(3), 189–206.

Ghosh, Tilottama, Elvidge, Christopher D., Sutton, Paul C., Baugh, Kimberly E., Ziskin, Daniel, & Tuttle, Benjamin T. (2010). Creating a global grid of distributed fossil fuel CO2 emissions from nighttime satellite imagery. *Energies*, *3*(12), 1895–1913. https://doi.org/10.3390/en3121895

Giorgino, Toni. (2009). Computing and Visualizing Dynamic Time Warping Alignments in R : The dtw Package. *Journal of Statistical Software*, *31*(7). https://doi.org/10.18637/jss.v031.i07

Glaeser, Edward L. (2011). Cities, productivity, and quality of life. *Science (New York, N.Y.)*, *333*(6042),

592–594. https://doi.org/10.1126/science.1209264

Glass, David C., & Singer, Jerome E. (1972). Urban stress: Experiments on noise and social stressors.

Gober, Patricia. (2010, August 1). Desert urbanization and the challenges of water sustainability. *Current Opinion in Environmental Sustainability*. Elsevier. https://doi.org/10.1016/j.cosust.2010.06.006

Gonçalves, R. R. V., Zullo, J., Amaral, B. F., Coltri, P. P., M.Sousa, E. P., & Romani, L. A. S. (2014). LAND USE TEMPORAL ANALYSIS THROUGH CLUSTERING TECHNIQUES ON SATELLITE IMAGE TIME SERIES, 2173–2176.

Gordon, P., Richardsonll, H. W., & Wong, H. L. (1986). The distribution of population and employment in a polycentric city : the case of Los Angeles f, *18*(November 1984), 161–173.

Grahn, Patrik, & Stigsdotter, Ulrika A. (2003). Landscape planning and stress. *Urban Forestry and Urban Greening*, *2*(1), 1–18. https://doi.org/10.1078/1618-8667-00019

Granger, C. W. J. (1969). Investigating Causal Relations by Econometric Models and Cross-spectral Methods Author (s): C . W . J . Granger Published by : The Econometric Society Stable URL : http://www.jstor.org/stable/1912791 Accessed : 08-07-2016 18 : 00 UTC Your use of the JST. *Econometrica: Journal of the Econometric Society*, *37*(3), 424–438.

Green, A. A., Berman, M., Switzer, P., & Craig, M. D. (1988). A transformation for ordering multispectral data in terms of image quality with implications for noise removal. *IEEE Transactions on Geoscience and Remote Sensing*, *26*(1), 65–74. https://doi.org/10.1109/36.3001

Griffiths, Patrick, Hostert, Patrick, Gruebner, Oliver, & der Linden, Sebastian Van. (2010). Mapping megacity growth with multi-sensor data. *Remote Sensing of Environment*, *114*(2), 426–439. https://doi.org/10.1016/j.rse.2009.09.012

Grimm, N. B., Faeth, S. H., Golubiewski, N. E., Redman, C. L., Wu, J., Bai, X., & Briggs, J. M. (2008). Global Change and the Ecology of Cities. *Science*, *319*(5864), 756–760. https://doi.org/10.1126/science.1150195

Groffman, Peter M., Cavender-Bares, Jeannine, Bettez, Neil D., Grove, J.Morgan, Hall, Sharon J., Heffernan, James B., Hobbie, Sarah E., Larson, Kelli L., Morse, Jennifer L., Neill, Christopher, Nelson, Kristen, O'Neil-Dunne, Jarlath, Ogden, Laura, Pataki, Diane E., Polsky, Colin, Chowdhury, Rinku Roy, & Steele, Meredith K. (2014). Ecological homogenization of urban USA. *Frontiers in Ecology and the Environment*, *12*(1), 74–81. https://doi.org/10.1890/120374

Grossman, Gene M., & Krueger, Alan B. (1991). Environmental Impacts of a North American Free Trade Agreement. *National Bureau of Economic Research Working Paper Series*, *No. 3914*(3914), 1–57. https://doi.org/10.3386/w3914

Guérois, Marianne, & Pumain, Denise. (2008). Built-up encroachment and the urban field: A comparison of forty European cities. *Environment and Planning A*, *40*(9), 2186–2203. https://doi.org/10.1068/a39382

Handayani, Wiwandari, & Rudiarto, Iwan. (2014). Dynamics of Urban Growth in Semarang Metropolitan – Central Java: An Examination Based on Built-Up Area and Population Change. *Journal of Geography and Geology*, *6*(4), 80–87. https://doi.org/10.5539/jgg.v6n4p80

Hansen, M. C., Roy, D. P., Lindquist, E., Adusei, B., Justice, C. O., Alstatt, A. (2008). A method for

integrating MODIS and Landsat data for systematic monitoring of forest cover and change in the Congo Basin. *Remote Sensing of Environment*, *112*(5), 2495–2513.

Hawelka, Bartosz, Sitko, Izabela, Beinat, Euro, Sobolevsky, Stanislav, Kazakopoulos, Pavlos, & Ratti, Carlo. (2014). Geo-located Twitter as proxy for global mobility patterns. *Cartography and Geographic Information Science*, *41*(3), 260–271. https://doi.org/10.1080/15230406.2014.890072

Heckscher, Eli Filip. (1919). *The effect of foreign trade on the distribution of income*.

Heiden, Uta, Segl, Karl, Roessner, Sigrid, & Kaufmann, Hermann. (2007). Determination of robust spectral features for identification of urban surface materials in hyperspectral remote sensing data. *Remote Sensing of Environment*, *111*(4), 537–552. https://doi.org/10.1016/J.RSE.2007.04.008

Henderson, M., Yeh, E. T., Gong, P., Elvidge, C., & Baugh, K. (2003). Validation of urban boundaries derived from global night-time satellite imagery. *International Journal of Remote Sensing*, *24*(3), 595–610. https://doi.org/10.1080/01431160304982

Hermosilla, Txomin, Wulder, Michael A., White, Joanne C., Coops, Nicholas C., & Hobart, Geordie W. (2015). An integrated Landsat time series protocol for change detection and generation of annual gap-free surface reflectance composites. *Remote Sensing of Environment*, *158*, 220–234.

Heynen, Nik, Perkins, Harold A., & Roy, Parama. (2006). The Political Ecology of Uneven Urban Green Space: The Impact of Political Economy on Race and Ethnicity in Producing Environmental Inequality in Milwaukee. *Urban Affairs Review*, *42*(1), 3–25. https://doi.org/10.1177/1078087406290729

Heynen, Nikolas C., & Lindsey, Greg. (2003). Correlates of Urban Forest Canopy Cover. *Public Works Management & Policy*, *8*(1), 33–47. https://doi.org/10.1177/1087724X03008001004

Hill, Michael J., & Donald, Graham E. (2003). Estimating spatio-temporal patterns of agricultural productivity in fragmented landscapes using AVHRR NDVI time series. *Remote Sensing of Environment*, *84*(3), 367–384. https://doi.org/10.1016/S0034-4257(02)00128-1

Hodgson, Michael E., Jensen, John R., Tullis, Jason A., Riordan, Kevin D., & Archer, Clark M. (2003). Synergistic Use of Lidar and Color Aerial Photography for Mapping Urban Parcel Imperviousness. *Photogrammetric Engineering & Remote Sensing*, *69*(9), 973–980. https://doi.org/10.14358/PERS.69.9.973

Hoffmann, Robert, Lee, Chew-Ging, Ramasamy, Bala, & Yeung, Matthew. (2005). FDI and pollution: a granger causality test using panel data. *Journal of International Development*, *17*(3), 311–317. https://doi.org/10.1002/jid.1196

Hoornweg, Daniel, Bhada-Tata, Perinaz, & Kennedy, Chris. (2013). Waste production must peak this century. *Nature*, *502*(7473), 615–617. https://doi.org/10.1038/502615a

Hostert, Patrick, Röder, Achim, & Hill, Joachim. (2003). Coupling spectral unmixing and trend analysis for monitoring of long-term vegetation dynamics in Mediterranean rangelands. *Remote Sensing of Environment*, *87*(2–3), 183–197. https://doi.org/10.1016/80034-4257(03)00145-7

Hsiao, Cheng. (2007). Panel data analysis-advantages and challenges. *Test*, *16*(1), 1–22. https://doi.org/10.1007/s11749-007-0046-x

Huang, Qingxu, He, Chunyang, Gao, Bin, Yang, Yang, Liu, Zhifeng, Zhao, Yuanyuan, & Dou, Yue. (2015).

Detecting the 20 year city-size dynamics in China with a rank clock approach and DMSP/OLS nighttime data. *Landscape and Urban Planning*, *137*, 138–148. https://doi.org/10.1016/j.landurbplan.2015.01.004

Huete, A. R., Jackson, R. D., & Post, D. F. (1985). Spectral response of a plant canopy with different soil backgrounds. *Remote Sensing of Environment*, *17*(1), 37–53.

Huete, A. R., & Tucker, C. J. (1991). Investigation of soil influences in AVHRR red and near-infrared vegetation index imagery. *International Journal of Remote Sensing*, *12*(6), 1223–1242.

Hugo, Graeme. (2017). *New forms of urbanization: beyond the urban-rural dichotomy*. Routledge. Retrieved from https://books.google.ca/books?hl=en&lr=&id=aJwuDwAAQBAJ&oi=fnd&pg=PT10&ots=KpH9Fs2b3h&sig=a07XGKAAWOtwo3LY_zSzXabEgw0#v=onepage&q&f=false

Im, Kyung So;, & Pesaran, M. H. (2003). on the Panel Unit Root Tests Using Nonlinear Instrumental Variables. *SSRN*.

Janelle, Donald G., & Beuthe, Michel. (1997). Globalization and research issues in transportation. *Journal of Transport Geography*, *5*(3), 199–206. https://doi.org/10.1016/S0966-6923(97)00017-3

Jensen, Jr, & Cowen, Dc. (1999). Remote sensing of urban suburban infrastructure and socio-economic attributes. *Photogrammetric Engineering and Remote Sensing*, *65*(5), 611–622.

Ji, Wei, Ma, Jia, Twibell, Rima Wahab, & Underhill, Karen. (2006). Characterizing urban sprawl using multi-stage remote sensing images and landscape metrics. *Computers, Environment and Urban Systems*, *30*(6), 861–879. https://doi.org/10.1016/j.compenvurbsys.2005.09.002

Jim, C. Y., & Chen, Wendy Y. (2006). Impacts of urban environmental elements on residential housing prices in Guangzhou (China). *Landscape and Urban Planning*, *78*(4), 422–434. https://doi.org/10.1016/j.landurbplan.2005.12.003

Johansen, Søren. (1988). Statistical analysis of cointegration vectors. *Journal of Economic Dynamics and Control*, *12*(2–3), 231–254. https://doi.org/10.1016/0165-1889(88)90041-3

Jones, Gavin W. (2002). Southeast Asian urbanization and the growth of mega-urban regions. *Journal of Population Research*, *19*(2), 119–136. https://doi.org/10.1007/BF03031973

Kahn, Matthew E. (2000). The environmental impact of suburbanization. *Journal of Policy Analysis and Management*, *19*(4), 569–586. https://doi.org/10.1002/1520-6688(200023)19:4<569::AID-PAM3>3.0.CO;2-P

Keast, Allen. (2013). *Biogeography and ecology in Australia*. Springer.

Keogh, Eamonn, & Ratanamahatana, Chotirat Ann. (2005). Exact indexing of dynamic time warping. *Knowledge and Information Systems*, *7*(3), 358–386. https://doi.org/10.1007/s10115-004-0154-9

Keshava, Nirmal, & Mustard, John F. (2002). Spectral unmixing. *IEEE Signal Processing Magazine*, *19*(1), 44–57. https://doi.org/10.1109/79.974727

Kestens, Yan, Thériault, Marius, & Des Rosiers, François. (2004). The Impact of Surrounding Land Use and Vegetation on Single-Family House Prices. *Environment and Planning B: Planning and Design*, *31*(4), 539–567. https://doi.org/10.1068/b3023

Klotz, M., Kemper, T., Geiß, C., Esch, T., & Taubenböck, H. (2016). How good is the map? A multi-scale cross-comparison framework for global settlement layers: Evidence from Central Europe. *Remote Sensing of Environment*, *178*, 191–212. https://doi.org/10.1016/j.rse.2016.03.001

Knapp, Tom, & Mookerjee, Rajen. (1996). Population growth and global CO2 emissions. *Energy Policy*, *24*(1), 31–37. https://doi.org/10.1016/0301-4215(95)00130-1

Kong, Fanhua, Yin, Haiwei, & Nakagoshi, Nobukazu. (2007). Using GIS and landscape metrics in the hedonic price modeling of the amenity value of urban green space: A case study in Jinan City, China. *Landscape and Urban Planning*, *79*(3–4), 240–252. https://doi.org/10.1016/j.landurbplan.2006.02.013

Kottek, Markus, Grieser, Jürgen, Beck, Christoph, Rudolf, Bruno, & Rubel, Franz. (2006). World map of the Köppen-Geiger climate classification updated. *Meteorologische Zeitschrift*, *15*(3), 259–263.

Kumagai, Kiichiro. (n.d.). ANALYSIS OF VEGETATION DISTRIBUTION IN URBAN AREAS: SPATIAL ANALYSIS APPROACH ON A REGIONAL SCALE. Retrieved from https://pdfs.semanticscholar.org/92bf/9658e5c5a739d9b625df8fc7de9b45fa7029.pdf

Kummu, Matti, Ward, Philip J., De Moel, Hans, & Varis, Olli. (2010). Is physical water scarcity a new phenomenon? Global assessment of water shortage over the last two millennia. *Environmental Research Letters*, *5*(3), 34006. https://doi.org/10.1088/1748-9326/5/3/034006

Kuznets, Simon. (1955). Economic growth and income inequality. *The American Economic Review*, 1–28.

Kyba, Christopher, Garz, Stefanie, Kuechly, Helga, de Miguel, Alejandro, Zamorano, Jaime, Fischer, Jürgen, & Hölker, Franz. (2014). High-Resolution Imagery of Earth at Night: New Sources, Opportunities and Challenges. *Remote Sensing*, *7*(1), 1–23. https://doi.org/10.3390/rs70100001

Lee, Taedong. (2013). Global cities and transnational climate change networks. *Global Environmental Politics*, *13*(1), 108–127.

Levin, Andrew, Lin, Chien Fu, & Chu, Chia Shang James. (2002). Unit root tests in panel data: Asymptotic and finite-sample properties. *Journal of Econometrics*, *108*(1), 1–24. https://doi.org/10.1016/S0304-4076(01)00098-7

Li, Xi, Chen, Xiaoling, Zhao, Yousong, Xu, Jia, Chen, Fengrui, & Li, Hui. (2013). Automatic intercalibration of night-time light imagery using robust regression. *Remote Sensing Letters*, *4*(1), 45–54. https://doi.org/10.1080/2150704X.2012.687471

Lin, Jinyao, Liu, Xiaoping, Li, Kai, & Li, Xia. (2014). A maximum entropy method to extract urban land by combining MODIS reflectance, MODIS NDVI, and DMSP-OLS data. *International Journal of Remote Sensing*, *35*(18), 6708–6727. https://doi.org/10.1080/01431161.2014.960623

Liu, Jiyuan, Zhan, Jinyan, & Deng, Xiangzheng. (2005). Spatio-temporal Patterns and Driving Forces of Urban Land Expansion in China during the Economic Reform Era. *AMBIO: A Journal of the Human Environment*, *34*(6), 450–455. https://doi.org/10.1579/0044-7447-34.6.450

Liu, Ting, & Yang, Xiaojun. (2015). Monitoring land changes in an urban area using satellite imagery, GIS and landscape metrics. *Applied Geography*, *56*, 42–54. https://doi.org/10.1016/j.apgeog.2014.10.002

Liu, Zhifeng, He, Chunyang, Zhang, Qiaofeng, Huang, Qingxu, & Yang, Yang. (2012). Extracting the

dynamics of urban expansion in China using DMSP-OLS nighttime light data from 1992 to 2008. *Landscape and Urban Planning*, *106*(1), 62–72. https://doi.org/10.1016/j.landurbplan.2012.02.013

Lo, Fu-chen, & Marcotullio, Peter J. (2000a). Globalisation and Urban Transform ations in the Asia-Pacific Region : A Review. *Urban Studies*, *37*(1), 77–111.

Lo, Fu-chen, & Marcotullio, Peter J. (2000b). Globalisation and Urban Transform ations in the Asia ± Paci ® c Region : A Review, *37*(1), 77–111.

Lu, Ming, & Chen, Zhao. (2004). Urbanization, Urban-Biased Economic Policies and Urban-Rural Inequality [J]. *Economic Research Journal*, *6*(5), 50–58.

Luck, Gary W., Smallbone, Lisa T., & O'Brien, Rachel. (2009). Socio-Economics and Vegetation Change in Urban Ecosystems: Patterns in Space and Time. *Ecosystems*, *12*(4), 604–620. https://doi.org/10.1007/s10021-009-9244-6

Lyon, John G., Yuan, Ding, Lunetta, Ross S., & Elvidge, Chris D. (1998). A change detection experiment using vegetation indices. *Photogrammetric Engineering and Remote Sensing*, *64*(2), 143–150.

Ma, Ting, Zhou, Chenghu, Pei, Tao, Haynie, Susan, & Fan, Junfu. (2012). Quantitative estimation of urbanization dynamics using time series of DMSP/OLS nighttime light data: A comparative case study from China's cities. *Remote Sensing of Environment*, *124*, 99–107. https://doi.org/10.1016/j.rse.2012.04.018

Maechler, Martin, Rousseeuw, Peter, Struyf, Anja, Hubert, Mia, & Hornik, Kurt. (2012). Cluster: cluster analysis basics and extensions. *R Package Version*.

Major, D. J., Baret, F., & Guyot, G. (1990). A ratio vegetation index adjusted for soil brightness. *International Journal of Remote Sensing*, *11*(5), 727–740.

Mann, Henry B. .. (1945). Nonparametric Tests Against Trend. *The Econometric Society*, *13*(3), 245–259.

Marconcini, Mattia, Metz, Annekatrin, Esch, Thomas, & Zeidler, Julian. (2014). GLOBAL URBAN GROWTH MONITORING BY MEANS OF SAR DATA. *German Aerospace Center*, (April 2012), 1477–1480.

Marshall, Richard. (2013). *Emerging urbanity: global urban projects in the Asia Pacific Rim*. Routledge.

Martinus, Kirsten, & Tonts, Matthew. (2015). Powering the world city system: energy industry networks and interurban connectivity. *Environment and Planning A*, *47*(7), 1502–1520.

Masek, J. G., Lindsay, F. E., & Goward, S. N. (2000). Dynamics of urban growth in the Washington DC metropolitan area, 1973-1996, from Landsat observations. *International Journal of Remote Sensing*, *21*(18), 3473–3486. https://doi.org/10.1080/014311600750037507

McKinney, Michael L. (2002). Urbanization, Biodiversity, and Conservation: The impacts of urbanization on native species are poorly studied, but educating a highly urbanized human population about these impacts can greatly improve species conservation in all ecosystems. *BioScience*, *52*(10), 883–890. https://doi.org/10.1641/0006-3568(2002)052[0883:UBAC]2.0.CO;2

McKinney, Michael L. (2006). Urbanization as a major cause of biotic homogenization. *Biological Conservation*, *127*(3), 247–260. https://doi.org/10.1016/j.biocon.2005.09.005

Michishita, Ryo, Jiang, Zhiben, & Xu, Bing. (2012). Monitoring two decades of urbanization in the Poyang Lake area, China through spectral unmixing. *Remote Sensing of Environment*, *117*, 3–18.

https://doi.org/10.1016/j.rse.2011.06.021

Mieg, Harald A., & Töpfer, Klaus. (2013). 8 Privatization, urban fragmentation, and sustainable development. In *Institutional and Social Innovation for Sustainable Urban Development* (p. 130).

Mike Jenks, Daniel Kozak, Pattaranan Takkanon. (2008). *World Cities and Urban Form: Fragmented, Polycentric, Sustainable?*

Montgomery, Mark R. (2008). The Urban Transformation of the Developing World. *Science*, *761*(February), 761–765. https://doi.org/10.1126/science.1153012

Mozumder, Pallab, & Marathe, Achla. (2007). Causality relationship between electricity consumption and GDP in Bangladesh. *Energy Policy*, *35*(1), 395–402. https://doi.org/10.1016/j.enpol.2005.11.033

Murakami, Akinobu, Medrial Zain, Alinda, Takeuchi, Kazuhiko, Tsunekawa, Atsushi, & Yokota, Shigehiro. (2005). Trends in urbanization and patterns of land use in the Asian mega cities Jakarta, Bangkok, and Metro Manila. *Landscape and Urban Planning*, *70*(3–4), 251–259. https://doi.org/10.1016/J.LANDURBPLAN.2003.10.021

Ng, Mee Kam. (2010). International Planning Studies Sustainable Urban Development Issues in Chinese Transitional Cities : Hong Kong and Shenzhen Sustainable Urban Development Issues in Chinese Transitional Cities : Hong Kong and Shenzhen, *3475*(October 2012), 37–41. https://doi.org/10.1080/1356347022011258

Nicolaou, N., Siddique, N., & Custovic, A. (2005). Allergic disease in urban and rural populations: increasing prevalence with increasing urbanization. *Allergy*, *60*(11), 1357–1360.

Nowak, David J. (2002). The effects of urban trees on air quality. *USDA Forest Service*, 96–102.

Nowak, David J., Crane, Daniel E., & Stevens, Jack C. (2006). Air pollution removal by urban trees and shrubs in the United States. *Urban Forestry and Urban Greening*, *4*(3–4), 115–123. https://doi.org/10.1016/j.ufug.2006.01.007

Nowak, David J., & Dwyer, John F. (2007). Understanding the Benefits and Costs of Urban Forest Ecosystems. *Handbook of Urban and Community Forestry in the North East*, 25–46. https://doi.org/10.1007/978-1-4020-4289-8{_}2

Ohlin, Berth. (1952). *Interregional And International Trade. Vol. 39*. Harvard University Press.; Cambridge.

Oke, Timothy R. (1982). The energetic basis of the urban heat island. *Quarterly Journal of the Royal Meteorological Society*, *108*(455), 1–24.

Panayotou, Theodore. (1997). Demystifying the environmental Kuznets curve: turning a black box into a policy tool. *Environment and Development Economics*, *2*(4), S1355770X97000259. https://doi.org/10.1017/S1355770X97000259

Pandey, Bhartendu, Joshi, P. K., & Seto, Karen C. (2013). Monitoring urbanization dynamics in India using DMSP/OLS night time lights and SPOT-VGT data. *International Journal of Applied Earth Observation and Geoinformation*, *23*, 49–61. https://doi.org/https://doi.org/10.1016/j.jag.2012.11.005

Pandey, Bhartendu, Zhang, Qingling, & Seto, Karen C. (2017). Comparative evaluation of relative calibration methods for DMSP/OLS nighttime lights. *Remote Sensing of Environment*, *195*, 67–78.

https://doi.org/10.1016/j.rse.2017.04.011

Pettorelli, Nathalie, Vik, Jon Olav, Mysterud, Atle, Gaillard, Jean-Michel, Tucker, Compton J., & Stenseth, Nils Chr. (2005). Using the satellite-derived NDVI to assess ecological responses to environmental change. *Trends in Ecology & Evolution*, *20*(9), 503–510. https://doi.org/10.1016/J.TREE.2005.05.011

Phinn, Stuart, Stanford, M., Scarth, P., Murray, A. T., & Shyy, P. T. (2002). Monitoring the composition of urban environments based on the vegetation-impervious surface-soil (VIS) model by subpixel analysis techniques. *International Journal of Remote Sensing*, *23*(20), 4131–4153.

Pickett, Steward T. A., & Zhou, Weiqi. (2015). Global urbanization as a shifting context for applying ecological science toward the sustainable city. *Ecosystem Health and Sustainability*, *1*(1), art5-art5. https://doi.org/10.1890/EHS14-0014.1

Quigley, Martin F. (2002). Franklin Park: 150 years of changing design, disturbance, and impact on tree growth. *Urban Ecosystems*, *6*(3), 223–235.

Quigley, Martin F. (2004). Street trees and rural conspecifics: will long-lived trees reach full size in urban conditions? *Urban Ecosystems*, *7*(1), 29–39.

Rath, T. M., & Manmatha, R. (2003). Word image matching using dynamic time warping. *2003 IEEE Computer Society Conference on Computer Vision and Pattern Recognition, 2003. Proceedings.*, *2*, II-521-II-527. https://doi.org/10.1109/CVPR.2003.1211511

Ridd, Merrill K. (1995). Exploring a VIS (vegetation-impervious surface-soil) model for urban ecosystem analysis through remote sensing: comparative anatomy for cities. *International Journal of Remote Sensing*, *16*(12), 2165–2185.

Roberts, D. A., Gardner, M., Church, R., Ustin, S., Scheer, G., & Green, R. O. (1998). Mapping Chaparral in the Santa Monica Mountains Using Multiple Endmember Spectral Mixture Models. *Remote Sensing of Environment*, *65*(3), 267–279. https://doi.org/10.1016/S0034-4257(98)00037-6

Román, Miguel O., Wang, Zhuosen, Sun, Qingsong, Kalb, Virginia, Miller, Steven, Molthan, Andrew, Schultz, Lori, Bell, Jordan, Stokes, Eleanor, Pandey, Bhartendu, Seto, Karen, Hall, Dorothy, Oda, Tomohiro, Wolfe, Robert, Lin, Gary, Golpayegani, Navid, Devadiga, Sadashiva, Davidson, Carol, et al. (2018). NASA's Black Marble Nighttime Product Suite. *Remote Sensing of Enviroment*, *Revision S*(November 2017), 113–143. https://doi.org/10.1016/j.rse.2018.03.017

Rottensteiner, Franz, & Briese, Christian. (2002). A new method for building extraction in urban areas from high-resolution LIDAR data. *International Archives of Photogrammetry Remote Sensing and Spatial Information Sciences*, *34*(3/A), 295–301.

Rousseeuw, Peter J. (1987). Silhouettes: A graphical aid to the interpretation and validation of cluster analysis. *Journal of Computational and Applied Mathematics*, *20*(C), 53–65. https://doi.org/10.1016/0377-0427(87)90125-7

Salvador, Stan, & Chan, Philip. (2007). Toward accurate dynamic time warping in linear time and space. *Intelligent Data Analysis*, *11*(5), 561–580.

Satterthwaite, David. (2009). The implications of population growth and urbanization for climate change. *Environment and Urbanization*, *21*(2), 545–567. https://doi.org/10.1177/0956247809344361

Schaltegger, Stefan, & Synnestvedt, Terje. (2002). The link between "green" and economic success: environmental management as the crucial trigger between environmental and economic performance. *Journal of Environmental Management*, *65*(4), 339–346. https://doi.org/https://doi.org/10.1006/jema.2002.0555

Schmidt, Gail, Jenkerson, Calli, Masek, Jeffrey, Vermote, Eric, & Gao, Feng. (2013). *Landsat ecosystem disturbance adaptive processing system (LEDAPS) algorithm description*.

Schneider, A. (2012). Monitoring land-cover change in urban and peri-urban areas using dense time stacks of Landsat satellite data and a data mining approach. *Remote Sensing of Environment*, *124*, 689–704. https://doi.org/10.1016/j.rse.2012.06.006

Schneider, A., Friedl, Mark A., & Potere, D. (2009). A new map of global urban extent from MODIS satellite data. *Environmental Research Letters*, *4*(4), 44003. https://doi.org/10.1088/1748-9326/4/4/044003

Schneider, A., & Woodcock, C. E. (2008). Compact, Dispersed, Fragmented, Extensive? A Comparison of Urban Growth in Twenty-five Global Cities using Remotely Sensed Data, Pattern Metrics and Census Information. *Urban Studies*, *45*(3), 659–692. https://doi.org/10.1177/0042098007087340

Secord, John, & Zakhor, Avideh. (2006). Tree detection in aerial lidar and image data. *Proceedings - International Conference on Image Processing, ICIP*, *4*(2), 2317–2320. https://doi.org/10.1109/ICIP.2006.312850

Selden, Thomas M., & Song, Daqing. (1994). Environmental Quality and Development: Is There a Kuznets Curve for Air Pollution Emissions? *Journal of Environmental Economics and Management*, *27*(2), 147–162. https://doi.org/https://doi.org/10.1006/jeem.1994.1031

Sen, Pranab Kumar. (1968). Estimates of the Regression Coefficient Based on Kendall's Tau. *Journal of the American Statistical Association*, *63*(324), 1379–1389. https://doi.org/10.1080/01621459.1968.10480934

Seto, Karen C., & Fragkias, Michail. (2005). Quantifying spatiotemporal patterns of urban land-use change in four cities of China with time series landscape metrics. *Landscape Ecology*, *20*(7), 871–888. https://doi.org/10.1007/s10980-005-5238-8

Seto, Karen C., & Kaufmann, Robert K. (2003). Modeling the Drivers of Urban Land Use Change in the Pearl River Delta, China: Integrating Remote Sensing with Socioeconomic Data. *Land Economics*, *79*(1), 106–121. https://doi.org/10.3368/le.79.1.106

Seto, Karen Ching-Yee. (2014). *Rethinking Global Land Use in an Urban Era*. *Rethinking global land use in an urban era*. The MIT Press. https://doi.org/10.7551/mitpress/9780262026901.001.0001

Sexton, Joseph O., Song, Xiao Peng, Huang, Chengquan, Channan, Saurabh, Baker, Matthew E., & Townshend, John R. (2013). Urban growth of the Washington, D.C.-Baltimore, MD metropolitan region from 1984 to 2010 by annual, Landsat-based estimates of impervious cover. *Remote Sensing of Environment*, *129*, 42–53. https://doi.org/10.1016/j.rse.2012.10.025

Shafik, Nemat. (1994). Economic Development and Environmental Quality : An Econometric Analysis Source. *Oxford Economic Papers*, *46*(Special Issue on Environmental Economics), 757–773. Retrieved from http://www.jstor.org/stable/2663498

Shelley, Louise I. (1981). *Crime and modernization: The impact of industrialization and urbanization on*

crime. Southern Illinois University Press Carbondale.

Shen, Li, Guo, Xulin, Xiao, Kang, & Access, Open. (2015). Spatiotemporally characterizing urban temperatures based on remote sensing and GIS analysis : a case study in the city of Saskatoon, 27–39. https://doi.org/10.1515/geo-2015-0005

Singh, Kunwar K., Vogler, John B., Shoemaker, Douglas A., & Meentemeyer, Ross K. (2012). LiDAR-Landsat data fusion for large-area assessment of urban land cover: Balancing spatial resolution, data volume and mapping accuracy. *ISPRS Journal of Photogrammetry and Remote Sensing*, *74*, 110–121. https://doi.org/10.1016/j.isprsjprs.2012.09.009

Small, Christopher. (2003). High spatial resolution spectral mixture analysis of urban reflectance. *Remote Sensing of Environment*, *88*(1–2), 170–186. https://doi.org/10.1016/j.rse.2003.04.008

Small, Christopher, & Elvidge, Christopher D. (2013). Night on Earth: Mapping decadal changes of anthropogenic night light in Asia. *International Journal of Applied Earth Observation and Geoinformation*, *22*, 40–52. https://doi.org/10.1016/j.jag.2012.02.009

Small, Christopher, Elvidge, Christopher D., Balk, Deborah, & Montgomery, Mark. (2011). Spatial scaling of stable night lights. *Remote Sensing of Environment*, *115*(2), 269–280. https://doi.org/10.1016/j.rse.2010.08.021

Small, Christopher, & Lu, Jacqueline W. T. (2006). Estimation and vicarious validation of urban vegetation abundance by spectral mixture analysis. *Remote Sensing of Environment*, *100*(4), 441–456. https://doi.org/10.1016/j.rse.2005.10.023

Small, Christopher, Pozzi, Francesca, & Elvidge, C. D. (2005). Spatial analysis of global urban extent from DMSP-OLS night lights. *Remote Sensing of Environment*, *96*(3–4), 277–291. https://doi.org/10.1016/j.rse.2005.02.002

Stern, David I. (1998). Progress on the Environmental Kuznets Curve? *Environment and Development Economics*, *3*(2), 173–196. https://doi.org/doi:null

Stern, David I. (2004). The Rise and Fall of the Environmental Kuznets Curve. *World Development*, *32*(8), 1419–1439. https://doi.org/10.1016/j.worlddev.2004.03.004

Stern, David I., Common, Michael S., & Barbier, Edward B. (1996). Economic growth and environmental degradation: The environmental Kuznets curve and sustainable development. *World Development*, *24*(7), 1151–1160. https://doi.org/10.1016/0305-750X(96)00032-0

Sutton, Paul C., Elvidge, Christopher D., Ghosh, Tilottama, & others. (2007). Estimation of gross domestic product at sub-national scales using nighttime satellite imagery. *International Journal of Ecological Economics & Statistics*, *8*(S07), 5–21.

Sutton, Paul, Roberts, Dar, Elvidge, Christopher, & Baugh, Kimberly. (2001). Census from Heaven: An estimate of the global human population using night-time satellite imagery. *International Journal of Remote Sensing*, *22*(16), 3061–3076.

Swetnam, R. D., Fisher, B., Mbilinyi, B. P., Munishi, P. K. T., Willcock, S., Ricketts, T., Mwakalila, S., Balmford, A., Burgess, N. D., Marshall, A. R., & Lewis, S. L. (2011). Mapping socio-economic scenarios of land-cover change: A GIS method to enable ecosystem service modelling. *Journal of Environmental Management*, *92*(3), 563–574. https://doi.org/10.1016/J.JENVMAN.2010.09.007

Theil, Henri. (1992). A Rank-Invariant Method of Linear and Polynomial Regression Analysis (pp. 345–381). Springer, Dordrecht. https://doi.org/10.1007/978-94-011-2546-8_20

Tian, Yichen, Yin, Kai, Lu, Dengsheng, Hua, Lizhong, Zhao, Qianjun, & Wen, Meiping. (2014). Examining Land Use and Land-cover Spatiotemporal Change and Driving Forces in Beijing from 1978 to 2010. *Remote Sensing*, *6*(11), 10593–10611. https://doi.org/10.3390/rs61110593

Todd, Stella W., & Hoffer, Roger M. (1998). Responses of spectral indices to variations in vegetation cover and soil background. *Photogrammetric Engineering and Remote Sensing*, *64*, 915–922.

Tooke, Thoreau Rory, Coops, Nicholas C., Goodwin, Nicholas R., & Voogt, James A. (2009). Extracting urban vegetation characteristics using spectral mixture analysis and decision tree classifications. *Remote Sensing of Environment*, *113*(2), 398–407. https://doi.org/10.1016/j.rse.2008.10.005

Tyrväinen, Liisa, Pauleit, Stephan, Seeland, Klaus, & De Vries, Sjerp. (2005). Benefits and uses of urban forests and trees. In *Urban Forests and Trees: A Reference Book* (pp. 81–114). https://doi.org/10.1007/3-540-27684-X_5

UNDESA. (2014). *P.D. World Urbanization Prospects the 2014 Revision, Highlights*. New York.

UNDESA. (2017). *P.D. World Population Prospects the 2017 Revision, Key Findings*. New York.

UNESCAP. (2012). *Statistical Yearbook for Asia and the Pacific 2012*.

UNESCO. (2014). Asia and the Pacific.

United Nations. (2002). World Urbanization Prospects. The 2001 Revision Data Tables and Highlights. *World Urbanization Prospects: The 2003 Revision*, (March), 1–195. https://doi.org/ESA/P/ WP/173

Van Der Meer, F., & De Jong, S. M. (2000). Improving the results of spectral unmixing of Landsat Thematic Mapper imagery by enhancing the orthogonality of end-members. *International Journal of Remote Sensing*, *21*(15), 2781–2797. https://doi.org/10.1080/01431160050121249

Varshney, Avnish. (2013). Improved NDBI differencing algorithm for built-up regions change detection from remote-sensing data: An automated approach. *Remote Sensing Letters*, *4*(5), 504–512. https://doi.org/10.1080/2150704X.2013.763297

Venter, Oscar, Sanderson, Eric W., Magrach, Ainhoa, Allan, James R., Beher, Jutta, Jones, Kendall R., Possingham, Hugh P., Laurance, William F., Wood, Peter, Fekete, Balázs M., Levy, Marc A., & Watson, James E. M. (2016). Sixteen years of change in the global terrestrial human footprint and implications for biodiversity conservation. *Nature Communications*, *7*, 1–11. https://doi.org/10.1038/ncomms12558

Vikhamar, Dagrun, & Solberg, Rune. (2003). Snow-cover mapping in forests by constrained linear spectral unmixing of MODIS data. *Remote Sensing of Environment*, *88*(3), 309–323. https://doi.org/10.1016/J.RSE.2003.06.004

Wang, Lanying, Wang, Shiqian, Li, Wei, & Li, Jonathan. (2014). Monitoring urban expansion of the Greater Toronto area from 1985 to 2013 using Landsat images. In *International Geoscience and Remote Sensing Symposium (IGARSS)* (pp. 4264–4267). https://doi.org/10.1109/IGARSS.2014.6947431

Waqar, Mirza Muhammad, Mirza, Johum Fatimah, Mumtaz, Rafia, & Hussain, Ejaz. (2012). Development of New Indices for Extraction of Built-Up Area & Bare Soil. *Open Access*, *1*(1), 1–4.

https://doi.org/10.4172/scientificreports.13

Ward, Douglas, Phinn, Stuart R., & Murray, Alan T. (2000). Monitoring Growth in Rapidly Urbanizing Areas Using Remotely Sensed Data. *The Professional Geographer*, *52*(3), 371–386. https://doi.org/10.1111/0033-0124.00232

Welch, R. (1980). Monitoring urban population and energy utilization patterns from satellite Data. *Remote Sensing of Environment*, *9*(1), 1–9. https://doi.org/10.1016/0034-4257(80)90043-7

Weng, Qihao. (2012). Remote sensing of impervious surfaces in the urban areas: Requirements, methods, and trends. *Remote Sensing of Environment*, *117*, 34–49. https://doi.org/10.1016/j.rse.2011.02.030

Wentz, Elizabeth A., Anderson, Sharolyn, Fragkias, Michail, Netzband, Maik, Mesev, Victor, Myint, Soe W., Quattrochi, Dale, Rahman, Atiqur, & Seto, Karen C. (2014). Supporting global environmental change research: A review of trends and knowledge gaps in urban remote sensing. *Remote Sensing*, *6*(5), 3879–3905. https://doi.org/10.3390/rs6053879

Wheaton, William C., & Shishido, Hisanobu. (1981). Urban Concentration, Agglomeration Economies, and the Level of Economic Development. *Economic Development and Cultural Change*, *30*(1), 17–30. https://doi.org/10.1086/452537

White, J. C., Wulder, M. a., Hobart, G. W., Luther, J. E., Hermosilla, T., Griffiths, P., Coops, N. C., Hall, R. J., Hostert, P., Dyk, a., & Guindon, L. (2014). Pixel-based image compositing for large-area dense time series applications and science. *Canadian Journal of Remote Sensing*, (August 2014), 00–00. https://doi.org/10.1080/07038992.2014.945827

Woodcock, Curtis E., Allen, Richard, Anderson, Martha, Belward, Alan, Bindschadler, Robert, Cohen, Warren, Gao, Feng, GOWARD, SAMUEL N., HELDER, DENNIS, HELMER, EILEEN, NEMANI, RAMA, OREOPOULOS, LAZAROS, SCHOTT, JOHN, THENKABAI, PRASAD S., VERMOTE, ERIC F., VOGELMANN, JAMES, WULDER, MICHAEL A., & WYNNE, RANDOLPH. (2008). Free Access to Landsat Imagery. *Science*, *320*(May), 1011–1012.

World Population Statistics. (2013). *Shanghai Population 2013*. Retrieved from http://www.worldpopulationstatistics.com/shanghai-population-2013/

Wu, Peilin, & Tan, Minghong. (2012). Challenges for sustainable urbanization: a case study of water shortage and water environment changes in Shandong, China. *Procedia Environmental Sciences*, *13*, 919–927. https://doi.org/10.1016/j.proenv.2012.01.085

Wulder, Michael A., & Coops, Nicholas C. (2013). Make Earth observations open access. *Nature*, *2013*(February), 2013–2014.

Wulder, Michael A., Hilker, Thomas, White, Joanne C., Coops, Nicholas C., Masek, Jeffrey G., Pflugmacher, Dirk, & Crevier, Yves. (2015). Virtual constellations for global terrestrial monitoring. *Remote Sensing of Environment*, *170*, 62–76. https://doi.org/10.1016/j.rse.2015.09.001

Wulder, Michael A., White, Joanne C., Goward, Samuel N., Masek, Jeffrey G., Irons, James R., Herold, Martin, Cohen, Warren B., Loveland, Thomas R., & Woodcock, Curtis E. (2008). Landsat continuity: Issues and opportunities for land-cover monitoring. *Remote Sensing of Environment*, *112*(3), 955–969. https://doi.org/10.1016/j.rse.2007.07.004

Xian, George, & Crane, Mike. (2006). An analysis of urban thermal characteristics and associated land-

cover in Tampa Bay and Las Vegas using Landsat satellite data. *Remote Sensing of Environment*, *104*(2), 147–156. https://doi.org/10.1016/J.RSE.2005.09.023

Xu, Xinliang, & Min, Xibi. (2013). Quantifying spatiotemporal patterns of urban expansion in China using remote sensing data. *Cities*, *35*, 104–113. https://doi.org/10.1016/j.cities.2013.05.002

Yang, Jun, Huang, Conghong, Zhang, Zhiyong, & Wang, Le. (2014). The temporal trend of urban green coverage in major Chinese cities between 1990 and 2010. *Urban Forestry & Urban Greening*, *13*(1), 19–27. https://doi.org/10.1016/j.ufug.2013.10.002

Yang, X., & Lo, C. P. (2002). Using a time series of satellite imagery to detect land use and land-cover changes in the Atlanta, Georgia metropolitan area. *International Journal of Remote Sensing*, *23*(9), 1775–1798. https://doi.org/10.1080/01431160110075802

Yang, Yetao, Wong, Louis Ngai Yuen, Chen, Chao, & Chen, Tao. (2014). Using multitemporal Landsat imagery to monitor and model the influences of landscape pattern on urban expansion in a metropolitan region. *Journal of Applied Remote Sensing*, *8*(1), 83639. https://doi.org/10.1117/1.JRS.8.083639

Zha, Y., Gao, J., & Ni, S. (2003). Use of normalized difference built-up index in automatically mapping urban areas from TM imagery. *International Journal of Remote Sensing*, *24*(3), 583–594. https://doi.org/10.1080/01431160304987

Zhang, Q., Pandey, B., & Seto, K. C. (2016). A Robust Method to Generate a Consistent Time Series From DMSP / OLS Nighttime Light Data. *IEEE Transactions on Geoscience and Remote Sensing*, *54*(10), 5821–5831. https://doi.org/10.1109/TGRS.2016.2572724

Zhang, Qingling, Schaaf, Crystal, & Seto, Karen C. (2013). The Vegetation adjusted NTL Urban Index: A new approach to reduce saturation and increase variation in nighttime luminosity. *Remote Sensing of Environment*, *129*, 32–41. https://doi.org/10.1016/j.rse.2012.10.022

Zhang, Xiaoyang, Friedl, Mark A., Schaaf, Crystal B., Strahler, Alan H., Hodges, J. C. F., Gao, Feng, Reed, Bradley C., & Huete, Alfredo. (2003). Monitoring vegetation phenology using MODIS. *Remote Sensing of Environment*, *84*(3), 471–475. https://doi.org/10.1016/S0034-4257(02)00135-9

Zhao, Shuqing, Liu, Shuguang, & Zhou, Decheng. (2016). Prevalent vegetation growth enhancement in urban environment. *Proceedings of the National Academy of Sciences*, *113*(22), 6313–6318. https://doi.org/10.1073/pnas.1602312113

Zheng, Xinyu, Yu, Zhoulu, Ao, Weijiu, Wang, Youfu, Tahmassebi, Amir Reza, You, Shucheng, Deng, Jinsong, & Wang, Ke. (2014). Rural impervious surfaces extraction from Landsat-8 imagery and rural impervious surface index. In Thomas J. Jackson, Jing Ming Chen, Peng Gong, & Shunlin Liang (Eds.), *SPIE Asia Pacific Remote Sensing* (Vol. 9260, p. 926030). https://doi.org/10.1117/12.2068807

Zhu, Zhe, & Woodcock, Curtis E. (2012). Object-based cloud and cloud shadow detection in Landsat imagery. *Remote Sensing of Environment*, *118*, 83–94. https://doi.org/10.1016/j.rse.2011.10.028

Ziter, Carly. (2016). The biodiversity-ecosystem service relationship in urban areas: A quantitative review. *Oikos*, *125*(6), 761–768. https://doi.org/10.1111/oik.02883

Appendix 1

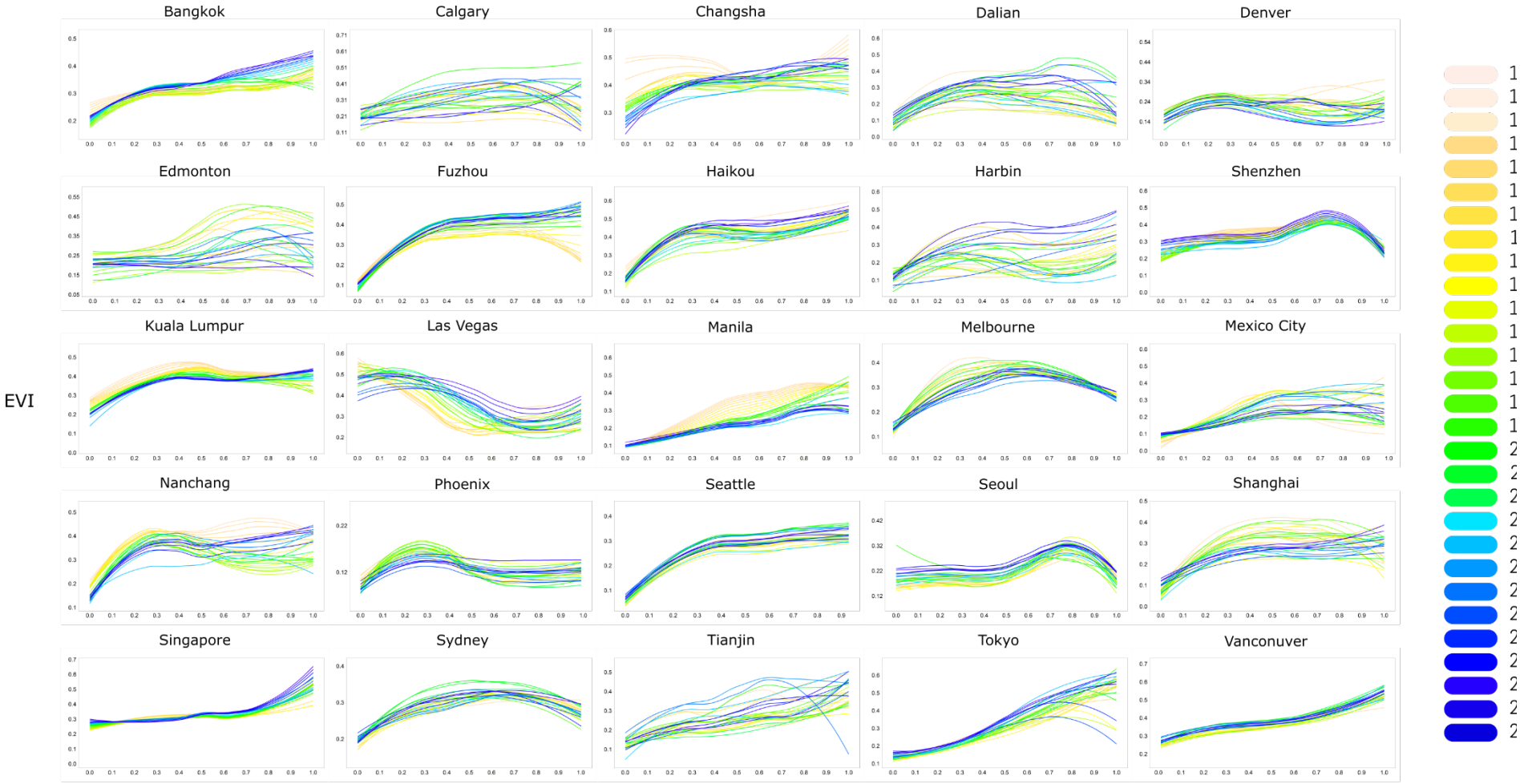
Bangkok
Calgary
Changsha
Dalian
Denver
Edmonton
Fuzhou
Haikou
Harbin
Shenzhen
Kuala Lumpur
Las Vegas
Manila
Melbourne
Mexico City
Nanchang
Phoenix
Seattle
Seoul
Shanghai
Singapore
Sydney
Tianjin
Tokyo
Vanconuver
EVI
Distance Index
1
1
1
1
1
1
1
1
1
1
1
1
1
2
2
2
2
2
2
2
2
2
2
2

Appendix 2

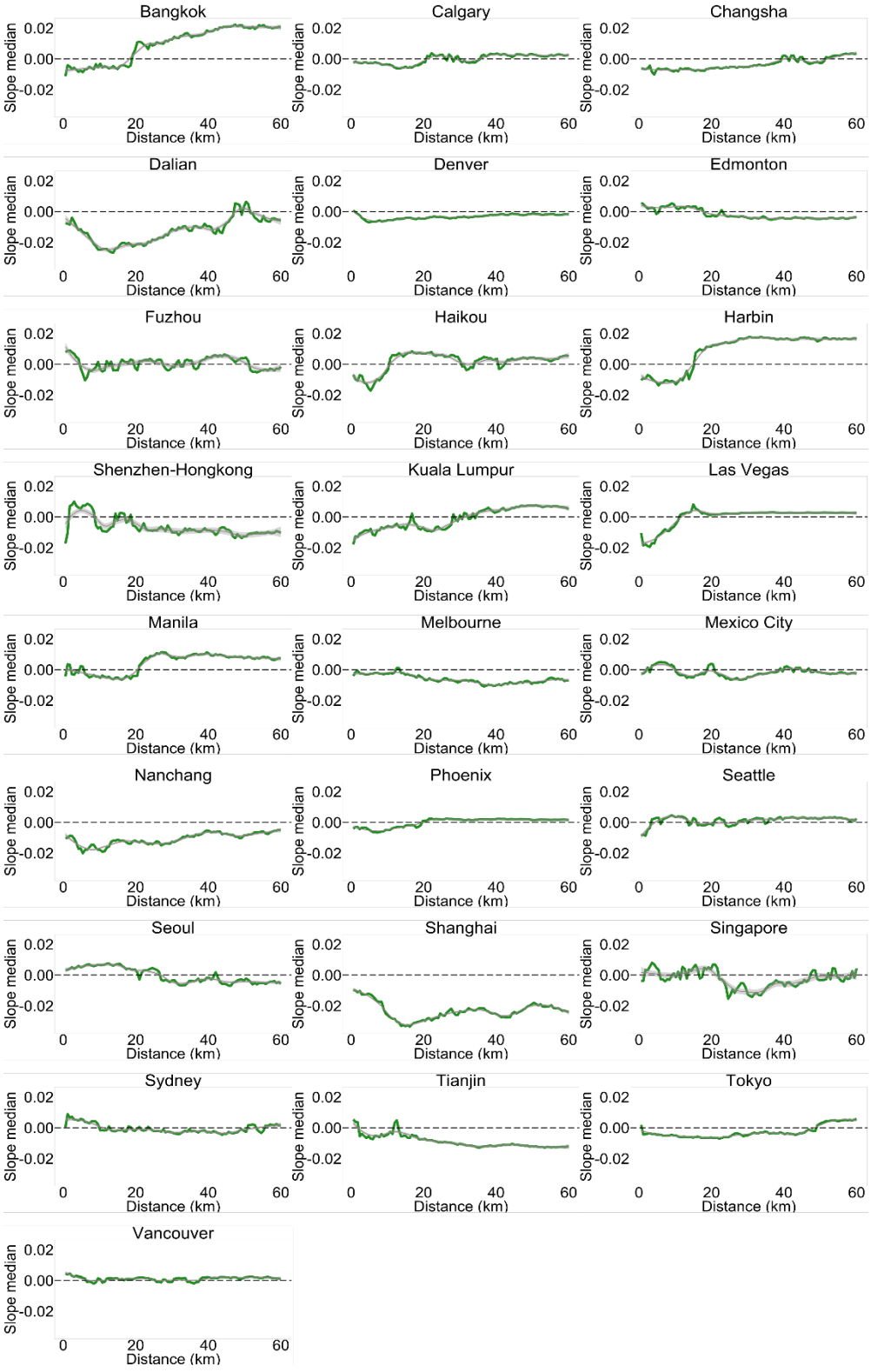
Bangkok
Calgary
Changsha
Dalian
Denver
Edmonton
Fuzhou
Haikou
Harbin
Shenzhen-Hongkong
Kuala Lumpur
Las Vegas
Manila
Melbourne
Mexico City
Nanchang
Phoenix
Seattle
Seoul
Shanghai
Singapore
Sydney
Tianjin
Tokyo
Vancouver
Slope median
0.02
0.00
-0.02
0
20
40
60
Distance (km)

Appendix 3

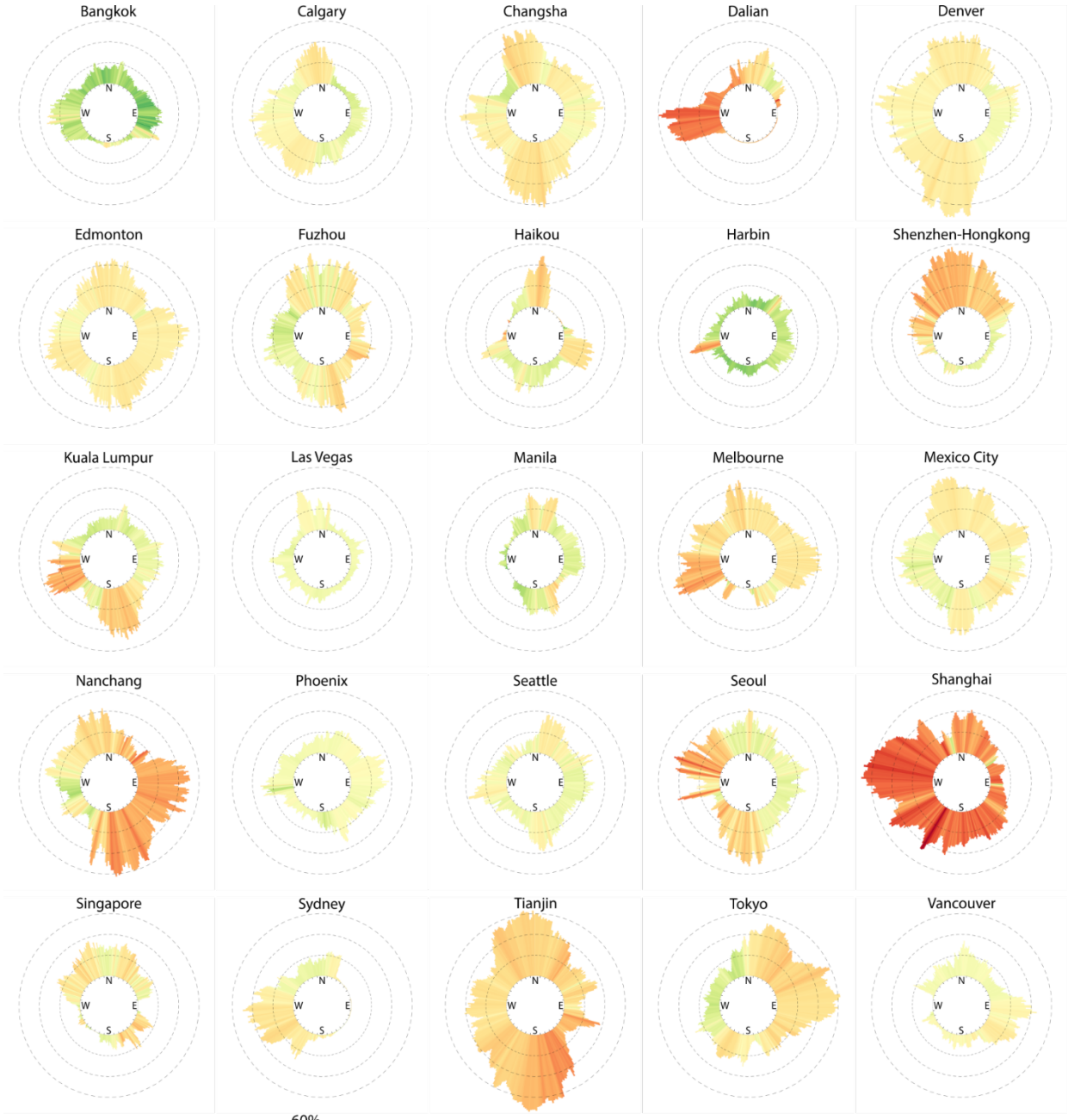
Bangkok
Calgary
Changsha
Dalian
Denver
Edmonton
Fuzhou
Haikou
Harbin
Shenzhen-Hongkong
Kuala Lumpur
Las Vegas
Manila
Melbourne
Mexico City
Nanchang
Phoenix
Seattle
Seoul
Shanghai
Singapore
Sydney
Tianjin
Tokyo
Vancouver
N
W
E
S

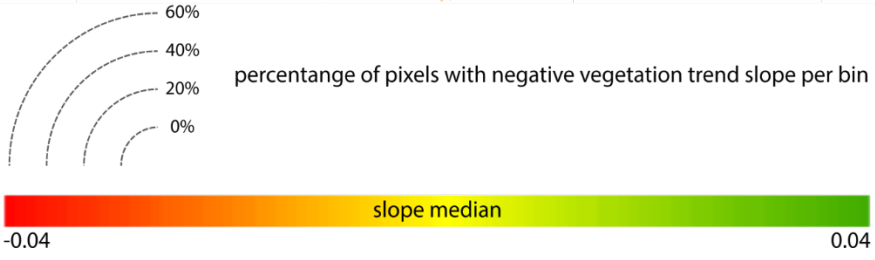
60%
40%
20%
0%
percentange of pixels with negative vegetation trend slope per bin
slope median
-0.04
0.04

Appendix 4

Panel unit root tests indicated that not all panel data sets were stationary in level. T_{DN} was stationary in level ($p < 0.01$) as indicated by both LLC and IPS procedures. However, the test results were mixed for other socio-economic panel time series. T_{GDP_Total} contained a panel unit root in level and achieved stationarity at 1st difference. T_{POP_Total} was stationary in both level and 1st using IPS procedure but contained panel unit roots in levels using LLC test. Given the mixed test results, I used only the 1st difference panel data sets for subsequent analysis.

	Level	**1st difference**	**Level**	**1st difference**
	LLC	LLC	IPS	IPS
T_{DN}	-2.94605 ***	-13.8317 ***	-4.26640 ***	-14.7862 ***
T_{POP_Total}	-0.15784	-5.36286 ***	-2.65526 ***	-5.97486 ***
T_{GDP_Total}	2.06186	-8.51984 ***	-0.18361	-8.16482 ***
10% (*), 5% (**), 1% (***)				

Johansen Fisher co-integration test indicated a significant presence of long-run relationship between T_{DN}, T_{POP_Total}, and T_{GDP_Total}. I rejected the null hypothesis – no long-run relationship, at the 1% significance level for all pairs of panel data sets. The existence of a long term equilibrium allowed for testing Granger causality between nighttime lights and socio-economic changes.

Time Series Pairs	**H0: number of cointegration vectors**	**Fisher statistic (trace test)**	**Fisher statistics (max-eigen test)**
TDN ~ TPOP_Total	None	140.6***	128.3***
	At most 1	55.27	55.27
TGDP_Total ~ TPOP_ Total	None	144.6***	137.4***
	At most 1	73.44	73.44
T_{DN} ~ T_{GDP_Total}	None	202.0***	178.3***
	At most 1	66.83	66.83
10% level (*), 5% level (**), 1% level (***)			